IZMIR DEMOCRACY UNIVERSITY

NATURAL &APPLIED SCIENCES JOURNAL

IDUNAS

Table of Contents

A Novel Hybrid: Neuro-Immuno-Engineering

Review Article

Arzu L. Aral[1]* iD , Gönül Ö. Peker[2] iD

[1] Department of Immunology, Faculty of Medicine, Izmir Democracy University, Izmir, Turkey

[2] Department of Physiology, Faculty of Medicine, Ege University, Izmir, Turkey (retired)

Author E-mails
arzuaral@gmail.com
*Correspondance to: Assoc. Prof. Dr. Arzu Latife Aral, Department of Immunology, Faculty of Medicine, Izmir Democracy University, Izmir, Turkey
Tel: +90 232 260 1001
DOI: 10.38061/idunas.754647

Abstract

Although the central nervous system has been known as immune-privileged for many decades, the psycho-neuro-endocrine-immune relationships studied in integrity, in recent years has opened a new era called neuroimmunology. Illumination of the bi-directional cross-talk between immune and central nervous systems, both of which are of cardinal importance for homeostasis, survival, progress and wellbeing, and, is highly expected to provide an integrated understanding of neuropathological and degenerative processes. Bioengineering is another novel inter-discipline, which has been developing with great momentum recently. Adaptability, ownership, and mastery of the recipient and the durability and optimal performance of the devices used, seem to be the outmost priority requirement for success. In the context of translational medicine, collaboration between medicine with bioengineering, systems engineering, and material science is definitely the first inevitable requirement for survival and progressive development in the next century.
Keywords: Neuroimmunology, neuro-engineering, immuno-engineering, neuro-immune homeostasis

1. INTRODUCTION

Restoring and enhancing lost structures and their optimal function but also traveling into the somewhat unknowns of the body with "brain-inspired technics" needs a synergy between living and artificial bio-mimetic systems. Bio-engineering is the discipline resulting from the merge of biology and electronics, and it effectively impacts both individuals' and nations well-being and welfare. A wide variety of bio-materials are used in the central nervous system (CNS) including drug or gene carriers, scaffolds, chips, neural electrodes, and mini labs in site, but also living robots and intelligent neuro-prostheses. These technologies need to be as "near-physiologic" as possible, energy efficient to be handy, and accepted and tolerated by the defence systems of our organism. Additionally, diagnostic and therapeutic tools, and "lab-

on-chip" methods for research open another vast field to investigate the interesting interactions with or within biology.

Bio-electronics is interested in a range of topics at the interface of biology and electronics. Electronic technics help to analyze biological materials on the cellular and subcellular level. This combination has a wide range of application area in biology, medicine, and even security. Physically interfacing electronic devices with biological systems is also a focus area of bio-electronics (e.g., brain-machine, cell-electrode, or protein-electrode). Assistive technologies for individuals with brain and nervous system disease or injury such as paralysis, blindness and deafness, and new technologies for protein structure-function measurements are also among these areas (Walker et al., 2009).

In addition to biomaterials and bioelectronics, there is another new concept called "bio-hybrid". This system is "formed by at least one natural and one artificial entity that establish close physical interactions at the molecular, cellular, or systems level, eventually leading to information flow and processing in one or both directions" (Vassanelli and Mahmud, 2016).

Whether synthetic or hybrid, such biomechanical devices need to be accepted both by the immune system and by the community, thru overcoming biological, ethical, and social concerns as "foreign". This is only possible with a successful communication within social or biological systems. In this context, it is important to understand the bi-directional cross-talk between the immune system and the CNS to improve the success of neuro-immuno-engineering.

"The overarching technical drivers pushing bioelectronics are the constant advances in semi-conductor technology and in surface chemistry related to the interface of biology and man-made devices" (Walker et al., 2009). Both efforts for understanding biological systems and processes at the macro- to nano-scale, and the huge challenge of our century's cross-disciplinary research involving electrical engineering, medicine, biology, chemistry, physics and material science are growing rapidly. In contrast to decades of reductionist biology, today, "systems biology", which "embodies a new perspective from which to view biological systems and knowledge culled from its endeavours leading to advances in medicine and security". This new approach in biomedical research aims to perceive the larger picture by putting all pieces together from the level of organism, tissue, cell, and subcellular organelle to molecule (Walker et al., 2009).

2. EXCLUSIVE IMMUNITY OF THE NERVOUS SYSTEM

Sensing and recognition of endangerment, alarming other homeostatic and organ systems for coping with the particular threat, and information storage and retrieval capacity are indispensable for life. Two major unique systems sharing this privilege are the nervous and immune systems. The nervous system and the brain in particular have been considered as "immune privileged" since 1940s. Privilege of immunity is a concept that involves highly controlled maintenance of adaptive immunity and inflammation. However, existence of lymph drainage in the CNS, passage of T and B lymphocytes through blood brain barrier (BBB) and the antigen processing capacity of microglia showed that it actually is not. And today, the bidirectional crosstalk between these systems is a key tool to explain some homeostatic but also pathological conditions (Louveau et al., 2015).

Fundamentals of the Immune System

The immune system defends our body against foreign invaders such as bacteria, viruses, fungi, parasites, and even allergens. It may recognize the non-self, such as an infectious agent or a damaged cell, by pattern recognition receptors. After assuming it as dangerous, immune system starts to fight this agent recruiting its tools and mechanisms. There are two main components of the immune system called innate and adaptive systems, and they both use humoral and cell mediated immunity to perform their function. Humoral immunity recruits antibodies, cytokines and other soluble mediators, while cellular immunity use many different types of cells as its warriors.

The first response of the immune system to non-self is established by the innate immunity. Main actors of innate immunity are neutrophils, mast cells, macrophages, natural killer (NK) cells, basophils and eosinophils. When the non-self is not sufficiently inactivated by the innate system, the adaptive immune system starts to fight using its tailor-made warriors called lymphocytes. T helper lymphocytes are divided mainly into two subgroups called pro-inflammatory Th1 and anti-inflammatory Th2. Another group of lymphocytes, named cytotoxic T cells, play role in cellular killing mechanisms, while helper T cells produce pro- or anti-inflammatory cytokines depending on their profile. The main goal of B lymphocyte is to produce antibodies, which are the main tools of humoral immune system. Dendritic cells are professional antigen presenting cells (APC), aiming the T lymphocytes. With the help of the costimulatory molecules expressed as secondary signals by the T cells, an adaptive immune response moves towards the target. One of the most unique characteristics of the immune system is memory. So once faced, it may recognize the danger and when exposed again, it may retrieve the necessary information more rapidly. Immune system should react to the pathogens or cancer cells properly. All these responses should be in control to maintain an immune homeostasis. When this control breaks down, either an excessive immune response to the pathogens or a regular response to self may cause autoimmune disorders. The list and information about main cells of innate and adaptive immunity are given in Table 1.

Glial cells: Friends or Foes?

The immune activity in the brain has its own rules in addition to the peripheral ones, and these rules are brought to life with both cellular and humoral actors of immunity. In addition to peripheral cells, which monitor the body regularly to detect and destroy infected or transformed cells, a second group called resident immune cells are mainly responsible for the homeostatic processes in CNS (David et al., 2015).

Glial cells are non-neuronal cells in central and peripheral nervous systems (Figure 1). Since they do not produce electrical impulses, for many years glial cells had unfortunately been identified as just "glue cells" owing to their sole and passive task of so-called physical support to neurons. Later however, there had been tremendous amount of contrary data to change this understanding, especially following the histological identification of Einstein's post-mortem brain. According to Diamond's studies performed on the thick slices from a single region of the genius' brain, glial cell counts were much higher compared to those of his regular and healthy age-matched controls (Diamond et al., 1985). In addition to providing mechanical and metabolic support, and protection for neurons, glial cells also maintain messenger homeostasis and endurance of immune activity via soluble mediators such as cytokines and chemokines in the brain (Ramesh et al., 2013). Glial cells perform a vital role in establishing and maintaining the function of the nervous system. Brain's exclusively own and particularly nocturnal glial cleansing machinery called the "glymphatic system" plays a major role in draining the environmental metabolites and possible toxins during sleep, also functioning as the determinant of the fate of neurons via apoptosis or else following injury or neuropathology (Jessen et al., 2015).

There are mainly four different types of glial cells called microglia, astrocytes, oligodendrocytes and ependymal cells (Figure 1). Astrocytes provide protective and metabolic support for neurons with some of the factors called as gliotransmitters while "microglia are involved in synaptic pruning, canvassing extracellular space and phagocytosing apoptotic cells" (Sochocka et al., 2017). Other group of the glial cells called oligodendrocytes also support neurons metabolically and they provide a source of myelin, which surrounds nerve cell axons to insulate them, and increase the rate at which electrical impulses are passed along the axon (Bean et al., 2007). Loss of the trophic support of the glial cells may cause excitotoxicity, weakening of synaptic plasticity, inflammation, and loss of myelination. All these negative effects impair neuronal activity, ultimately affecting behavior (Elsayed and Magistretti, 2015).

Under homeostatic conditions, the brain hosts several heterogeneous populations of myeloid cells (Prinz and Priller, 2014), which may be classified as microglia, meningeal macrophage, choroid plexus macrophage and perivascular space macrophage. Microglia are responsible for both mediating healthy

function and initiating inflammatory cascades. "While normal inflammation is a tissue healing response; sustained or situationally inappropriate inflammation can exacerbate or directly facilitate the death of adjacent neural and glial cells" (Neher et al., 2012; Brown et al., 2015; Tsui et al., 2019). In the case of injury, microglia stimulate astrocytes to generate a glial scar by differentiating, migrating, proliferating, and secreting fibrous sugar-based matrices. This partitions the injury and poses a physical and chemical barrier preventing axonal regeneration. "The environment within the scar is often dominated by reactive microglia and astrocytes that create cytotoxic conditions, which in turn would signal the death of neurons, first causing the loss of proximal biological circuitry, and later resulting in locomotor and cognitive deficits" (Gaudet and Fonken, 2018; Tsui et al., 2019). Therapeutic devices implanted in the CNS need attenuated microglial activity to improve the lifetime. Biomaterial design and engineering needs immune modulatory approaches to improve device compatibility.

3. NEUROIMMUNOLOGY

Neuroimmunology is a broad area playing a major role in achieving a healthy life. Aberrant synaptic pruning during development, obscure modulation of the brain-blood barrier (BBB) for immune cell recruitment, axonal degeneration and demyelination, cellular repair and regeneration, and immune mediated aggregate removal, especially in the late phase of life are several of the conditions where a balanced neuro-inflammation is absolutely necessary (Kierdorf and Prinz, 2017). A daring approach briefly defined as *psycho-neuro-endocrino-immunology* is interested in these mechanisms and their complicated interactions, which can be divided into several areas of research, and may be depicted as the studies of the following avenues (Kipnis and Filiano, 2017):
a**)** Bidirectional information trafficking between immune and nervous systems under physiological and pathological conditions and their impact on neural activity
b) The role of microglia in fine-tuning of developing neuronal circuits as well as in the maintenance of neuronal synapses.
c) "'Protective immunity', addressing beneficial immune infiltrates into the CNS following injury and in neurodegenerative diseases"
d) The mechanisms underlying the gut–immune–brain axis (Kipnis and Filiano, 2017).
Neural influences on the immune system are effective via neurotransmitters and neurotrophic growth factors, including NGF and BDNF. There are also hormonal influences acting via epinephrine, norepinephrine, and glucocorticoids (ThyagaRajan and Priyanka, 2012). Oxytocin, a remarkable hormone produced by neurohypophysis, and melatonin, another important hormone produced by epiphysis have very significant regulatory effects on the immune system (Li et al., 2017, Carrillo-Vico et al., 2013). On the other hand; understanding the modulation of nerve cell function by immune and inflammatory mediators such as cytokines, and reactive oxygen and nitrogen species are important mechanisms to fill up the gaps in the neuroimmunologic network. Other physical similarities common to the nervous and immune systems in terms of communication can be stated as synapses and ion channels, both of which are also considered remarkable in understanding the complicated connections, relations, and cross-talks (Hu et al., 2015).

4. NEUROINFLAMMATION

In a variety of neurological diseases including cerebrovascular disease (e.g. stroke), neurodegeneration (e.g. Alzheimer's disease), demyelinating diseases (e.g. Multiple Sclerosis) and malign neoplasms, neuroinflammation is an important factor playing role in pathophysiology. Different cell types and molecular mediators of the immune system participating in homeostasis, immune surveillance, regeneration, and repair at controlled situation, may lead to damage of brain tissue under pathological conditions (Figure 2). Activation of microglia, accompanied mostly by BBB breakdown, cytokine and

chemokine release and blood-borne leukocyte infiltration is one of the hallmarks of neuroinflammation (Pulli and Chen, 2014). Myeloid cells may cause to damage to myelin sheath and neurons through oxidative stress, phagocytosis and protein damage, while lymphocytes may stimulate antibody-dependent cytotoxicity (Pulli and Chen, 2014).

"Neuroinflammation is a highly relevant diagnostic and therapeutic target, but several characteristics of the brain such as BBB and cranial bones, which complicate the access to the brain, make both goals more difficult than at other sites in the body" (Pulli and Chen, 2014). Additionally, the limited regeneration capacity of the brain makes secondary and tertiary prevention more difficult and early diagnosis is of utmost importance (Pulli and Chen, 2014). Non-invasive molecular imaging of key actors in neuroinflammation may be useful tools to solve this problem. Neuroinflammation can be identified even in molecular levels by using magnetic resonance imaging (MRI), positron emission tomography (PET), single photon emission computed tomography (SPECT), and optical imaging. Visualizing the adhesion molecules such as vascular adhesion molecule-1 (VCAM-1), intercellular adhesion molecule (ICAM)-1, integrin and E- and P-selectin, show endothelial cell activation, while oxidative stress, granule release and phagocytosis are related with function of the leukocytes (Pulli and Chen, 2014).

The most important consequences caused by inflammation are demyelination and neuronal death, which both may be visualized via cellular/molecular imaging technics. 11C-flumazenil is a helpful example to show the different effects of the same molecule in different conditions: In MS, at early stage, 11C-flumazenil PET is of prognostic value; neuronal loss correlates significantly with disease progression and irreversible disability. The central benzodiazepine receptor expressing neurons can be targeted with 11C-flumazenil enhanced PET and are accepted as a good marker for neuron integrity in stroke (Sette et al., 1993, Heiss et al., 1997; Pulli and Chen, 2014). Also, in Alzheimer's disease, reduction of 11C-flumazenil binding corresponded precisely with areas of neuronal loss (Pascual et al., 2012; Pulli and Chen, 2014). Another example, "annexin-V, is a protein binding with high affinity to apoptotic cells expressing phosphatidylserine (PS) on their cell surface. With 99mTc labeled annexin-V, apoptosis successfully detected on SPECT" (Koopman et al., 1994; Pulli and Chen, 2014).

5. NEURO- AND IMMUNO-ENGINEERING

Neuro-engineering is one of biochemical engineering interdisciplinary areas that uses engineering techniques to understand, repair, replace or enhance neural systems. With the contribution of neuroscience, molecular biology, device development, computation, and mathematics, it has become one of the most exciting novel ventures in science and technology today. This concept brings insights from neuroscience and cognitive science with rapidly changing state-of-the-art technologies to create significant innovations inspired by or directed to the brain. Technologies for imaging, sensing, or affecting real-time brain activity and behavior, computing paradigms, augmented and adaptive systems, and brain-computer interfaces are all accounted in tools used for neuro-engineering (Figure 3).

Neuro-engineering can develop devices and sophisticated computing to assist those with neural disorders. Since, nearly one billion people worldwide are affected by traumatic or neurodegenerative pathologies, it is one of the most important tools of neuro-restoration and neuro-rehabilitation approaches (Prochazka 2017). While revealing how computations are done by natural neural systems, neuro-engineering inspire new algorithms, mathematics, technologies, and robotics between engineering and living systems. Diagnostic devices, such as functional MRI examining the inner workings of the nervous system, high performance sensory devices helping to restore the missing neural function, smart prostheses competing to replace missing limbs and modulatory devices to correct nervous system dysfunction are all examples for the emerging field of "therapeutic neuro-engineering". There are also ultra high resolution and real time investigation devices observing, sensing, and monitoring. Micro-electrode array dishes or 2-photon fluorescence microscopes showing the living network in action to explore the "*terra incognita*" of neuroscience are some of the novel inventions.

Immuno-engineering applies engineering principles to the discovery and design of the immune system. Therapies, including engineering-based approaches, should harness the immune system and benefit from engineering optimization (Kim et al., 2019). Combining the know-how from both fields could lead to boosting of potency of vaccines, regulating tolerance and biocompatibility of medical implants, and enhancing tissue regeneration. Immuno-engineering may also help to improve the functionality and increase the lifetime of neurological devices by reducing the rejection caused by inflammation. Since that astrocytes and microglia have been identified as essential in many neuro-regenerative processes, they are assumed to be the foregoing keys in future design of drug delivery systems, implants, and scaffolds (Tsui et al., 2018), as briefly mentioned below:

Nanoparticles: Nano-neuroscience

"A nanoparticle is a microscopic particle with at least one dimension less than 100 nm. Nanoparticle research is currently an area of intense scientific research, due to a wide variety of potential applications in biomedical, optical, and electronic fields" (Shahid et al., 2009). Design of a nanoparticle should consider the target cell, mechanism of uptake and potential uptake by phagocytic cells in the brain such as microglia (Tsui et al., 2018). An ideal nanoparticle should compose of an inert or functional vehicle. It should also traverse the BBB and selectively interact with the target. Since microglia are sensitive to nanoparticles, they also need to be able to avoid phagocytosis and clearance by microglia (Xue et al., 2012). Nanoparticles have been extensively used in neuroscience to investigate their potential applications for the diagnosis, treatment and monitoring of several neurological diseases (Berger 2019).

Nano-neuroscience research aims to "regenerate and protect the CNS by developing nano-engineered substrates, for example, to help guide axon growth after damage or degeneration. Other therapeutic strategies for CNS disorders require getting a device or drug to a specific site in the CNS" (Vidu et al., 2015). Nanomaterials may be used as vessels to deliver drugs. Nanoparticles are promising tools "to provide chips that will interface with the brain and allowing to detect and correcting online any potential miss-function of the brain's microcircuits bridging the perception with the executive control of behavior" (Vidu et al., 2015).

Hydrogels

Hydrogels are three-dimensional networks which are formed from hydrophilic polymers. They are comprised of up to 90% of water. Hydrogels could provide mechanical support and are important tools for neuroregenertion. "Hyaluronic acid, collagen type I, alginate, chitosan, methylcellulose, Matrigel, fibrin, gellan gum, self-assembling peptides and proteins, poly (ethylene glycol), methacrylates, and methacrylamides are all hydrogels which may be used in brain injury therapy or give promising results in brain injury research studies" (Kornev et al., 2018).

Hydrogels may help the axonal regeneration after traumatic brain injury. When the newly formed cavity is filled with hydrogels, they may promote axonal regeneration while providing a suitable substrate for axonal growth (Carballo and Velasco, 2015). Koss et al. introduced "basal lamina mixture into the hydrogel formula thereby demonstrating the feasibility of augmenting the resulting scaffold with bioactive substrates, and improving cell integration into the scaffold" (Koss et al, 2017). Culturing microglia in hydrogels is also feasible because of the advantageous in offering systematic and high-throughput modelling of the CNS in vitro and they can be used to model various injuries (Koss et al., 2016). In summary, hydrogels promote axonal regeneration after injury and reduce glial scarring or attenuate neuroinflammation (Koss et al., 2016), but they also may help drug release, bridging between the lesioned tissue and others and presenting models for research (George et al., 2019).

Microelectrode Implants

A neural implant, or an electrode, is a device placed inside the body and interacts with neurons via electrical impulses in particular patterns. The study on neural implants started early in 1970's (Calvello 2013). People may regain their abilities that have been lost via injuries or degenerative disorders with the help of neural devices. An electrical circuitry which is implanted as a neural device may either stimulate the nervous system or record the electrical activity of the nerve cell. "This device enhances senses, physical movement, and memory. To restore cognitive function, a neural implant must gather data from one area of the brain, process this information correctly, and then deliver the resulting signal to another brain region, bypassing any damaged tissue. In the past few decades, humans have developed advanced technologies that produced major improvements in the quality of life, their survivability, or their performance in a job. However, scientists predict that within the next twenty years neural interfaces will be designed to not only increase the dynamic range of senses, but will also enhance memory and enable cyberthink, which is invisible communication with others" (Ach and Lüttenberg, 2008).

Treating brain disorders using implants may use tools including electrode arrays, neuro-modulation chips and control module microprocessors (Figure 4). "A common and ongoing limitation of neural prosthetics is their inconsistent recording quality and long-term stability due to neuro-inflammation which is altering electrical and chemical activity around implanted probes" (Tsui et al., 2019). Following an implantable device, microglia become activated and call astrocytes to recruit at the site of implant. This reaction is called astrogliosis resulting with a scar formation (Tsui et al. 2019). Activation of microglia and astrocytes stimulate the production of prooinflammatory cytokines such as IL-1, IL-6 and TNF, which inhibit the regeneration process and support excessive cell death. The encapsulated layer around the implant is also produced by the activated microglia and astrocytes and limits regeneration (Tsui et al., 2019). Implantation of neural probes leads to overproduction of reactive oxygen species which stimulate the foreign body response, and facilitate neuronal death, corrosion and delamination of the microelectrode surface (Ereifej et al., 2018).

"An *in vitro* model of glial scarring around neuroelectrodes chronically implanted in CNS" (Polikov et al., 2006), was developed either by using mechanical scrape or microwire as foreign body placement in a primary cell-based system. Polikov et al. evaluated the roles of microglia and astrocytes in a cell culture implant model 6h and 10 days. Scrape wound was used for acute and microwire insertion was used for chronic implantation. Although microglia invaded the scraped wound at early timepoints, activated astrocytes came to the lesion area first after 7 days. A glial scar developed at day 10 of the microwire insertion with a microglial core in the middle and surrounding astrocytes around. During the implantation process neurons were electrically active but did not repopulate around the lesion (Polikov et al., 2006). Primary glial cell responses observed *in vivo* were correlated well with cell culture. The surface material coating the electrode and implant duration does also matter by distribution and quantification of especially microglia on the surface of retrieved microelectrodes (Leung et al., 2008). According to the results of these studies, understanding the role of glial cells in implantable device rejection would help gain several improvements in material design (Polikov et al., 2006; Leung et al., 2008).

The major failure modes of microelectrode arrays are based on several problems. First, the place of replacement is important, the top of the electrode should become encased in a thin layer of the arachnoid to get stabilized (Prochazka 2017). Second, biological failure such as bleeding, hardware infection, meningitis, gliosis, meningeal encapsulation and extrusion are important to disrupt the tolerance of the immune system to the implanted device. Material and mechanical failures also regulate the glial cell coverage and may be an inducer of undesirable inflammatory activity. Mechanically adaptive electrodes may have regulatory effects on implant induced inflammation. Material stiffness, micromotion and tethering are all factors which must be considered in electrode design (Prochazka 2017). Devices which are initially rigid but become compliant after implantation show reduced neuroinflammatory response in long term implantation in addition to early reduced immune response to mechanically compliant intracortical implants (Nguyen et al.,

2014). Large diameter and tethered implants strongly influence tissue reactions in the CNS (Thelin et al., 2011).

There are several technical modifications of classical microelectrodes in current research and treatment. Cell grafting onto electrode implants can secrete neuroprotective factors into the surrounding area and potentially inhibit harmful cytotoxic and biochemical mechanisms for implantation (Gaillard et al., 2007). Compared to single electrodes, the use of microelectrode arrays can also produce relevant host response to the insertion (Nolta et al., 2015); but all these modifications need further *in vitro* and especially, *in vivo* investigation before claiming to be useful in clinics.

Other Materials and Laboratory Technics in Neuroimmunoengineering

Bioengineering research may be basically analyzed in four groups which all should be harnessed and coordinated to take part in the challenge. Drivers are important for early detection and treatment of the disease. They also may include artificial sensory organs including eyes, nose, etc. Measurements and analyses are sensing the states of individual cells. Devices such as μ-energy sources and nano-delivery devices are important in bio-devices, bio-system monitoring and management. With the contribution of technologies such as wireless network and two-way interfaces with bio-tissues, intelligent micro-bioelectronics systems are getting stronger and resistant (Walker et al., 2009).

Drug delivery systems for neural prosthetic-induced inflammation involve the use of conducting polymers and they are preferred in many degenerative disorders as regulatory tools of the immune system (Green and Abidian, 2015). Disc-shaped polymer patches and cellular backpacks may also be used for drug delivery. Gold is another effective substrate for drug delivery coatings and also biosensor construction and nanoelectrical device coatings (Tsui et al., 2019). All these biomaterials and applications have notable advantages, but also challenges that will determine the future directions in clinics.

In the last decades bioengineering technics have opened a brilliant area for researchers in many areas including bio-medicine. *In vitro* and *in vivo* research tools have detailed many cellular and molecular pathways which give promising translational ideas for the clinics. Genomic, proteomic and cellular technics and imaging tools in every step of research are successful offsprings of neuroimmunoengineering. In addition, miniaturized lab-on-a-chip devices which integrate and automate many laboratory technics on a single chip provide cost efficiency, low volume reagents, high parallelization, ergonomy, high diagnostic speed, high sensitivity, and high expandability for researchers (Yılmaz and Yılmaz, 2017).

6. CONCLUSION

The application of engineering, especially electronics technology to biology and medicine is not a new concept. The entire medical imaging industry, cardiac pacemakers and cochlear implants had been successful examples of bioengineering for decades. In neuroscience, understanding the molecular basis of nerve and muscle function with the help of high-impedance amplifiers was another challenge in the late 1940's. These studies combining the quantitative biology and practical clinical neuroscience led directly to many Nobel Prizes in history. As a next step, stakeholders from government, academic and industry should build intelligent collaborations and interdisciplinary working groups to overcome the new challenges of the century. Progress in these sectors requires innovation in areas including measurement and characterization, fabrication, and power sources. In addition, development of nanoscale bioelectronics will be important in genomics and proteomics studies and open a new era for molecular-based personalized medicine.

Neurostimulation procedures, devices and imaging technics in global market is growing with a sharp acceleration in our century. "Government, industry, and academic leaders from different sectors and disciplines must be willing to commit to joint efforts where interdisciplinary contributions are necessary for success" (Walker et al., 2009). Moreover, this merge of systems biology, neuroscience, medicine,

bioengineering, and neuro-rehabilitation may lead the way to a need for contribution of other interdisciplinary areas called neuro-law and neuro-ethics.

Collectively, innovative material science is anticipated for non-corrosive, durable, tolerable/unrejectable products, with higher specifity, higher sensitivity, high resolution and high-speed features. Optimized semiconductors and chips, miniaturization to the highest possible measures, and also highly compliable computer software for precise data processing and storage are all strongly needed. Finally, integrating modern engineering technics with systems biology, material science and medicine will definitely result in "equally profound quantum leaps" (Walker et al., 2009).

Brain is wider than the sky and deeper than the sea (E. Dickinson), but those who have been privileged to get to know the brain and the nervous system should also have the mission to act or interact (A. Einstein).

7. REFERENCES

1. Ach, J.S., Lüttenberg, B. Ethical Aspects of ICT Implants in the Human Body. Opinion of the European Group on Ethics in Science and New Technologies to the European Commision. (2008). In: Nanobiotechnology, Nanomedicine and Human Enhancement. Eds: Ach, J.S., Lüttenberg, B. LIT Verlag Münster. 157-186.

2. Bean, B.P. (2007). The action potential in mammalian central neurons. Nature Reviews Neuroscience. 8, 451-465.

3. Berger, M. (2017). Nanotechnology for neuroscience. https://www.nanowerk.com/spotlight/spotid=48348.php

4. Brown, G.C., Vilalta, A. (2015). How microglia kills neurons. Brain Research. 1628, 288-297.

5. Calvello T. Human Enhancement: Brain Chips (Neural Implants). (2013) https://humanenhancementusingbrainchips.weebly.com/neural-implants.html

6. Carballo-Molina, O.A., Velasco, I. (2015). Hydrogels as scaffolds and delivery systems to enhance axonal regeneration after injuries. Frontiers in Cellular Neuroscience. 9, 13.

7. Carrillo-Vico, A., Lardone, P.J., Alvarez-Sanchez, N., Rodriguez-Rodriguez, A., Guerrero, J.M. (2013). Melatonin: buffering the immune system. International Journal of Molecular Sciences.14 (4), 8638-8683. **8.** Lee,K. Y., &

Mooney, D. J. (2012). Alginate: propertis and biomedical applications. Progress in polyme science, 37(1), 106–126. https://oi.org/10.1016/j.progpolymsci.2011.06.003

8. David, S., Kroner, A., Greenhalgh, A.D., Zarruk, J.G., Lopez-Vales, R.J. (2018). Myeloid cell responses after spinal cord injury. Neuroimmunology. 321, 97-108.

9. Diamond, M.C., Scheibel, A.B., Murphy, G.M. Jr., Harvey, T. (2017). On the Brain of a Scientist: Albert Einstein. Experimental Neurology. 88, 198-204.

10. Elsayed, M., Magistretti, P.J. (2015). A New Outlook on Mental Illnesses: Glial Involvement Beyond the Glue. Frontiers in Cellular Neuroscience. 9, 468.

11. Ereifej, E.S., Rial, G.M., Hermann, J.K., Smith, C.S., Meade, S.M., Rayyan, J.M., Chen. (2018). Implantation of Neural Probes in the Brain Elicits Oxidative Stress. Frontiers in Bioengineering and Biotechnology. 6:9.

12. Gaillard A., Prestoz, L., Dumartin, B., Cantereau, M., Morel, F., Roger, M., Jaber, M. (2017). Reestablishment of damaged adult motor pathways by grafted embiyonic cortical neurons. Nature Neuroscience, 10 (10), 1294-1299.

13. Gaudet, A.D., Fonken, L.K. (2018). Glial Cells Shape Pathology and Repair After Spinal Cord Injury. Neurotherapeutics. 15 (3), 554-577.

14. George, J., Hsu, C., Nguyen, L.T.B., Ye, H., Cui, Z. (2019). Neural tissue engineering with structured hydrogels in CNS models and therapies. Biotechnology Advances. 03, 009.

15. Green, R., Abidian, M.R. (2015). Conducting polymers for neural prosthetic and neural interface applications. Advanced Materials. 27 (46), 7620-7637.

16. Heiss, W.D., Graf, R., Fujita, T., Ohta, K., Bauer, B., Löttgen, J., Wienhard, K. (1997). Early detection of irreversibly damaged ischemic tissue by flumazenil positron emission tomography in cats. Stroke. 28, 2045–2051.

17. Hu, X, Leak, R.K., Shi, Y., Suenaga, J., Gao, Y., Zheng, P., Chen, J. (2015). Microglial and macrophage polarization – new prospects for brain repair. Nature Reviews Neurology. 11, 56.

18. Jessen, K.R., Mirsky, R., Lloyd, A.C. (2015). Schwann cells: development and role in nerve repair. Cold Spring Harbor Perspectives in Biology. 7.

19. Kim, J.K., Shin, Y.J., Ha, L.J., Kim, D.H., Kim, D.H. (2019). Unraveling the Mechanobiology of the Immune System. Advanced Healthcare Materials. 8 (4), e1801332.

20. Kipnis, J., Filiano, A.J. (2017). The central nervous system: privileged by immune connections. Nature Reviews Immunology. 18, 83-84.

21. Koopman, G., Reutelingsperger, C.P., Kuijten, G.A., Keehnen, R.M., Pals, S.T., van Oers, M.H.J. (1994). Annexin V for flow cytometric detection of phosphatidylserine expression on B cells undergoing apoptosis. Blood. 84, 1415-1420.

22. Kornev, V.A., Grebenik, E.A., Solovieva, A.B., Dmitriev, R.I., Timashev, T.S. (2018). Hydrogel-assisted neuroregeneration approaches towards brain injury therapy: A state-of-the-art review.

Computational and Structural Biotechnology Journal. 16, 488-502.

23. Koss, K.M., Unsworth, L.D. (2016). Neural tissue engineering: bioresponsive nanoscaffolds using engineered self-assembling peptides. Acta Biomaterialia. 44, 2-15.

24. Koss, K.M., Churchward, M.A., Jeffery, A.F., Mushahwar, V.K., Elias, A.L., Todd, K.G. (2017). Improved 3D hydrogel cultures of primary glial cells for in vitro modelling of neuroinflammation. Journal of Visualized Experiments. 1-11.

25. Leung, B.K., Biran, R., Underwood, C.J., Tresco, P.A. (2008). Characterization of microglial attachment and cytokine release on biomaterials of differing surface chemistry. Biomaterials. 29, 3289-3297.

26. Li, T., Wang, P., Wang, S.C., Wang, Y.F. (2017). Approaches mediating Oxytocin Regulation of the Immune System. Frontiers in Immunology. 7, 693.

27. Louveau, A., Harris, T.H., Kipnis, J. (2015). Revisiting the mechanisms of CNS immune privilege. Trends in Immunology. 36 (10), 569-577.

28. Neher, J.J., Neniskyte, U., Brown, G.C. (2012). Primary phagocytosis of neurons by inflamed microglia: potential roles in neurodegeneration. Frontiers in Pharmacology. 3.

29. Nguyen, J.K., Park, D.J., Skousen, J.L., Hess-Dunning, A.E., Tyler, D.J., Rowan, S.J., Weder, C., Cpadona, J.R. (2014). Mechanically-compliant intrasortical implants reduce the neuroinflammatory response. Journal of Neural Engineering. 11 (5).

30. Nolta, N.F., Christensen, M.B., Crane, P.D., Skousen, J.L., Tresco, P.A. (2015). BBB leakage, astrogliosis, and tissue loss correlate with silicon microelectrode array recording performance. Biomaterials. 53, 753-762.

31. Pascual, B., Prieto, E., Arbizu, J., Marti-Climent, J.M., Peñuelas, I., Quincoces, G., Zarauza,

R., Pappata, S., Masdeu, J.C. (2012). Decreased carbon-11-flumazenil binding in early Alzheimer's disease. Brain. 135, 2817-2825.

32. Polikov, V.S., Block, M.L., Fellous, J.M., Hong, J.S., Reichert, W.M. (2006). In vitro model of glial scarring around neuroelectrodes chronically implanted in the CNS. Biomaterials. 27, 5368-5376.

33. Prinz, M., Priller, J. (2014). Microglia and brain macrophages in the molecular age: from origin to neuropsychiatric disease. Nature Reviews Neuroscience. 15 (5), 300-312.

34. Prochazka A. (2017). Biology of Neuroengineering Interfaces-Neurophysiology and neural engineering: a review. Journal of Neurophysiology. 118 (2), 1292-1309.

35. Pulli, B., Chen, J.W. (2014). Imaging Neuroinflammation-from Bench to Bedside. Journal of Clinical and Cellular Immunology. 5, 226.

36. Ramesh, G., MacLEan, A.G., Phillipp, M.T. (2013). Cytokines and chemokines at the crosroads of neuroinflammation, neurodegeneration, and neuropathic pain. Mediators Inflammation. 480739.

37. Sette, G., Baron, J.C., Young, A.R., Miyazawa, H., Tillet, I., Barre, L., Travere, J.M., Derlon, J.M., MacKenzie, E.T. (1993). In vivo mapping of brain benzodiazepine receptor changes by positron emission tomography after focal ischemia in the anesthetized baboon. Stroke. 24, 2046-2057.

38. Shahid, M., Khan, H.M., Mustafa, S., Shujaatullah, F. (2009). Nanotechnology: Implications of nanoparticles in medical science. In: Biotechnology Emerging Trends. Eds: Sayyed RZ, Patil AS. Scientific Publishers. pp. 529-550.

39. Sochocka, M., Diniz, B.S., Leszek, J. (2017). Inflammatory response in the CNS: Friend or Foe? Molecular Neurobiology. 54 (10), 8071-8089.
40. Thelin, J., Jörntell, H., Psouni, E., Garwicz, M., Schouenborg, J., Danielsen, N., Linsmeier, C.E. (2011). Implant size and fixation mode strongly influence tissue reactions in the CNS. PLoS One. 6.

41. ThyagaRajan, S., Priyanka, H.P. (2012). Bidirectional communication between the neuroendocrine system and the immune system: relevance to health and diseases. Annals of Neurosciences. 19 (1), 40-46.

42. Tsui, C., Koss, K., Churchward, M.A., Todd, K.G. (2019). Biomaterials and glia: Progress on designs to modulate neuroinflammation. Acta Biomaterialia. 83, 13-28.

43. Vassanelli, S., Mahmud, M. (2016). Trends and challenges in neuroengineering: toward "intelligent" neuroprotheses through brain-"brain inspired systems" communication. Frontiers in neuroscience. 10, 438.

44. Vidu, R., Rahman, M., Mahmoudi, M., Enaschescu, M., Poteca, D.T., Opris, I. (2015). Nanostructures: a platform for brain repair and augmentation. Frontiers in Systems Neuroscience. 8, 91.

45. Walker, G.M., Ramsey, J.M., Cavin, R.K., Herr, D.J.C., Merzbacher, C.I., Zhirnov, V. (2009). https://www.nist.gov/system/files/documents/pml/div683/bioelectronics_report.pdf

46. Xue, D., Zhao, M., Wang, Y.J., Wang, L., Yang, Y., Wang, S.W., Zhang, R., Zhao, Y., Liu, R.T. (2012). A multifunctional peptide rescues memory deficits in Alzheimer's disease transgenic mice by inhibiting Aβ42-induced cytotoxicity and increasing microglial phagocytosis. Neurobiology of Disease. 46 (3), 701-709.

47. Yılmaz B, Yılmaz F. (2017). Lab-on-a-chip technology and its application. In: Omics Technologies and Bioengineering. Eds: Brah D, Azevedo V. Elsevier. pp. 145-153.

Bioinks for Bioprinting Tissues and Organs

Review Article

Yağmur Can ⁱᴰ, **Rümeysa Karaca** ⁱᴰ, **Funda Özbek** ⁱᴰ, **Gizem Boz** ⁱᴰ, **Açelya Yılmazer** ⁱᴰ, **Pınar Yılgör Huri**[1]* ⁱᴰ

[1] Department of Biomedical Engineering, Faculty of Engineering, Ankara University, Ankara, Turkey

Author E-mails
phuri@ankara.edu.tr
*Correspondance to: Assoc. Prof. Dr. Pinar Yilgor Huri, Department of Biomedical Engineering, Faculty of Engineering, Ankara University, Ankara, Turkey
Tel: +903126000100
DOI: 10.38061/idunas.782768

Özet

Üç boyutlu (3B) baskı teknolojisinin kullanılması, doku mühendisliği ve rejeneratif tıptaki uygulamaları büyük ölçüde etkilemiştir. Özellikle, biyobaskı alanındaki son gelişmeler, canlı ve fonksiyonel doku ve organların üretimi için umut vadetmektedir. 3B biyobaskı, dokuların katman-katman üretiminde biyo-mürekkeplerin kullanılmasını içerir ve gerekli şekli sağlamak, hücre fonksiyonlarını ve canlılığını korumak gibi önemli rollere sahiptir. Biyomürekkepler, doğal veya sentetik kökenli biyomalzemelerdir ve hücrelerin yeni doku oluşturmak için çoğalmaları ve farklılaşmaları için doğal hücre dışı matris ortamını taklit ederler. Bu derlemede, 3B biyobaskı yöntemi ve biyomürekkep çeşitleri ile biyobaskı alanındaki kilometre taşı uygulamalar ayrıntılı olarak incelenmiştir.
Anahtar Sözcükler: 3B baskı, Biyomürekkep, Hidrojel, Doku Mühendisliği, Rejeneratif Tıp

Abstract

Compared to the other imaging modalities Magnetic Resonance Imaging (MRI) system has many the use of three-dimensional (3D) printing technology greatly impacted the applications in tissue engineering and regenerative medicine. Especially, recent developments in the bioprinting field holds promise for the production of viable and functional tissues and organs. 3D bioprinting process involves the use of bioinks in the layer-by-layer production of tissues and has such important roles as providing the shape and preserving the cell function and vitality. Bioinks are biomaterials, of natural or synthetic origin, and they mimic the natural extracellular matrix environment for cells to proliferate and differentiate into to form the new tissue. In this review, 3D bioprinting methods and types of bioinks are discussed in detail, with special emphasis on the milestone applications in the bioprinting field.
Keywords: 3D bioprinting, Bioink, Hydrogel, Tissue engineering, Regenerative medicine

1. INTRODUCTION

3D bioprinting is a promising technology to fabricate variety of tissues and organs in the laboratory using cells and biomaterials. Emerging as a new biofabrication method, 3D bioprinting has significant control over reproducible tissue structures. Homogeneous seeding and growth of the cells within 3D structures, which is among the difficulties encountered in tissue engineering technique, can be surmounted with the bioprinting method. Also, with this technique, various cell types can be delicately positioned to specific locations within complex 3D structures and it is possible to reach high cell densities. Bioprinting is performed with materials containing live cells. These materials, called bioinks, are biocompatible hydrogels that form a gel in accordance with some external stimuli fine-tuned according to the bioprinting technique used (such as chemical cross-linking, photo cross-linking etc.). Bioinks are designed to mimic the extracellular matrix environment structurally and mechanically and they promote the cell adhesion, proliferation and differentiation. These polymer-based matrices should be able to form a highly stable gel since this is needed to obtain high printing accuracy.

There are four different types of bioprinting techniques, and each technique has strengths and weaknesses. For instance, in extrusion printing, which is the most suitable technique in terms of vertical configuration, cell viability and printing speed are lower than other techniques. Stereolithography has the fastest printing speed among other techniques, and due to this feature, it protects cells from non-physiological conditions. The bioink to be selected for each bioprinting technique contains different requirements. Bioinks are generally developed from natural or synthetic biomaterials or from a combination of these materials. An ideal bioink should have appropriate mechanical, rheological and biological properties to perform the function of a tissue and organ. The selection of bioink is critical because its properties are essential for printability, including achievable structural resolution, shape stability and cell viability before, during and after gelling (Güngör-Özkerim, İnci, Zhang, Khademhosseini & Dökmeci, 2018; Kačarević et al., 2018). In this review, recent developments in the bioprinting technology are examined and summarized by focusing on various bioprinting techniques and bioink properties.

What is a Bioink?

3D printing, which has recently emerged as a rapid fabrication technique, is a method that gains great importance day by day. 3D printing is a technique that has many different processes and are frequently used in the production of functional tissues and organs. Bioprinting method provides the opportunity to place various cell types on the printed tissue scaffolds. Scaffolds with a suitable microarchitecture should be produced and also the effect of production on cell viability should be taken into account. Bioprinting can be performed clinically in different environments to satisfy the need of a patient with damaged tissue. The application steps of the bioprinting technique in the clinical setting are shown in Figure 1 (Güngör-Özkerim et al., 2018; Kačarević et al., 2018).
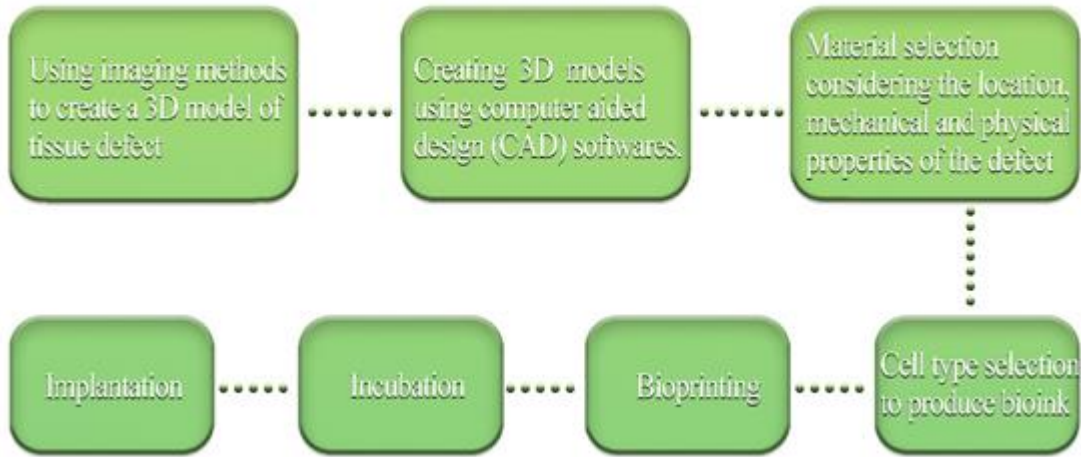
Figure 1. Stages of bioprinting in clinical applications. Digital 3D images are used by various softwares to design the appropriate scaffold. Bioprinting process is performed after selecting the appropriate material and cells for the application. The 3D culture which is obtained from incubation is evaluated for implantation by various methods.

The aim of bioprinting is to present a new method to tissue implants and to minimize the process by eliminating the problems of the patients who can have difficulties in this process. In addition, it is to prevent animal experiments used in therapeutic tests. Furthermore to the advantages and challenges of each technique, the current research status for the various tissue types of each technique is addressed. These four techniques have been observed to have various effects on cell viability, resolution, and printing accuracy. Additionally, a significant effect of material selection and concentrations on printing properties was observed (Kačarević et al., 2018). Figure 2 summarizes the process of bioink formation for bioprinting.
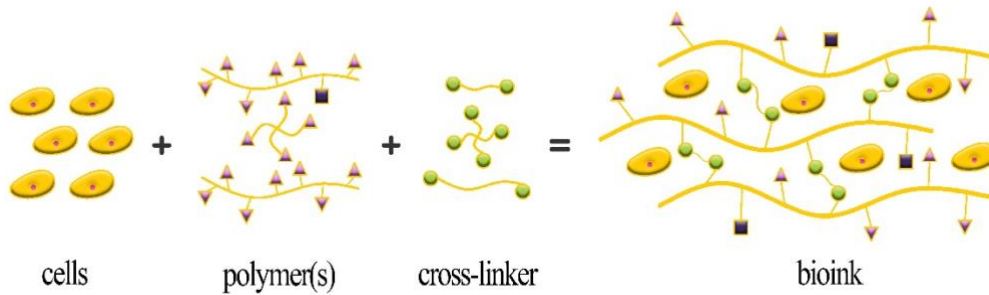
Figure 2. Bioink formation for 3D bioprinting. Bioinks are formed by the combination of cells and polymers. They are then used to print 3D tissues.

2. GENERAL FEATURES OF BIOPRINTING TECHNOLOGIES

Inkjet-Based Bioprinting

Inkjet bioprinting has two types, thermal based inkjet printing and piezoelectric elements which is the first printer used to print live cells. Some problems were encountered while developing inkjet bio-printing. The first of these problems is that the cells die due to drying on the substrate during printing. As a result of the studies, it was seen that the problem was solved by trapping the cells in a polymer structure. Thus, studies on cell-containing hydrogels have increased and new developments have been obtained. Now, the exact positioning of the cells can be achieved with inkjet bioprinting.

As seen in Figure 3, there are two types of inkjet bioprinters, one using a thermal actuator and one with a piezoelectric actuator. Thermal-based inkjet printing uses an element (heater) heated from 100°C to 300°C to nucleate a balloon. Since the balloon causes an increase in pressure in the head, it allows the droplets to be sprayed from the mouth. It does not harm the cells since it does not use low temperature and is not used for a long time.
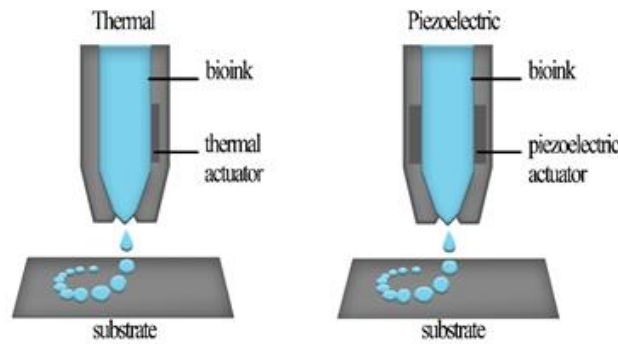

Figure 3. Schematic diagram of inkjet bioprinting.

The piezoelectric inkjet printer needs waves to extract the liquid from the mouth. These waves are acoustic waves and use piezoelectric crystals for their formation. A problem encountered when using this technique is that the viscosities of the mechanism limits the use of high-concentration and viscous bio-inks, as they reduce the acoustic/pressure waves applied and prevent the droplets from ejecting. There are some parameters to consider for the production of three-dimensional structures. The two most important parameters in inkjet printing are concentration and surface tension. While more functional structures are produced with high concentration solutions, opposite structures are formed in low concentration.

In the Table 1, some parameters of inkjet printing and their values are specified. As seen, these low cost printers have a great value in terms of cell viability. However, besides these advantages, it has some limitations in terms of cell packaging due to its inks not having high concentrations. (Hölzl et al., 2016; Kačarević et al., 2018).

Table 1. Overview of important bioink parameters for inkjet-based bioprinting.

Inkjet-based bioprinting	
Parameters	**Values**
Viscosity	<10 mPas
Cell density	Low $< 10^6$ cells ml^{-1}
Resolution	10–50 μm
Single cell control	Low
Speed	Fast
Cell viability	<85%

Laser-based bioprinting

Laser-based bioprinting is one of the nozzle-free bioprinting methods that uses a laser to push cells from a solution to the surface. The basic principle is to create a pulse on the absorbent surface using a focused laser. The laser heats some of the solution so that some of the bioink is pushed towards the surface with the help of the air pocket. Its main advantage is that it does not contain nozzles and it can use high viscosity materials. But when printing on these printers, it is necessary to pay attention to the heat because high temperature can damage the cells. Figure 4 shows the elements of laser-based bioprinting and gives information about the working principle.
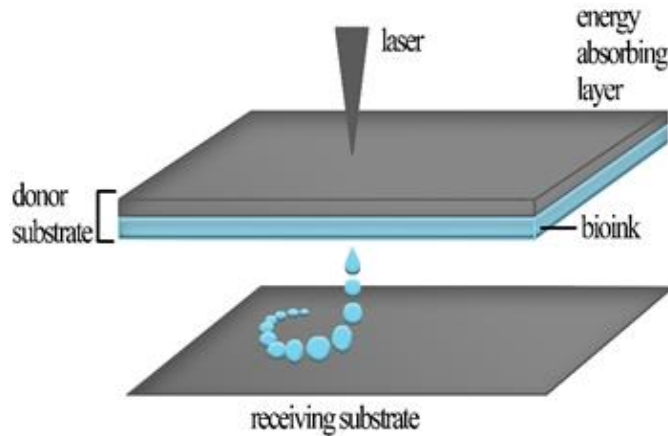
Figure 4. Schematic of laser-based bioprinting technique.

The most important advantage of laser-based bioprinting is that it is not affected by shear stress. However, there are some parameters that are specific for this technique. Viscosity and temperature are the two most important of these and are among the factors that play an important role in 3D tissue formation (Table 2) (Hölzl et al., 2016; Kačarević et al., 2018).

Table 2. Overview of important bioink parameters for laser-based bioprinting.

Laser-based bioprinting	
Parameters	**Values**
Viscosity	1-300 mPas
Cell density	Medium
Resolution	10–100 μm
Single cell control	Medium
Fabrication speed	Medium
Cell viability	>95%

Extrusion-Based Bioprinting (Fused Deposition Modeling)

In extrusion based printing, which is one of the most preferred methods for the production of 3D models, bioink is placed in disposable syringes and dispensed with a nozzle by pneumatic or mechanical pressure (Figure 5). It can distribute high viscosity bioink by providing more control with screw based accumulation. Briefly, the working principle is as follows. After the filament fed from the coil inside the system is accumulated, the print head is guided according to the tissue structure to be created with the help of a computer. The print head, which moves horizontally to create the first layer, is then moved vertically to create a new layer. The control of the head is completely personal and its speed can be adjusted according to the state of the print.
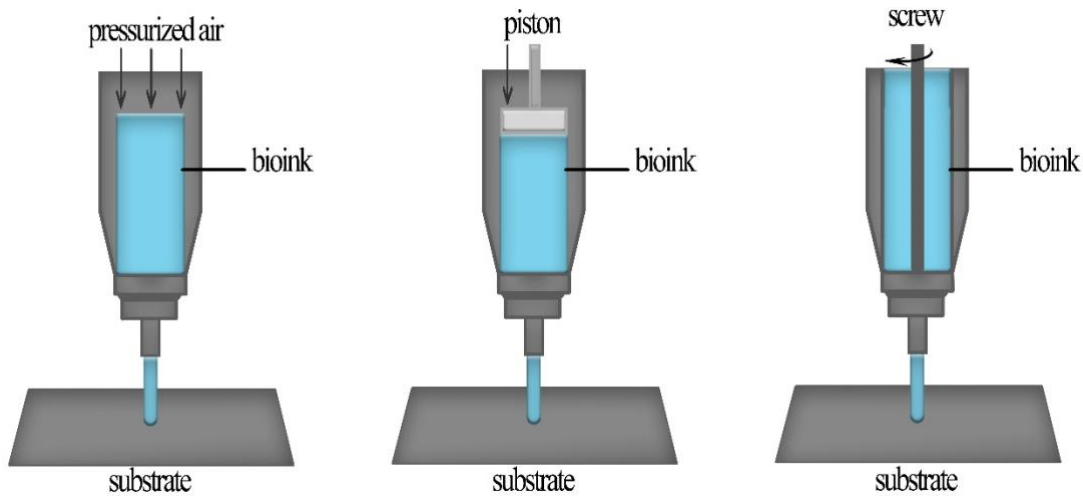
Figure 5. Working principle of extrusion-based bioprinting.

Extrusion-based printing has some disadvantages. It has lower resolution compared to other bioprinting techniques. This feature is an undesirable limitation for functional tissue formation. Also in bioprinting methods, low pressure drops are desired to prevent cell viability from being damaged and cell deaths, but this technique cannot provide them. Therefore, studies should be carried out to make sure that the hydrogel provides the necessary qualities before hydrogel printing. Hydrogels with low viscosity and additives should not be used. Extrusion-based printing is also very important in the rheological behavior of bioink. Viscosity of bioinks generally change with cutting speed. However, increased viscosity causes more cell deaths. Therefore, the concentration of the combination of bioink and biomaterial must be well adjusted. Otherwise, cell deaths cannot be prevented and the desired functional tissue cannot be obtained (Hölzl et al., 2016; Kačarević et al., 2018).

Stereolithography

Stereolithography, the oldest 3D printing technology, is based on the technique of curing the liquid photopolymer in a boat with a low power ultraviolet (UV) laser. SLA, which is highly preferred in biomodel production due to its high resolution, increases efficiency and reproduces internal structures while producing large objects. Continuous liquid interface production (CLIP), a recently developed SLA modification, simplifies SLA by increasing the production speed. In this technique, the polymer material is condensed with light. Micromirror arrays are used to control the light intensity in these areas as it is a necessity. This technique has many advantages. For example, hydrogels are not affected by the number and complexity of the layers, the printing time is the same for each layer. Thus the SLA technique can

significantly reduce the duration of the printing process. It is also a nozzle-free technique with high cell viability and resolution (Figure 6).
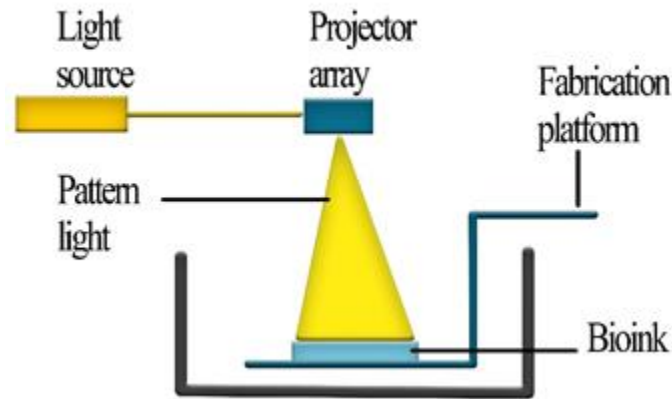

Figure 6. Schematic of stereolithography as a 3D bioprinting technique.

As a medical practice, SLA is often used for the manufacturing of anatomical models for pre-surgical planning. Although it has many advantages, its main disadvantage is the scarcity of hydrogels with SLA processing properties. Another disadvantage is that there are no compositional gradients along the horizontal planes (Melchels, Feijen & Grijpma, 2010; Chae et al., 2015).

In Table 3, the properties of various bioprinting techniques are compared.

Table 3. Comparison of existing bioprinting techniques.

	Inkjet-based	Extrusion-based	Laser-based	Stereolithography
Viability	> 85	40-80	>95	> 85
Speed	Fast	Slow	Medium	Fast
Cost	Low	Medium	High	Low
Vertical Structure	Poor	Good	Medium	Good

3. TYPES OF BIOINKS

Bioinks are important components of bioprinting and consists of living cells and biomaterials that mimics the extracellular matrix environment necessary for the attachment of cells. Bioinks are used to encapsulate desired cell types and to create tissue structures. Cell-loaded bioinks are based on hydrogel, which almost all of its content is water which is beneficial for cell viability and protection of the cells from production-dependent forces. To support cell proliferation and functions after printing, bioinks should have favorable rheological, mechanical, physical and chemical properties. These features can be listed as in the Figure 7. The features shown in the Figure 7 can significantly affect printing accuracy, cell viability, proliferation and morphology after printing.
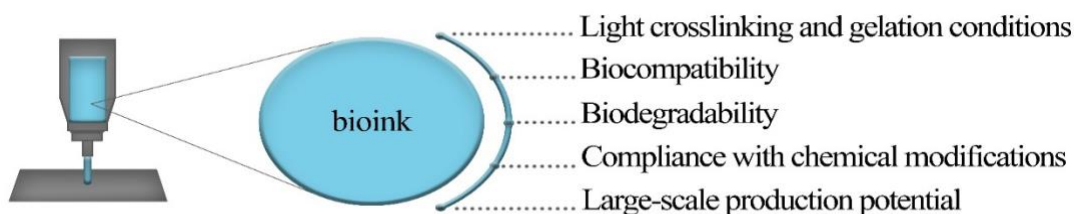
Figure 7. Bioinks should have important properties such as being biocompatible and biodegradable. They should be modifiable and cross-linkable to be able to form the 3D shape. Moreover, bionks should carry the potential to be produced in large-scales.

The bioinks are different for each bioprinter and the same bioink cannot be used in all of the bioprinter types. Bioinks are specific for every application, hence they should be suitable to modification. When selecting bioinks, it is suggested to choose the ones that can be modified in order to obtain better results according to the properties of the tissues and organs trying to be obtained. Therefore, many natural and synthetic biomaterials and mixtures of these materials have been used as bioinks.

The polymers obtained from plants and animals then used as biomaterials are called natural biomaterials. Animal-sourced bioinks enable much better cell reproduction and function compared to plant-based bioinks. These natural biomaterials have biocompatibility, biodegradation and biomimicking of ECM structure advantages over synthetic materials. In contrast with, synthetic polymers provide the feature that is not easily possible in natural biomaterials, such as controlling mechanical stability, pH and temperature responses. While the limited modification capacity and the difficulty of these modifications should be considered, the use of natural biomaterials as bioinks gives better results in terms of cell viability and growth than synthetic ones.

Adjustable properties are obtained in bioinks to be used for 3D bioprinters by combining natural polymers with either synthetic or another natural polymer. As mentioned earlier, although synthetic biomaterials do not have as much potential as natural biomaterials in terms of cell viability and growth, they allow to improvement of properties such as mechanical properties and crosslinking, which are important in 3D bioprinting.

In this section, the most widely used bioink materials for 3D bioprinting are discussed and also summarized in Table 4.

Table 4. Types of bioinks and comparison of their advantages and disadvantages.

Source	Bioink	Printing Tech.	Advantages	Disadvantages
Natural	Alginate	Extrusion, laser-based	Rapid gelation, low cost	No cell binding areas
	Agarose	Extrusion, laser-based	Nontoxic crosslinking, biocompability, high mechanical strength	Poor cell adhesion
	Collagen	Extrusion, laser-based	Biocompatibility, cell adhesion	Low viscosity, low mechanical integrity
	Gelatin	Extrusion	Biocompatibility	Low viscosity, low stability
	HA	Extrusion, laser-based	Cell viability	Poor mechanical properties, low stability

	Fibrin	Extrusion, inkjet	Cell adhesion, cell viability	Poor mechanical properties
	Cellulose	Extrusion	Biocompability, low cost, high mechanical strength	-
	Silk	Extrusion, inkjet, laser-based	High viscosity, slow degration time	Low cell viability, lack of cell binding sites
	dECM	Extrusion	Providing complex structure of the natural ECM	Poor shape fidelity, poor resolution, rapid degradation, immunogenic (animal-derived)
	Chitosan	-	High mechanical strength, biodegrability	Low cell viability
Synthetic	Pluronic	Extrusion	High resolution, good shape fidelity	Poor mechanical properties
	PEG	Extrusion, laser-based	Adjustable mechanical properties, low cost	Cytotoxicity (due to UV), poor cell adhesion

Natural Biomaterial-Based Bioinks

Biomaterials derived from natural sources are called natural biomaterials. These natural biomaterials with properties such as biocompatibility and biodegradation are often used with different versions of natural biomaterials as bioink for 3D bioprinting.

Alginate-based Bioinks

Alginate or alginic acid, is a naturally occurred polysaccharide primarily attained from the cell walls of brown algea and used for many biomedical applications due to its favorable properties (Axpe & Oyen, 2016). One of these is that the ability of alginates to form a hydrogel polymer that stands out with its resemblance to the extracellular matrix by crosslinking through the existence of bivalent cations such as Ca^{+2}, Mg^{+2}. Alginates show low toxicity and are relatively low cost compared to other biomaterials. Through ease of gelation, high biocompatibility and other features, they have been adopted as bioinks (Abasalizadeh et al., 2020).

Depending on their concentration, alginates can form hydrogels in a range from low viscosity soft hydrogels to viscous hydrogels (Lee & Mooney, 2012). They have shear thinning features which provides stress relief. Thus, during the printing process, alginates safeguard to the cells from stress. Although their use in lower concentrations is recommended because it increases cell viability, alginates are not cell adhesive. Furthermore, in 3D printing applications of alginate at lower concentration cannot achieve a good resolution. Previous researches towards improving the resolution of alginate printing suggests mixing alginate with high molecular weighted polymers.

Alginates are generally formulated as bioinks for inkjet printing. Many examples of usage of alginates as bioinks for 3D bioprinting of different tissue engineering models were reported. While the prominent of these studies are related to alginate based hydrogels produced with different combinations, stem cell bioprinting by using alginate bioinks are also frequently included in these studies. For 3D bioprinting of engineered scaffold bone tissue, an alginate based hydrogel developed by combining with polyvinyl alcohol-hydroxyapatite were reported in 2017 (Bendtsen, Quinnell, & Wei, 2017). In another study, a technique has been reported, using alginate/gelatin methacryloyl (GelMA) bioink, which allows direct bioprinting of endothelial cells into microfibrous hydrogel scaffolds to form an endothelialized human myocardium (Zhang et al., 2016). In the studies for stem cell bioprinting, there is a study in 2017, whose detailed explaination can be found in the fourth section of this article, where alginate was used as bioink with nanofibrillated cellulose (NFC) for 3D bioprinting of induced pluripotent stem cells (iPSCs) to support cartilage manufacture (Nguyen et al., 2017). In 2015, alginate based bioink was used in the 3D bioprinting of human pluripotent stem cells (hPSCs) to produce a three-dimensional mini liver. Alginate-RGD (Arg-Gly-Asp) bioink was created for this study (Faulkner-Jones et al., 2015).

These studies reveal that alginate based bioink can be used for multiple purposes and because of its numerous advantages, it is mostly preferred as bioink materials in 3D bioprinting.

Agarose-based Bioinks

Agarose, a polysaccharide derived by extracting from seaweed, is used as a biopolymer for different purposes in the biomedical field. It has been used as a bioink because of its gel formation at low temperatures with non-toxic crosslinking and high stability, biocompatibility, and mechanical strength. Due to the non-crosslinker gelling feature of agarose, printing of complex structures is possible. However, poor cell adhesion ability to support cell growth appears as a problem. To overcome of this, various efforts have been conducted by combining agarose with other biomaterials to improve the cell adhesion properties of the agarose gel. In a study, the ability of agarose to support endothelial and fibroblast cell growth was shown when blended with collagen and fibrinogen (Kreimendahl et al., 2017). Agarose-based hydrogels are commonly used for 3D bioprinting of cartilage tissue since the requirement for cell sprouting is minimal in this case. An example for these applications, the use of collagen and sodium alginate blend with an agarose-based bioink has been reported. It was shown that mechanical properties of the material was improved while not effecting the gelation properties (Yang et al., 2018). Among the different hydrogels tested as bioinks for cartilage in tissue engineering, the agarose-alginate mixture showed the highest potential (Daly, Critchley, Rencsok, & Kelly, 2016a). The most advanced hyaline-like cartilage result has been reported to be obtained in trials using alginate and agarose hydrogels as bioinks (Daly et al., 2016a; Roberts & Martens, 2016). Since good gelation property alone is not sufficient for using of agarose as bioink, chemical modifications or blending are required to develop the above-mentioned deficient properties.

Collagen-based Bioinks

Collagen is a natural polymer found in almost all biological tissues especially in the connective tissues of skins and bones and is derived from natural extracellular matrix. Due to its high biocompatibility, collagen has been adopted as a natural bioink material in 3D bioprinting and has been used for many years. Collagen can be preferred either alone or in combination in 3D bioprinting usages. It should be noted that its low viscosity makes pure collagen hydrogel difficult for bioprinting. In order to overcome this problem, modifying the collagen by blending with other materials is the most preferred method. The characteristics of collagen are affected by molecular structure, molecular weight, and temperature. These effects can change the viscosity and formation of the collagen hydrogel. Despite almost 30 types of collagen protein present in human cells, due to its abundance, type I collagen is frequently preferred and used for tissue

engineering applications. Collagen molecules consisting of three polypeptide chains, forms a triple helix structure by extending these chains which contains cell adhesion sites based on the transmembrane receptor binding motifs of arginine-glycine-aspartic (RGD) residues (J. E. Kim, S. H. Kim, & Jung, 2016). Cell adherence sites on the chains provide a higher potential to support cell growth to collagen-based bioinks. Also during printing, collagen protects the cells. Collagen has the ability to crosslink using temperature or pH change. The crosslinks formed allow the structure to increase its mechanical properties. Thus, the tensile strength and viscoelastic properties of crosslinked collagen increases compared to non-crosslinked collagen. Crosslinking or gelation of collagen takes longer than other biomaterials, however improved mechanical properties are more preferred for 3D bioprinting.

Studies using collagen as bioink in extrusion, inkjet, droplet-based, electromechanical jetting and laser-based printing have been reported. In a study dated 2018, corneal structures resembling the natural human corneal stroma structure were 3D bioprinted with collagen-based bioinks containing encapsulated corneal keratocytes (Isaacson, Swioklo, & Connon, 2018). In another study, collagen hydrogel bioinks were preferred to create the vascularized mouse thyroid gland structure (Bulanova et al., 2017). Collagen I has been studied as bioinks with keratinocytes and fibroblast cells for the forming of human skin by 3D bioprinting (Lee et al., 2014).

Gelatin-based Bioinks

Gelatin is a biopolymer that derives from the hydrolysis of collagen, and because it is derived from collagen, it has the potential to have almost the same properties as collagen. The biocompatible structure of collagen, as cited before, is also seen in gelatin which is its hydrolyzed form. Since gelatin is obtained naturally from sources at sea, it does not have the risk of carrying disease as those obtained from other sources. The fact that the structure of gelatin has properties that support cell growth and that it easily forms hydrogels with physical crosslinks at low temperatures such as room temperature causes it to be used as a biomaterial in 3D bioprinting applications. Unfortunately, besides this advantage of ease thermal gelation, whereas gelatin has a very low melting point, which is lower than the human body temperature, that comes with a conclusion as restricting its vivo administration. Fortunately, it offers a structure in which these features can be easily adjusted for 3D bioprinting. In order to improve poor bioprinting solubility, shape fidelity and to achieve better results, blending of gelatin with other polymers has also been a preferred method for increasing the low viscosity of their hydrogels (Ahangar, Cooke, Weber, & Rosenzweig, 2019). Mixing gelatin methacrylamide (GELMA) with gellan gum, one of the studies in which gelatin is blended with different viscous polymers to increase the viscosity, has the most popular research results (Panwar & Tan, 2016). This mixture hydrogel structure which offers adjustable physical properties to researchers, is used and developed in many biomedical applications other than 3D bioprinting. The GELMA structure crosslinking takes place chemically. Since this process requires exposure to UV light, care must be taken to avoid potential DNA damage due to UV radiation. These easily adjustable properties of GELMA hydrogel mentioned before enable the usage of it in extrusion, inkjet and SLA-based bioprinting.

Hyaluronic Acid-based Bioinks

Hyaluronic acid (HA), a component of the extracellular matrix, is a glycosaminoglycan composed of repeating disaccharide units. Already taking part in regulatory tasks such as cell growth, migration and differentiation within the cell makes it indispensable for biomedical applications especially in tissue engineering and regenerative medicine. HA protects the cells from pressure stress during printing and offers an environment to improve cell vitality and function by its nature. Hydrogels of HA have high viscosity, which is one of the generally preferred properties in three dimensional bioprinting. However, the rareness of crosslinking in these gels weakens the mechanical strength properties of the HA hydrogel. Therefore, methods such as thiolation and methacrylation to increase the degree of cross-linking have been used in

researchs to modify HA hydrogels. Studies that have successfully crosslinked hyaluronic acid hydrogels physically and photochemically have been reported (Noh et al., 2019). Methacrylated HA (HA-MA), a modified form of HA, has been observed to form stable crosslinks along with the photoinitiator in the media when exposed to UV light (Merceron & Murphy, 2015). These methods were used to improve shape fidelity and good results have been obtained. HA, which has a biocompatibility profile, can also be made more resistant to degradation by enzymes thanks to the cross-links in its hydrogels. They are preferred as bioink in extrusion printing and stereolithographic printing applications.

Fibrin-based Bioinks

Fibrin, a protein formed as a result of the enzymatic reaction of thrombin and fibrinogen in the blood, has taken its place in 3D bioprinting applications as bioinks thanks to its biocompatibility and biodegradability of hydrogels formed by these proteins, like many other hydrogels. However, studies for the use of fibrin for 3D bioprinting are fewer than those in other areas of tissue engineering applications. Due to the low viscosity of the hydrogels of fibrin, they are useful in inkjet bioprinting methods, and they are also used as an additive in extrusion bioprinting by increasing its mechanical strength with other biopolymers (Wang, 2019). The properties of this structure, which provides cell adhesion, support and viability, can be adjusted for its components using different proportions. Although the rapid crosslinking time of this biocompatible biomaterial is an advantage, its irreversible and rapid gelling at human body temperature and rapid degradation time limits its use in the bioprinting field (Merceron & Murphy, 2015). Studies have been developed in which it is blended with different polymers to develop poor mechanical properties. These include attempts to improve stability.

Cellulose-based Bioinks

Cellulose, which is the main ingredient of plant cell walls gives the plant a hard and strong structure. Cellulose is a natural polysaccharide used as itself or its derivatives as bioinks to provide structural and mechanical support to printed structures in 3D bioprinting. The method of blending cellulose with bioactive polymers is frequently used to improve the three-dimensional structure of the cells, increase the viability of the cells and enhance the mechanical properties of biomaterial printed via 3D bioprinter (Gopinathan & Noh, 2018). Examples to known derivatives of cellulose, nanofibrile cellulose (NFC), which is used as a shear-thinning agent in other bioinks, and methyl-cellulose (MC), which can form hydrogel reacts against external stimuli by easily changing its properties such as concentration or molecular weight, can be given.

Silk-based Bioinks

Silk which is protein rarely used alone in regenerative medicine and tissue engineering but mostly blended with other polymers is obtained by harvesting from silkworms and spiders (Gopinathan & Noh, 2018; Derakhshanfar et al., 2018). The versions of silk and itself are preferred as bioinks since they contain all of the properties that should be in an ideal biomaterial to develop a bioink such as high viscosity, slow condition of degrading, shear thinning and not causing an immune response. In addition, silk provides a protection to the cells against stress that occurs during bioprinting. However, high viscosity silk hydrogels, considered as an advantage for bioprinting, can clog the nozzle during printing. Although all of these mentioned possibilities exist in one material seems great, silk does not have cell binding sites that allow cell adhesion, which adversely affects cell growth and functionality. In order to improve these and the shape fidelity of the 3D bioprinted biomaterials, studies are made in which silk is blended with other polymers.

Decellularized Extracellular Matrix (dECM)-based Bioinks

dECM is a natural polymer mixture produced by the decellularization of animal tissues using chemical, physical or combining these methods, while ensuring the ECM remains the same without changing its properties which provides the necessary physical scaffold for cellular components. Using the ECM itself is important for tissue engineering and regenerative medicine applications, as the complex structure of the natural ECM to meet the cell needs by a single material cannot be fully represented when creating bioinks (Turunen et al., 2018). Bioinks are created using the powder form of dECM in a buffer solution (Gopinathan & Noh, 2018). Derivation of dECM from different tissues causes it to have a wide range in terms of cell growth and differentiation factors. However, because dECM is derived from animal tissues, it is likely to contain immunogens that can cause immune responses in host tissues (Dzobo, Motaung, & Adesida, 2019). Since dECM has generally low viscosity, it exhibits weak mechanical properties. Its shape fidelity and bioprinting resolution is poor and its biodegradation occurs very rapidly. Various studies have been carried out to overcome these problems, including physical and chemical cross-linking and blending of dECM with other polymers.

Chitosan-based Bioinks

Chitosan, which is used in medical applications, is derived from the chitin which is a biodegradable fiber developed from the shells of shellfish. A study has been reported that successful results were obtained where the hydrogel of chitosan which has high mechanical strength, antimicrobial property, bioactivity and biodegradability was used as bioink in 3D bioprinting for bone tissue engineering (Demirtaş, Irmak, & Gümüşderelioğlu, 2017; Zhang et al., 2019). Chitosan amino groups can be easily changed for different purposes in 3D bioprinting, and derivatives with suitable properties for applications can be obtained.

Synthetic Polymer-based Bioinks

Synthetic polymers are unique polymers that are artificially produced by chemical reactions of repeated structural units known as monomers. These polymers provide advantages over the natural biomaterial bioinks such as adjusting mechanical properties and degradation rate, which are important in bioprinting, as desired and functionalizing of them with a wide range of biofactors. However, since melting points of most biodegradable varieties reach up to 200°C which is almost quintuple of the human body temperature, and since synthetic ones cannot provide a suitable medium to support cell adhesion and viability compared to the natural biomaterial bioinks, synthetic polymers take place only in 10% of the bioinks used in three-dimensional bioprinting. Synthetic polymers that are being used as bioinks includes pluronic acid, polyethylene glycol (PEG), polyurethane (PU), poly(lactic-glycolic acid) (PLGA), poly(ε-caprolactone) (PCL), and poly(L-lactic acid) (PLLA) (Merceron & Murphy, 2015; Wang, 2019; Gopinathan & Noh, 2018).

Pluronic Acid-based Bioinks

Pluronics or poloxamers are nonimmunogenic synthetic tri-block copolymers composed by the sequences of poly (ethylene oxide), poly (propylene oxide), poly (ethylene oxide), shortly PEO-PPO-PEO structure are often used in tissue engineering. The hydrophilic property of ethylene oxide and the hydrophobic property of propylene oxide provide amphiphilic properties to the structure of pluronics that allow them to form self-assemble micelles in aqueous solutions. Since micelle formation affects the degradation properties of the biomaterial, it is taken into consideration when choosing bioinks for three-dimensional bioprinters. Most prominent feature of pluronic using as a bioink is its rapid and self-assembly gelation process at room temperature. Other properties can be continued as forming of viscous gels and

providing high resolution and good shape fidelity to the printed tissues or organs. Providing good resolution is a major factor in the use of pluronic as bioink in three-dimensional printing of vascular network, and viscous structure of their gels enables easy fabrication of complex 3D stuctures. Besides their advantages, the synthetic structures of these polymers create disadvantages such as low cell binding affinity and lack of ability for degradation. And also weak mechanical properties of pluronic are weak, thus, the good shape fidelity of the pluronic immediately after printing is not long-lasting. In a study, it has been reported that pluronic bioink lacks the ability to protect cells from stress during bioprinting (Panwar & Tan, 2016). Even though pluronic has these mentioned disadvantages, it is mostly used as sacrificial molding agent in 3D bioprinting.

Although the studies used of pluronic as bioink for different bioprinting methods other than extrusion-based bioprinting are almost nonexistent, a study has been reported where the mixture of pluronic with another hydrogel has been tried as a bioink for the inkjet bioprinting (Merceron & Murphy, 2015).

PEG-based Bioinks

This synthetic polymer, which comes up with different names according to its molecular weight, is simply known as polyethylene glycol (PEG). The differentiation in its molecular weights is achieved by ring-opening polymerization of ethylene oxide, and these polymerization levels give it the names PEG, poly (ethylene oxide) (PEO), and poly (oxyethylene) (POE). Having a so easily changeable molecular weight allows its rheological and mechanical properties to be tunable, making PEG an inevitable opportunity to use it as bioinks in 3D bioprinting applications. Also it offers different geometry configurations that can be synthesized from linear to multi-arm PEGs. So far this versatile structure allows it to be used for various purposes in many different fields such as medicine, biology, industry and commercial. Its biocompatibility, nonimmunogenic, hydrophilic structure, low cost and FDA approval make PEG and its varieties an excellent bioink candidate. So much so that PEGs are one of the most preferred bioink type among synthetic biomaterial based bioinks.

Since PEGs cannot form hydrogels alone, they require chemical modification to create a cross-linked three-dimensional structure. The two hydroxyl groups in its structure are converted into functional groups such as acrylate, methyloxyl, thiol, amine, carboxyl and acetylene through physical or covalent crosslinking, thus PEG can be easily adapted to the desired mechanical properties in three-dimensional bioprinting studies. PEG-diacrylate (PEGDA) and PEG-dimethylacrylate (PEGDMA) forms of PEG formed as a result of acrylation and methacrylation are the main types of PEG used when forming bioinks (Merceron & Murphy, 2015; Ashammakhi et al. 2019). Cross-links can occur in PEG forms using photo-initiation. Customizable mechanical properties of PEG makes it more advantageous than other synthetic polymers for printing multilayered structures. Furthermore, the hydrophilic structure of PEG allows cell encapsulation. Although its many advantages, and resistance of its hydrogels to protein adsorption, which allows to create desired biofunctionality, the lack of cell binding sites adversely affects cell adhesion, limiting the use of PEG-based bioinks in 3D bioprinting applications. RGD peptide modification applications have been developed and used to increase cell adhesion ability in PEGs for bioprinting.

While low viscosity prevents the use of PEG-based hydrogels in extrusion bioprinting applications, it offers the advantage of preserving shape fidelity in other bioprinting applications such as inkjet bioprinting. PEG-based hydrogels are mixed with other biomaterials for using in extrusion biopressure, and improving their properties accordingly. PEG can be used as a crosslinker to improve the bioprinting resolution of other bioinks.

Nanocomposite Bioinks

By combining polymers with nanofillers such as carbon nanotubes, silicates, ceramics and metals, nanocomposite bioinks are formed for creating a variety in three-dimensional bioprinting applications by

enhancing mechanical or chemical structural properties of these polymers. Although nanocomposite bioink studies have been developed and used for tissue engineering already, the potential of nanocomposite bioinks is not clear in three-dimensional bioprinting. However there is really powerful belief that nanocomposite bioinks can impart unique properties to 3D bioprinted structures.

4. BIOPRINTING FOR TISSUE ENGINEERING AND REGENERATIVE MEDICINE

Studies are rapidly propagating to the ultimate goal of producing functional living organs for transplantation using bioprinting. Some the findings on the use of bioinks for bioprinting are discussed below.

Bioprinting of keratinocyte cells by producing bioinks suitable for three-dimensional bioprinters were made. Tests, such as cell proliferation, viability analysis and cell distribution were performed and morphology of the epidermis tissue culture with hydrogel structure was determined for the obtained structure. The hydrogel most suitable for bio printing was determined using three different hydrogels like gelatin, alginate and chitosan. As a result of the researches, it was determined that got tissues were effectively produced using 3D bioprinting, and keratinocytes were able to join the hydrogels and retain their viability. The produced bioinks can be used as a treatment for skin injuries such as burns. (Ürkmez, Seçkin, Görgün, &Uyanıkgil, 2018)

The use of bioinks is a promising development in the field of regenarative medicine. Nevertheless, full success cannot be achieved as bioinks cannot meet the intrication of the natural extracellular matrix (ECM). To solve this problem, a research was made to whether bioinks can be made while preserving the natural extracellular matrix. In the first place, tissue printing was performed with a specific decellularized extracellular matrix biopsy covering live hASCs or hTMSCs. As an outcome of this research, the usage of bioinks prepared with cell-free (dECM) tissues for in vivo and in vitro tissue functions has been opened. (Pati et al., 2014)

The structure of bioinks has an important role in cell printing. If the crosslinks are installed incorrectly in bioinks, shaping will not be as desired while printing. For this reason, dECM bioinks with heat modules that allow cross-linking at the same time have been designed. As a result of the tests, it has been observed that it has more printability than bioinks without a heat module. At the same time, no cell death due to the heat module was found. In addition, it was determined that the viscoelasticity increased at higher bioink concentrations, hence, the collapse was less and it could support itself more easily. (Ahn et al., 2017)

Whether iPSCs are proper for bioprinting to assist cartilage production have been investigated. To facilitate the adaptation of iPSCs to their phenotypic properties, nanofibrilized cellulose composite has been used, which provides structural and mechanical support to create the physiological mimicry environment. Alginate and hyaluronic acid have also been used to assist cells. As a result of the research, together with these hydrogel combinations, iPSCs have been observed to be suitable for cartilage formation in 3D bioprinting. (Nguyen et al., 2017)

Despite three-dimensional bioprinting technology has drew great attention in the field of regenerative medicine, there are some engineering difficulties to overcome. For long-term shape stability, bioinks need to meet basic criteria such as printable, biocompatible and structural and mechanical stability. Especially when using DLP modality, the dynamics of the polymerization, changing the power of the light source, the printing speed, the type and concentrations of the photoinitiators should be adjusted. Silk fibroin-based bioinks were made. With this Sil-MA hydrogel, it was observed that complex structures can be printed in one press, higher print lengths can be achieved compared to other hydrogels, cell distribution and net printing can be achieved as designed even if the print size is small. Flexible and stretchable structures were obtained as the Sil-MA concentration increased. Based on the mechanical properties obtained as a result of the research, Sil-MA can be used for many clinical applications. (Kim et al., 2018)

Finding bioinks that meet physical, chemical and biological requirements and developing biomaterial ink (BmI) is the biggest challenge in biofabrication. In order for the tissues to be successful, BmIs and bioinks must act like natural cells. Bioinks hardness and porosity should be like to the natural extracellular matrix to assist cell growth and proliferation. As mentioned earlier, most of the materials developed cannot meet these requirements. The nucleotide lipid-based hydrogel forms soft scaffolds that can mimic the extracellular matrix have been observed. This hydrogel can be used as biomaterial ink or bioinks. (Dessane et al., 2020)

It is a very important issue to heal muscle defect injuries caused by the loss of the structural and functional properties of the natural skeletal muscle. Treatment of muscle injuries has clinical difficulties. Therefore, restoring the normal function of the skeletal muscle will be an important improvement in extensive muscle defect injuries. The effect of neural cell integration on muscle regeneration has been investigated. Human muscle progenitor cells (hMPC) and human neural stem cells (hNSC) were used to resolve problems caused by innervation. Neuromuscular junction (NMJ) formation was observed with the combined use of these cells. It was also observed that the innervation was facilitated and the functionality was recovered in some muscle defect injuries. (Kim et al., 2020)

Bioinks take an important place to improve the functions of 3D printed tissues. An ideal bioink should be printable, non-toxic, biocompatible and able to mimic the natural extracellular matrix. The properties of bioinks can be affected by various parameters. The impact of ionic strength of the solvent on alginate gelatin bioinks has been analyzed. As the ionic strength of the solvent used in bioinks increased, a lower viscosity was observed. It was also found that the solvent had low ionic strength, less swelling and degradation. In line with the research, it was understood that the ionic strength of the solvent had a significant effect on the printability, mechanical properties and characteristics of the cell of bioinks. (Li et al., 2018)

5. FUTURE PROSPECTS

Bioprinters are promising and emerging technologies for creating 3D tissue units of different structures and geometries using many living tissues and biomaterials (Güngör-Özkerim et al., 2018). These devices enable the production of specific scaffolding and tissue models with high complexity about structure and numerous design types for patients. It has the potential to be widely used in medicine due to its many advantages such as this one (Ji & Guvendiren, 2017). This usable potential has enabled the production and transplantation of various structures such as bone, heart tissue, cartilaginous tissues and many more (Hölzl et al., 2016). One of the main components of bioprinting is bioinks and they consist of various cells and biomaterials (Güngör-Özkerim et al., 2018). Cell-wool hydrogels are the most common bio-inks that offer new strategies (Ji & Guvendiren, 2017). In addition, ECM-based bioinks, cell-free bioinks, cell aggregates or spheres, bioinks used in 3D biological printing technology have promising results for the development of tissues and organs (Gopinathan & Noh, 2018). Although dECM-based bioinks provide an alternative approach, transaction of tissue which is decellularized enhances the cost of ink making (Ji & Guvendiren, 2017). The presence of bioink in many features and types, the availability of appropriate modeling tools and the ability to use these materials in different geometries reveal the advantages of biological printing. The bioink and bioprinting required for different applications have come a long way in a short time. Therefore, the materials planned to be used for biological printing have been systematically researched and adjusted to suit different technologies (Hölzl et al., 2016). Although biological printing is an area open to development, the production of bioinks that can fully meet the requirements sought has been restricted due to various biological, mechanical and similar reasons. Many studies are needed to develop bioink structures and to establish new standards (Güngör-Özkerim et al., 2018). In addition to the development of bioinks, it is thought that bioprinters have higher resolution and lower costs, which can increase the expectations of research areas (Gopinathan & Noh, 2018). Current manufacturing procedures are currently not sufficient to produce all organs because of complex nature, but

simple structures or tissues can be produced (Hacıoglu, Yılmazer & Ustundag, 2018). Moving of 3D bioprinted structures to the clinic still needs more arrangements (Ji & Guvendiren, 2017).

The future of bioink and 3D bioprinting is promising because new biomaterials containing supramolecular functionality, recycled crosslinking polymers and stimuli-sensitive hydrogels will greatly contribute to the development of this area. Such developments lead to the development of improved tissues and devices specific to the patients (Gopinathan & Noh, 2018). In some of the studies on bioprinters, models that allow evaluating the mechanic features of hydrogels which contains various cell distributions and densities are presented. These models can be expanded over time to include more complex 3D structure architectures and can be used for determining the estimated cellular loading, mechanical response and longitudinal behavior of cells which are printed in various hydrogel structures. Such studies can be squarely associated with organ development and tissue modeling (Hölzl et al., 2016). Two of the most interesting candidates for bioink design are supramolecular hydrogels with cross-linking mechanisms and stimulating materials for biomimetic 4D printing (Ji & Guvendiren, 2017).

Improving biological printing practices depends on many substances. Some of these are stem cell technology, material science technology, and production capabilities of bioink components. Moreover, principles such as post-pressure treatments, self-assembly and self-regulation can be considered as solutions to produce complex organs. When these problems are solved, biological pressure will be one of the most important inventions in the world (Hacıoglu, Yılmazer & Ustundag, 2018). Controlled and stimuli-responsive release of growth factors and immunomodulators will enable the ability to control the bioactivity of bioinks. Steps taken in the fields of nanomaterials, chemistry of polymer, material for 3D biological printing and technics of stem cell will make easier the improve of bioinks which are hydrogel (Chimene, Lennox, Kaunas & Gaharwar, 2016).

Some problems related with functionality, printability and safety of the material in biological printing methods are an issue to be investigated for therapeutic and non-therapeutic applications (Liu J et al., 2018). Bioprints with multiple printheads are the technologies required to generate heterogeneous and complex tissue structures quickly. These devices can accumulate versatile formulations concurrently to produce complex tissue structures which involves vascularized tissues. In recent studies, the use of multiple polymeric inks has been investigated. Mechanical development of multicomponent polymeric bioinks including shear thinning nanoparticles can be achieved. Adding microparticles and nanoparticles containing growth factor to the ink medium in the polymeric network will supply adjunct tools to check the cell destiny. One of the most important reasons for the complex tissue structures that are intended to be produced by operating 3D bioprinting is the restricted existence of multiple bioink. As a solution to this problem, multimaterial bio-inks have been one of the most researched areas, but many promising combinations of polymers have not been evaluated yet (Chimene et al., 2016). The use of naturally derived biopolymers as bioinks in biomedical and pharmaceutical executions is noted one of the most up and coming fields in the extension of 3D biological printing because these materials which have high abudance, low cost, biocompatibility and biodegradability. Apart from these features, difficulties such as mechanical properties, supplies imperfections, biocompatibility, tissue biomimicry and degradation kinetics in 3D printing which biopolymers have, used in medical fields are important requirements. The natural physiochemical properties of some biopolymers require innovations such as a change of printers which are commercial, change of natural biopolymers, advancing new solvent systems, and involving another bioactive. In future research, efforts can be made to enlarge the restricted diversity of naturally gained biopolymers. Some of these include the improvement of new solvent systems that are cell-friendly and can dissolve or disperse naturally derived biopolymers as ink formulations, the management of several biopolymers and the inclusion of different biomolecules like compound inks with properties such as the desired workability, printability, mechanics, bioactivity, biodegradability and chemical. The inclusion of components sensitive to physical stimuli in naturally derived biopolymers. When these challenges are overcomed, it can be estimated that there will be the use of naturally derived 'green' raw materials as future material for 3D bioprinting

technology. Such raw materials that can be used to make the potentially available 3D printing programmable and turn it into a future 4D print (Liu J et al., 2018).

6. CONCLUSION

3D biological printing is a hopeful process for the area of tissue engineering, including the creation of most complex structural architectures, vascularization of tissue structures and the orientation of stem cell differentiation. There are many types of bioprints that can be preferred in certain control and various designs, but several difficulties remain to create some complicated tissues, comprising several cell types. Most especially, bioink materials needs to be developed to clinically apply bioprine technology. Bioink formulation can be considered as one of the most important elements for the bioprinting process. A proper bioink must perform several rheological, mechanical and biological necessities during and after printing. Generally, according to the desired feature, they are branching under two main headings as natural-based and synthetic. Throughout this article, bioprinting methods and bioinks which have many different properties and are used for various purposes are indicated. At the same time, studies on tissue engineering and regenerative medicine and many promising possibilities for bioink are mentioned. Each method has its advantages and disadvantages according to its intended use. New techniques are being developed in order to eliminate these drawbacks.

Despite all the difficulties, 3D bioprinting has progressed towards its goal to enable functional tissue printing since its discovery, and this method has clearly proved fitting of ongoing research. Further time, working and multidisciplinary speciality will be required to perform the clinical potential of this technology, but the future is bright. Biological printing is ready to play an important role in personalized regenerative medicine.

7. ACKNOWLEDGEMENTS

8. REFERENCES

1. Güngör-Özkerim, P.S., İnci, I., Zhang, Y.S., Khademhosseini, A. & Dökmeci, M.R. (2018). Bioinks for 3D bioprinting: an overview. Biomaterials science, 6(5), 915-946. https://doi.org/10.1039/c7bm00765e

2. Hölzl, K., Lin, S., Tytgat, L., Van Vlierberghe, S., Gu, L., & Ovsianikov, A. (2016). Bioink properties before, during and after 3D bioprinting. Biofabrication, 8(3). https://doi.org/10.1088/1758-5090/8/3/032002

3. Kačarević, Ž.P., Rider, P.M., Alkildani, S., Retnasingh, S., Smeets, R., Jung, O.,…Barbeck, M. (2018). An Introduction to 3D Bioprinting: Possibilities, Challenges and Future Aspects. Materials (Basel, Switzerland), 11(11). https://doi.org/10.3390/ma11112199

4. Melchels, F.P., Feijen, J., & Grijpma, D.W. (2010). A review on stereolithography and its applications in biomedical engineering. Biomaterials, 31(24), 6121–6130. https://doi.org/10.1016/j.biomaterials.2010.04.050

5. Chae, M.P., Rozen, W.M., McMenamin, P.G., Findlay, M.W., Spychal, R.T., & Hunter-Smith, D.J. (2015). Emerging Applications of Bedside 3D Printing in Plastic Surgery. Frontiers in surgery, 2, 25. https://doi.org/10.3389/fsurg

6. Axpe, E., & Oyen, M. L. (2016). Applications of Alginate-Based Bioinks in 3D Bioprinting. International journal of molecular sciences, 17(12), 1976. https://doi.org/10.3390/ijms17121976

7. Abasalizadeh, F., Moghaddam, S. V., Alizadeh, E., Akbari, E., Kashani, E., Fazljou, S., Torbati, M.,

. . . Akbarzadeh, A. (2020). Alginate-based hydrogels as drug delivery vehicles in cancer treatment and their applications in wound dressing and 3D bioprinting. Journal of biological engineering, 14, 8. https://doi.org/10.1186/s13036-020-0227-7

8. Lee, K. Y., & Mooney, D. J. (2012). Alginate: properties and biomedical applications. Progress in polymer science, 37(1), 106–126. https://doi.org/10.1016/j.progpolymsci.2011.06.003

9. Bendtsen, S. T., Quinnell, S. P., & Wei, M. (2017). Development of a novel alginate-polyvinyl alcohol-hydroxyapatite hydrogel for 3D bioprinting bone tissue engineered scaffolds. Journal of biomedical materials research. Part A, 105(5), 1457–1468. https://doi.org/10.1002/jbm.a.36036

10. Zhang, Y. S., Arneri, A., Bersini, S., Shin, S. R., Zhu, K., Goli-Malekabadi, Z., . . . & Khademhosseini, A. (2016). Bioprinting 3D microfibrous scaffolds for engineering endothelialized myocardium and heart-on-a-chip. Biomaterials, 110, 45–59. https://doi.org/10.1016/j.biomaterials.2016.09.003

11. Nguyen, D., Hägg, D. A., Forsman, A., Ekholm, J., Nimkingratana, P., Brantsing, C., . . . & Simonsson, S. (2017). Cartilage Tissue Engineering by the 3D Bioprinting of iPS Cells in a Nanocellulose/Alginate Bioink. Scientific Reports, 7(1), 658. https://doi.org/10.1038/s41598-017-00690-y

12. Faulkner-Jones, A., Fyfe, C., Cornelissen, D. J., Gardner, J., King, J., & Courtney, A. (2015). Bioprinting of human pluripotent stem cells and their directed differentiation into hepatocyte-like cells for the generation of mini-livers in 3D. Biofabrication, 7(4), 044102. https://doi.org/10.1088/1758-5090/7/4/044102

13. Kreimendahl, F., Köpf, M., Thiebes, A. L., Duarte Campos, D. L., Blaeser, A., Schmitz-Rode, T., . . . & Fischer, H. (2017). 3D-Printing and Angiogenesis: Tailored Agarose-Type I Collagen Blends Comprise 3D Printability and Angiogenesis Potential for Tissue Engineered Substitutes. Tissue Engineering Part C, Methods, 23(10). https://doi.org/10.1089/ten.tec.2017.0234

14. Yang, X., Lu, Z., Wu, H., Li, W., Zheng, L., & Zhao, J. (2018). Collagen-alginate as bioink for three-dimensional (3D) cell printing based cartilage tissue engineering. Materials science & engineering. C, Materials for biological applications, 83, 195–201. https://doi.org/10.1016/j.msec.2017.09.002

15. Daly, A. C., Critchley, S. E., Rencsok, E. M., & Kelly, D. J. (2016a). A comparison of different bioinks for 3D bioprinting of fibrocartilage and hyaline cartilage. Biofabrication, 8(4), 1-10. https://doi.org/10.1088/1758-5090/8/4/045002

16. Roberts, J.J., & Martens, P. J. (2016). Engineering biosynthetic cell encapsulation systems. In L. Poole-Warren, P. Martens, & R. Green (Eds.), Biosynthetic Polymers for Medical Applications (Woodhead Publishing Series in Biomaterials) (pp. 205-239). Woodhead Publishing.

17. Kim, J. E., Kim, S. H., & Jung, Y. (2016). Current status of three-dimensional printing inks for soft tissue regeneration. Tissue Engineering and Regenerative Medicine, 13, 636–646. https://doi.org/10.1007/s13770-016-0125-8

18. Isaacson, A., Swioklo, S., & Connon, C. J. (2018). 3D bioprinting of a corneal stroma equivalent. Experimental Eye Research, 173, 188-193. https://doi.org/10.1016/j.exer.2018.05.010

19. Bulanova, E. A., Koudan, E. V., Degosserie, J., Heymans, C., Pereira, F. D., Parfenov, V. A., . . . & Mironov, V. A. (2017). Bioprinting of a functional vascularized mouse thyroid gland construct. Biofabrication, 9(3). https://doi.org/10.1088/1758-5090/aa7fdd

20. Lee, V., Singh, G., Trasatti, J. P., Bjornsson, C., Xu, X., Tran, T. N., & Karande, P. (2014). Design and fabrication of human skin by three-dimensional bioprinting. Tissue engineering. Part C, Methods,

20(6), 473–484. https://doi.org/10.1089/ten.TEC.2013.0335

21. Ahangar, P., Cooke, M. E., Weber, M. H., & Rosenzweig, D. H. (2019). Current Biomedical Applications of 3D Printing and Additive Manufacturing. Applied Sciences, 9(8). https://doi.org/10.3390/app9081713

22. Panwar, A., & Tan, L. P. (2016). Current Status of Bioinks for Micro-Extrusion-Based 3D Bioprinting. Molecules (Basel, Switzerland), 21(6), 685. https://doi.org/10.3390/molecules21060685

23. Noh, I., Kim, N., Tran, H. N., Lee, J., & Lee, C. (2019). 3D printable hyaluronic acid-based hydrogel for its potential application as a bioink in tissue engineering. Biomaterials Research, 23, 3. https://doi.org/10.1186/s40824-018-0152-8

24. Merceron, T., & Murphy, S. (2015). Hydrogels for 3D Bioprinting Applications. In: A. Atala, J. J. Yoo (Eds.), Essentials of 3D Biofabrication and Translation (pp. 249-270). USA: Academic Press an imprint of Elsevier

25. Wang, X. (2019). Advanced Polymers for Three-Dimensional (3D) Organ Bioprinting. Micromachines, 10(12), 814. https://doi.org/10.3390/mi10120814

26. Gopinathan, J., Noh, I. (2018). Recent trends in bioinks for 3D printing. Biomaterials Research, 22, 11. https://doi.org/10.1186/s40824-018-0122-1

27. Derakhshanfar, S., Mbeleck, R., Xu, K., Zhang, X., Zhong, W., & Xing, M. (2018). 3D bioprinting for biomedical devices and tissue engineering: A review of recent trends and advances. Bioactive materials, 3(2), 144–156. https://doi.org/10.1016/j.bioactmat.2017.11.008

28. Turunen, S., Kaisto, S., Skovorodkin, I., Mironov, V., Kalpio, T., & Vainio, S. (2018). 3D bioprinting of the kidney—hype or hope? AIMS Cell and Tissue Engineering, 2(3), 119-162. https://doi.org/10.3934/celltissue.2018.3.119

29. Dzobo, K., Motaung, K., & Adesida, A. (2019). Recent Trends in Decellularized Extracellular Matrix Bioinks for 3D Printing: An Updated Review. International journal of molecular sciences, 20(18). https://doi.org/10.3390/ijms20184628

30. Demirtaş, T. T., Irmak, G., & Gümüşderelioğlu, M. (2017). A bioprintable form of chitosan hydrogel for bone tissue engineering. Biofabrication, 9(3). https://doi.org/10.1088/1758-5090/aa7b1d

31. Zhang, Y., Zhou, D., Chen, J., Zhang, X., Li, X., Zhao, W. (2019). Biomaterials Based on Marine Resources for 3D Bioprinting Applications. Marine drugs, 17(10), 555. https://doi.org/10.3390/md17100555

32. Ashammakhi, N., Ahadian, S., Xu, C., Montazerian, H., Ko, H., Nasiri, R., . . . & Khademhosseini, A. (2019). Bioinks and bioprinting technologies to make heterogeneous and biomimetic tissue constructs. Materials Today Bio, 1. https://doi.org/10.1016/j.mtbio.2019.100008

33. Şendemir, A. Ü., Seçkin, U. D., Görgün, C., & Uyanıkgil, Y. (2018). Deri Doku Mühendisliği Üç Boyutlu Biyobaskı ve Keratinosit Kültürü. Dicle Medical Journal, 45(1), 9-18. https://doi.org/10.5798/dicletip.363931

34. Pati, F., Jang, J., Ha, D. H., Won Kim, S., Rhie, J. W., Shim, J. H., . . . & Cho, D. W. (2014). Printing three-dimensional tissue analogues with decellularized extracellular matrix bioink. Nature communications, 5. https://doi.org/10.1038/ncomms4935

35. Ahn, G., Min, K. H., Kim, C., Lee, J. S., Kang, D., Won, J. Y., . . . & Shim, J. H. (2017). Precise stacking of decellularized extracellular matrix based 3D cell-laden constructs by a 3D cell printing system equipped with heating modules. Scientific reports, 7(1). https://doi.org/10.1038/s41598-017-09201-5

36. Kim, S. H., Yeon, Y. K., Lee, J. M., Chao, J. R., Lee, Y. J., Seo, Y. B., . . . & Park, C. H. (2018). Precisely printable and biocompatible silk fibroin bioink for digital light processing 3D printing. Nature Communications, 9(1). https://doi.org/10.1038/s41467-018-03759-y

37. Dessane, B., Smirani, R., Bouguéon, G., Kauss, T., Ribot, E., Devillard, R., . . . & Crauste-Manciet S. (2020). Nucleotide lipid-based hydrogel as a new biomaterial ink for biofabrication. Scientific Reports, 10(1). https://doi.org/10.1038/s41598-020-59632-w

38. Kim, J. H., Kim, I., Seol, Y. J., Ko, I. K., Yoo, J. J., & Atala, A. (2020). Neural cell integration into 3D bioprinted skeletal muscle constructs accelerates restoration of muscle function. Nature communications, 11(1). https://doi.org/10.1038/s41467-020-14930-9

39. Li, Z., Huang, S., Liu, Y., Yao, B., Hu, T., Shi, H., . . . & Fu, X. (2018). Tuning Alginate-Gelatin Bioink Properties by Varying Solvent and Their Impact on Stem Cell Behavior. Scientific Reports, 8(1). https://doi.org/10.1038/s41598-018-26407-3

40. Ji, S., & Guvendiren, M. (2017). Recent Advances in Bioink Design for 3D Bioprinting of Tissues and Organs. Frontiers in bioengineering and biotechnology, 5, 23. https://doi.org/10.3389/fbioe.2017.00023

41. Gopinathan, J., & Noh, I. (2018). Recent trends in bioinks for 3D printing. Biomaterials research, 22: 11. https://doi.org/10.1186/s40824-018-0122-1

42. Hacıoglu, A., Yılmazer, H., & Ustundag, C. (2018). 3D Printing for Tissue Engineering Applications. Politeknik Dergisi, 21(1), 221-227. https://doi.org/10.2339/politeknik.389596

43. Chimene, D., Lennox, K. K., Kaunas, R. R., & Gaharwar, A. K. (2016). Advanced Bioinks for 3D Printing: A Materials Science Perspective. Annals of Biomedical Engineering, 44(6), 2090–2102. https://doi.org/10.1007/s10439-016-1638-y

44. Liu, J., Sun, L., Xu, W., Wang, Q., & Yu, S. (2018). Current advances and future perspectives of 3D printing natural-derived biopolymers. Carbohydrate Polymers, 207, 297-316. https://doi.org/10.1016/j.carbpol.2018.11.077

RF Marker Simulation Model for Interventional MRI Applications

Research Article

Engin Baysoy[1]* iD

[1] Biomedical Engineering Department, İzmir Democracy University, İzmir, Turkey

Author E-mails
engin.baysoy@idu.edu.tr
*Correspondance to: Engin Baysoy, Biomedical Engineering Department, İzmir Democracy University, İzmir, Turkey
Tel: +90 0232 260 1001
DOI: 10.38061/idunas.748352

Özet

Mevcut görüntüleme modaliteleri ile kıyaslandığında Manyetik Rezonans Görüntüleme (MRG) sisteminin sahip olduğu üstünlüklerin herkes tarafından kabul görmesiyle girişimsel kardiyovasküler ameliyatların MRG tarayıcı ile yapılması yönünde bir eğilim doğmuştur. Ancak halen güvenilir ve MRG uyumlu girişimsel aletlerin mevcut olmaması, bu klinik uygulamaların MRG rehberliğiyle yapılabilmesinin önündeki en büyük sorundur. Klinikteki kalp içi uygulamalarında MRG kullanımının yaygınlık kazanabilmesi için rehber tel ve kateterlerin ticari olarak üretiminde görüntülenebilirlik, küçültülebilirlik, esneklik ve güvenlik gibi kriterlerin dikkate alınması gerekmektedir.

Bu çalışmada, farklı şekillerde dizayn edilmiş RF işaretleyici yapılarının üretimini yapmaksızın güvenilir bir şekilde değerlendirebilmek için, konumdan bağımsız bir simülasyon modelinin uygulanabilirliği doğrulanmıştır. Model içerisinde kullanılan RF bobin tasarımları, daha önce deneysel yöntemler ile üretilmiş klinik olarak kullanılabilecek ve MRG uyumlu RF işaretleyiciler ile aynı ölçü ve özellikleri taşımaktadır [1]. Comsol Multiphysics programı simülasyonları ile sonlu eleman yöntemi kullanılarak, farklı RF bobin tasarımlarının elektriksel ve manyetik karakteristiği matematiksel olarak analiz edilmiştir. MRG ortamını resmeden kanıtlanmış bir benzetim ortamı, farklı RF işaretleyici prototip tasarımlarının üretimlerinin yapılmaksızın, birçok açıdan birbiriyle kıyaslanmasını mümkün kılacaktır. Bu çalışmada sunulan benzetim platformu gelecekte üretilmesi planlanan yeni RF işaretleyici tasarımlarının, görünürlük, güvenilirlik, sinyal gürültü oranı, ısınma miktarı ve kalite faktörü gibi özelliklerinin belirlenmesi açsından kullanışlı bir ortam sağlamaktadır.

Anahtar Sözcükler: Girişimsel MRG, RF işaretleyici, MRG uyumluluk, SEM simülasyonları.

Abstract

Compared to the other imaging modalities Magnetic Resonance Imaging (MRI) system has many advantages. There is a great demand to carry out interventional cardiovascular procedures under MRI scanner. However, the lack of visible markers and MRI compatible interventional instruments and devices,

is the main problem for realizing clinical applications with MRI guidance. In order to provide widespread usage of MRI for endovascular operations, commercial catheters and guidewires must be manufactured by considering many performance criteria including visualization, miniaturization, flexibility and safety.

In this study, an orientation independent simulation model was developed and validated to obtain a reliable method for evaluating the designed RF marker structures in a MRI environment. Utilized RF coil designs have similar size and properties with former constructed clinical grade MRI compatible RF markers in experimental works [1]. Finite Element Method (FEM) simulations were carried out for different RF coil designs to make the computational analysis of their electrical and magnetic characteristics by using COMSOL Multiphysics program.

By delineating an approved simulation platform of a MRI environment, various different designs of RF marker prototypes can be compared between each other in many aspects, instead of realizing these models. Proposed simulation platform enables a convenient facility to determine various parameters of micro coils that have significant effects on visibility and safety performance of the candidate designs including signal to noise ratio (SNR) and Quality (Q) factor, RF induced heating and specific absorption rate (SAR).

Keywords: Interventional MRI, MRI compatibility, RF marker, FEM simulations.

1. INTRODUCTION

Magnetic Resonance Imaging (MRI) guidance was intended to be a new platform by operators in order to realize catheter-based imaging and therapeutic procedures without usage of x-ray. Beside ionizing radiation free imaging modality benefits, operators favor MRI to perform complex interventional cardiovascular operations because of its accepted advantages including superior intrinsic soft tissue contrast and multi slice imaging technique [2]. Furthermore, compared to conventional x ray based modalities it is possible to collect reliable and real time physiologic cardiac parameters via MRI such as flow, volume, pressure, diffusion, perfusion, temperature, motion, and etc. [3].

Despite many promising progresses in many reports, unavailability of commercially proved MRI safe and visible instruments still makes interventional cardiovascular MRI (iCMRI) unrealistic for the treatment of cardiovascular diseases. Since MRI physical nature has a high magnetic field inside operation room, conventional interventional instruments and devices that consist of conductive materials cannot be utilized with interventional applications under MRI. Beside of MRI safety concerns with magnetic field effect and RF induced heating problems, medical devices implanted into patient body must be visible and possible for tracking while operator steering the catheter through the vessels and cardiac chambers of patient.

For semi-active and active catheter designs, in order to highlight the interventional medical devices under MRI, miniature size resonant frequency (RF) markers have to be placed over catheter shaft. Tuning of resonance frequency (RF) marker at Larmor frequency of MRI scanner, is the key for maximum interaction between RF marker and standard coil connected to MRI scanner.

Currently available RF markers in semi-active or active devices contain conventional components such as solenoid coils, nonmagnetic capacitors, diodes, and wires. However, all these rigid analog circuit components and the soldering process itself increase overall device profile and affect device mechanical properties (flexibility, endurance, and etc.) unfavorably.

An orientation independent simulation model was validated to obtain a reliable method for evaluation of the characteristics of the designed RF marker structures into the MRI platform without the need of fabrication. Finite Element Method (FEM) simulations were carried out for developed RF marker

prototype and different RF coil designs to obtain the computational analysis of their electrical and magnetic characteristics in COMSOL Multiphysics program.

Experimentally realized RF marker prototype was placed into a birdcage coil in a MRI simulation environment and its magnetic and electrical characteristics were examined in terms of electromagnetic field homogeneity and B1 field circularity in the volume of interest. Adding to that performance of different RF coil designs were studied when the RF coil was positioned into different orientations with respect to the birdcage coil in virtual MRI platform.

By delineating an approved simulation platform of a MRI environment, various different designs of RF marker prototypes can be compared between each other in many aspects, instead of realizing these models. Proposed simulation platform enables a convenient facility to determine various parameters of micro coils that have significant effects on visibility and safety performance of the candidate designs including signal to noise ratio (SNR) and Quality (Q) factor, RF induced heating and specific absorption rate (SAR).

2. MATERIALS & METHODS

Simulation Set Up in MRI for A Birdcage Coil

An orientation independent simulation model was constructed to evaluate the visibility performance of different RF marker designs in MRI environment. Designing a virtual platform for testing RF marker prototypes with different orientation according to standard birdcage coil helps to analyze the induced electromagnetic field, homogeneity distortion and B1 field circularity in the volume of interest.

Simulation Workflow

For setting up and solving a simulation model in Comsol Multiphysics 5.3, it is necessary to follow a standard workflow. Sequence of steps for a standard workflow was expressed below;

- Setting up a model environment
- Creating a geometry
- Specifying materials and their properties
- Defining physics and boundary conditions
- Creating a mesh
- Running simulation
- Postprocessing results

By following the regarding steps, we set up our simulation model, and evaluated the results according to our assumptions.

Validation of Finite Element Modeling of a Birdcage Coil

RF birdcage coils have become widespread in the field of MRI imaging. Their simplicity in design followed by a high homogenous magnetic field due to continuous sinusoidal current distribution on the surface of the coil led to their popularity. Modeling the birdcage coil in a 3D simulation environment helps to examine the electromagnetic field in the volume of interest, such as field homogeneity, B_1 field circularity [4]. Starting point of the simulation model studied in this study was an available model in COMSOL

Multiphysics model. Finite Element Method (FEM) model of low-pass birdcage coil in order to obtain a homogenous magnetic field and circular B_1 field inside the birdcage coil in 3 Tesla MRI was already prepared and shared by program supplier [5]. In our study, prepared and exist model by program supplier for 3 Tesla MRI, was modified and made suitable for 1.5 Tesla MRI scanner, given in Figure 1. Similar conditions were set up and evaluated for 1.5 Tesla MRI environment.
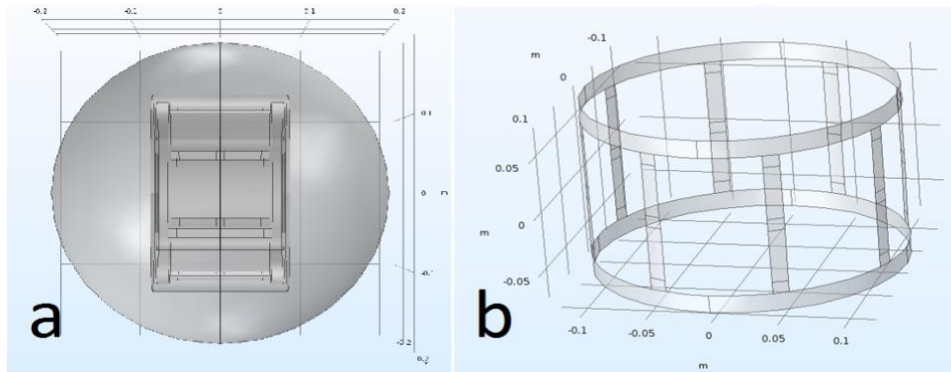

Figure 1. a) Geometric model of whole MRI virtual platform b) Geometric model of a low-pass birdcage coil inside MRI environment.

Geometric parameters of custom designed low-pass birdcage coil;

Radius of the sphere	: 20 cm
Radius of the birdcage coil	: 12 cm
Height of the birdcage coil	: 15 cm
Length of the capacitive elements	: 1 cm
Number of the capacitive elements	: 22
Number of the legs	: 8
Number of the activation ports	: 2

In order to validate the designed MRI platform, a phantom was placed into the middle of the model that has the similar properties with ASTM F2182 phantom (Relative permittivity: 80, relative permeability: 1, electrical conductivity: 0.47 S/m). Electric field distribution on the surface and the volume of the constructed phantom, shown in Figure 2, was compared with previously reported electric field distributions in the ASTM phantom [6].
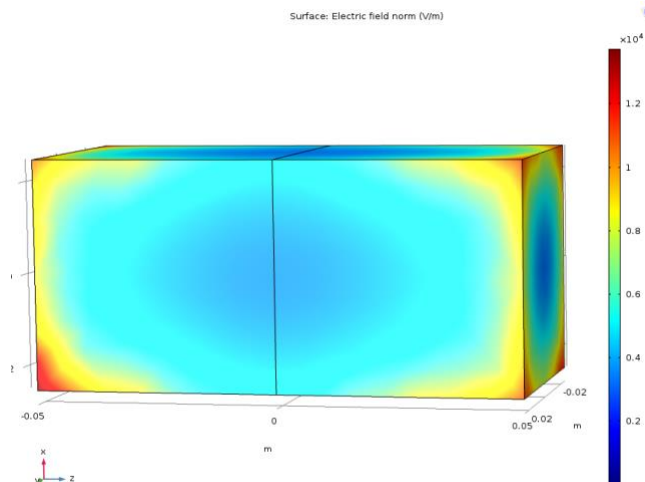

Figure 2. The phantom that simulates a saline water filled tank with 5 cm width, 5 cm depth and 10 cm length.

Quadrature Excitation in Frequency Domain Analysis

First part of our simulation studies was inspired by thesis studies [4,5] that utilized program of Comsol Multiphysics while inspecting effects of varied conditions, and parameters of instruments in MRI scanner environment. According to these former studies, in order to effectively design a birdcage coil, capacitance tuning is necessary to determine optimum capacitance value to obtain homogenous magnetic field distribution. In the simulation process, frequency domain analysis was used to find the optimal capacitance value at the Larmor frequency. Lumped ports were used to provide quadrature excitation. For low-pass birdcage coil, capacitors were placed accordingly to the type of coil to determine the resonant frequency and the uniformity of the field it produces. Boundary conditions were assigned to the surface of the coil elements and the outer boundary of the solution domain enclosing the coil geometry. Scattering boundary conditions were also used to avoid any electromagnetic wave reflection back to the coil. The coil surface and the RF shield around the coil were assigned the perfect electric conductor (PEC) condition. Firstly, air domain was used to study the performance of the low-pass birdcage coil. The homogeneity was attained by quadrature excitation and optimal capacitance values of lumped elements in the coil.

COMSOL Multiphysics allows us to specify more than one frequency in order to observe the variation of any electromagnetic field parameter with respect to the frequency. For instance, the return loss S_{11} can be inspected by running simulations for a range of frequencies (frequency sweep) to see where smaller return loss is occurred within specified capacitance value. In order to obtain both homogenous and circularly rotating B_1 field at the desired frequency, the capacitance was tuned by using the parametric sweep. The circularity of the field was evaluated by estimating the axial ratio of the magnetic field around the air phantom while the homogeneity of B_1 field, was calculated using the standard deviation of the electric field around phantom.

In the frequency domain analysis, quadrature excitation was used to obtain homogeneous and circularly polarized magnetic field in the birdcage coil by tuning the capacitors properly. Quadrature excitation was driven from two ports which are equal in magnitude but with a phase of 90^0 to generate circularly polarized field inside the coil. Quadrature excitation generates circularly polarized field which is more homogeneous than linear excitation as a result of equal currents distribution along the legs of the coil. In addition, quadrature driven birdcage coil is more power efficient compared with linear drive, by reducing the RF power requirement by a factor of two.

$$B_{linear} = B_1 \, cos(wt) \, x = (B_1^+) + (B_1^-) \tag{1}$$

where

$$B_1^{\pm} = \frac{B_1}{2}(cos\,(wt)x \pm sin\,(wt)y) \tag{2}$$

The first term represents a right-circularly polarized field while the second term represents left-circularly polarized field having equal magnitude of $B_1/2$.

Simulating The Low-Pass Birdcage Coil with The RF Marker Prototype

For the air phantom, we were able to get excellent magnetic field homogeneity and B_1 field circularity. However, it is necessary to check the alternation through the magnetic field homogeneity and B_1 field circularity when the RF marker coil is placed into the low-pass RF birdcage coil in MRI. Therefore, we

applied the same analysis while the designed RF coil marker was placed at the center of the low-pass birdcage coil domain. First optimum capacitance value was observed for the altered domain at the Larmor frequency. Secondly the effect of designed RF marker was examined with respect to the RF field homogeneity and B_1 field circularity.

First of all, precise geometry of the experimental fabricated RF marker prototype was built in model by using drawing tools in Comsol Multiphysics. Both geometric parameters of sketched RF marker in Figure 3 and properties of materials defined in Comsol Multiphysics, completely identical with the RF marker prototype implemented in laboratory studies.
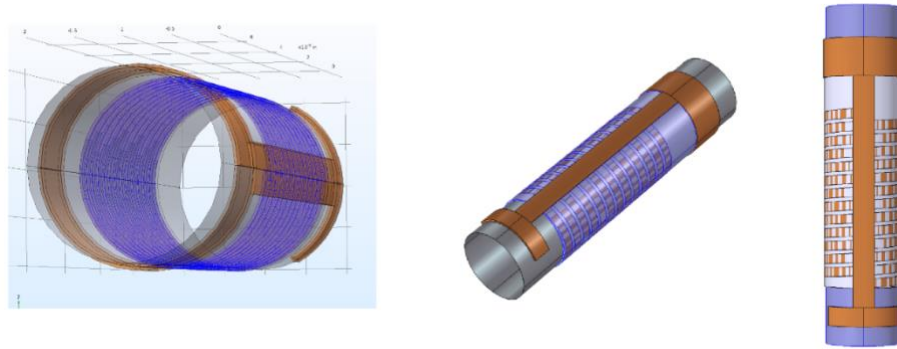
Figure 3. Dimensions of defined RF marker; radius: 1mm, number of turns of coil: 13, thickness of coil, capacitor plates and conductive layers: 30 μm, thickness of dielectric substance (Parylene C): 2.5 μm.

Designs of RF Coils

Helical Coil Design: In this part of this study, different RF coil in RF marker designs were performed to evaluate their performance into the birdcage coil in MRI platform. Figure 4 indicates one helical coil that can be used as a coil in a RF marker, while Figure 5 indicates designed helical RF coil placed into ASTM phantom that simulates a saline water filled tank.
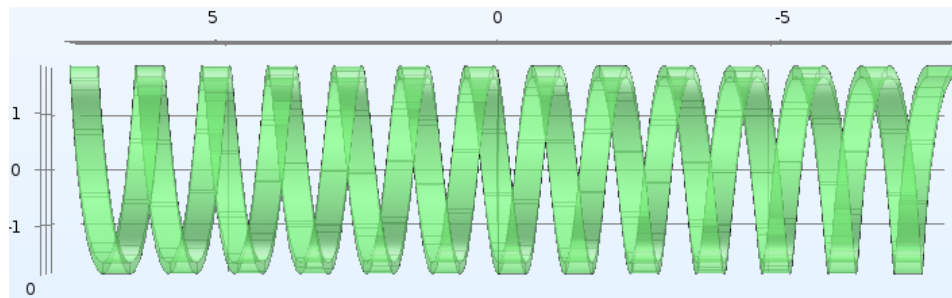
Figure 4. Designed helical RF coil image.

Geometric parameters of custom designed helical RF coil;

Radius of the RF marker coil	: 1.67 mm (length of 5 Fr catheter)
Length of the RF marker coil	: 5 mm
Number of the turns of the RF marker coil	: 13
Pitch between the two coil turns (wp)	: 100 μm
Width of each coil turn (ww)	: 200 μm

Figure 5. Image indicates designed helical RF coil placed into ASTM phantom that simulates a saline water filled tank with 5 cm width, 5 cm depth and 10 cm length.

Double Helical Coil Design: Figure 6 indicates double helical coil that can be used in a RF marker, while Figure 7 indicates designed double helical RF coil placed into ASTM phantom that simulates a saline water filled tank
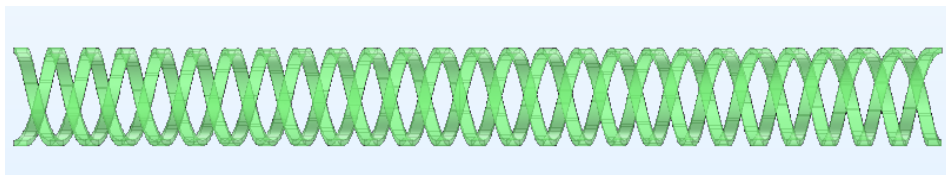
Figure 6. Image indicates designed double helical RF coils comprise 2 coils winded at the same direction but starting position of turns are different than each other.

Geometric parameters of custom designed double helical RF coil;

Radius of the RF marker coil   : 1.67 mm (length of 5 Fr catheter)
Length of the RF marker coil   : 3 cm
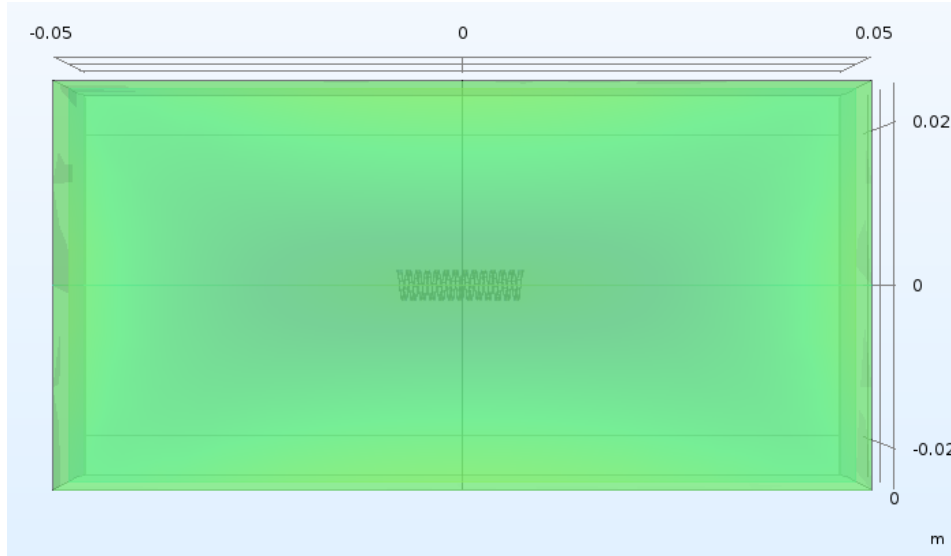Number of the turns of each coil   : 13
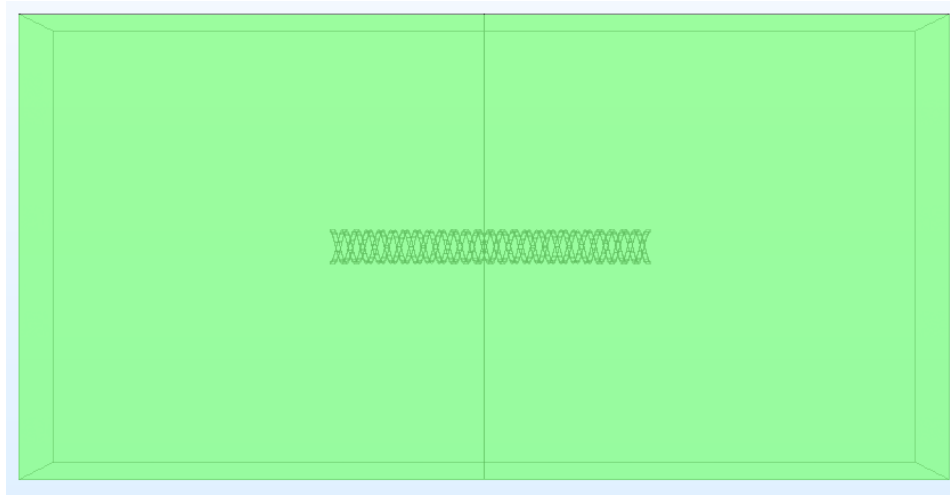
Figure 7. Image indicates designed double helical RF coil placed into ASTM phantom that simulates a saline water filled tank with 5 cm width, 5 cm depth and 10 cm length.

3. RESULTS & DISCUSSION

Simulating the Low-Pass Birdcage Coil without The RF Marker Prototype Capacitance Tuning Using Parametric Sweep

The designed birdcage coil has an inductor and many capacitors that have to resonate at the Larmor frequency of regarding MRI scanner. Initial tuning began by calculating the capacitance value, which is necessary for the coil to resonate at the desired frequency (63.8 MHz). Optimum capacitance value can be found by tuning the capacitor using a parametric sweep. The capacitance values range from 120 pF to 130 pF with a step capacitance of 0.5 pF were applied at 63.8 MHz, shown in Figure 8. The air phantom has a material property of electrical conductivity $\sigma = 0$ S/m, relative permeability $\mu r = 1$ and relative permittivity $\epsilon r = 1$.
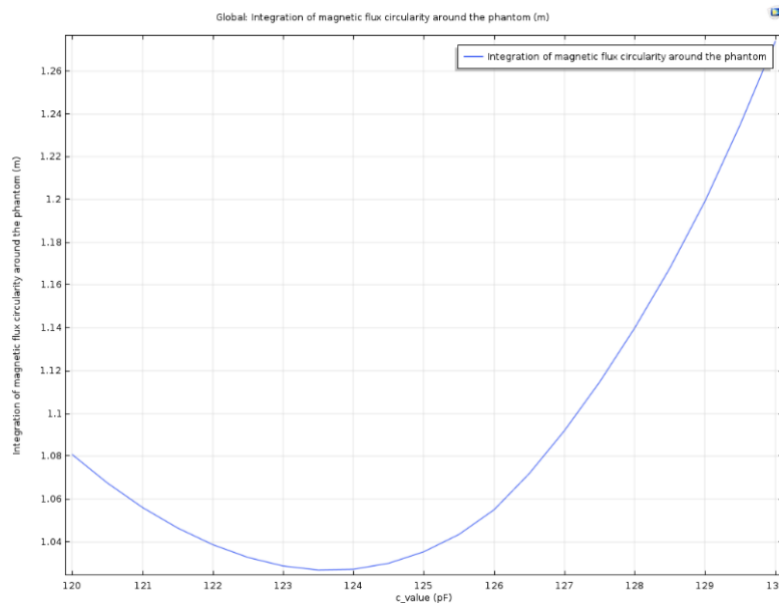
Figure 8. The axial ratio of the magnetic flux density for coil at 63.8 MHz (Larmor frequency of 1.5 Tesla MRI).

The circularity was evaluated by estimating the sum of the axial ratio of the magnetic field given as;

$$20 \log_{10}(B_{right} + B_{left})/(B_{right} - B_{left})) \tag{3}$$

where B_{left} denotes the left-hand rotating component of magnetic flux while B_{right} denotes the right-hand rotating component of magnetic flux.

Respectively the homogeneity of the field is calculated using the standard deviation of the electric field. The optimal capacitance value for field homogeneity is the same as that for circularity. It can be observed the optimal value of the capacitance is close to 123.5 pF as indicated in Figure 8.

**Magnetic Field Homogeneity Evaluation of the Low-Pass Birdcage Coil**

In order to evaluate the magnetic field homogeneity of the low-pass birdcage coil, a simulation was carried out for 8-leg low-pass birdcage coil loaded with air phantom as inspired studies mentioned before [4,5]. Capacitance value used on the rungs was 123.5 pF and the simulation frequency was 63.8 MHz. A homogenous magnetic field around the air phantom at 63.8 MHz was shown in Figure 9.

a) xy plane   b) yz plane   c) zx plane

Figure 9. Magnetic flux density distribution with real (red) and imaginary (blue) part of the magnetic flux density for coil at 63.8 MHz. a) indicates xy plane, b) indicates yz plane, c) indicates zx plane [4,5].

Simulating the Low-Pass Birdcage Coil with The RF Marker Prototype

Capacitance Tuning Using Parametric Sweep with The RF marker

Similar to the low-pass birdcage coil model without RF marker, optimum capacitance value was found by tuning the capacitor using a parametric sweep when designed RF marker was placed at the center of low-pass birdcage coil. The capacitance values range from 120 pF to 130 pF with a step capacitance of 0.5 pF were applied at 63.8 MHz as shown in Figure 10.
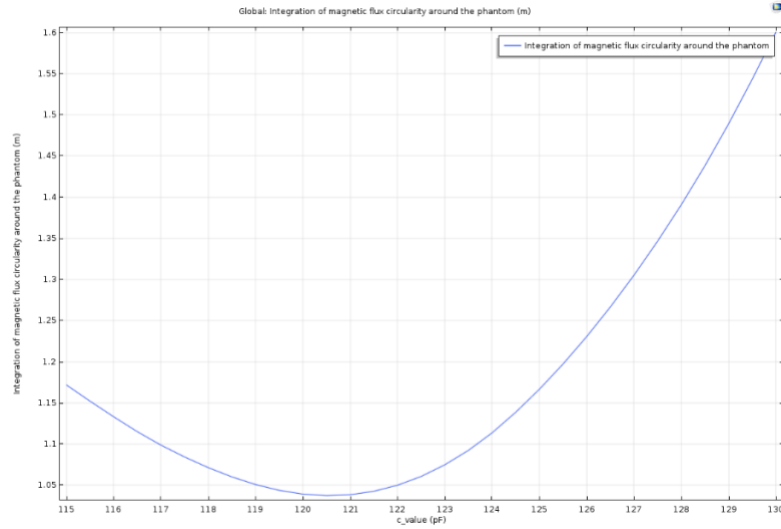
Figure 10. The axial ratio of the magnetic flux density for coil at 63.8 MHz (Larmor frequency of 1.5 Tesla MRI).

Magnetic Field Homogeneity Evaluation of the Low-Pass Birdcage Coil with The RF Marker

In order to analyze the effect of RF marker on magnetic field homogeneity, the simulation was run for 8-leg low-pass birdcage coil loaded with air phantom and RF marker prototype. Capacitance value used on the rungs was 120.5 pF and the simulation frequency was 63.8 MHz. A homogenous magnetic field both around the air phantom and RF marker at 63.8 MHz was shown in Figure 11.

a) xy plane   b) yz plane   c) zx plane

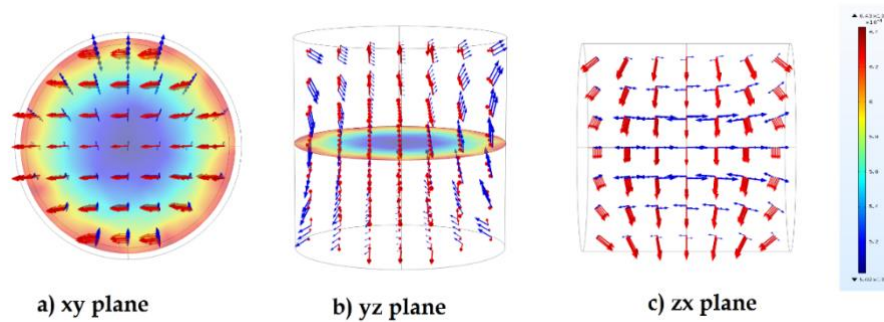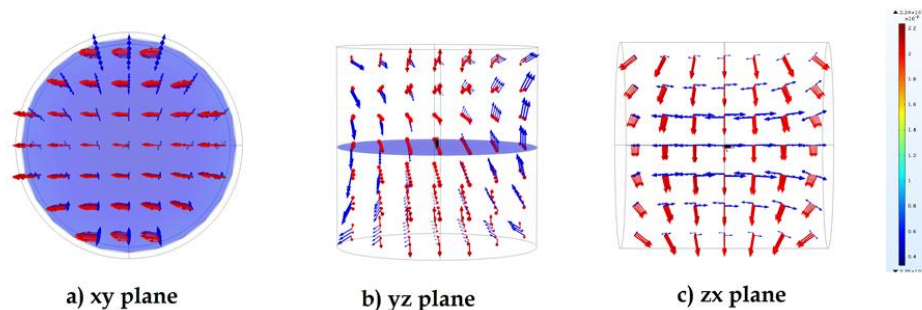**Figure 11.** Magnetic flux density norm distribution with real (red) and imaginary (blue) part of the magnetic flux density for coil at 63.8 MHz. a) indicates xy plane, b) indicates yz plane, c) indicates zx plane.

As it is noticed in Figure 11, existence of designed RF marker in the low-pass birdcage coil domain didn't cause a significant distortion on both homogeneity and circularity of B_1 field. However main reason for slightly alteration on the magnetic field homogeneity and circularity is RF marker induced additional non-uniform currents on the coil elements due to the different dielectric and permeability properties of the RF marker prototype.

Electric Fields Norm Analysis of Helical RF Coils in Different Designs

After validation of custom-made birdcage coil into MRI environment, orientation depended performance analysis of RF coils were performed into the birdcage coil. For this aim, electric field norms of 2 different RF coils into different orientations according to the birdcage coil were evaluated. Helical coil designs were constructed into virtual platform that have similar geometric size with real RF marker prototypes fabricated in experimental studies.

Electric Fields Norm Analysis of Single Helical RF Coil in Different Orientation

Electric fields norm of one helical RF coil into different orientations according to the birdcage coil were inspected as shown in Figure 12, in order to evaluate orientation dependency of the RF marker with respect to the standard MRI coils.

Figure 12. Image shows induced electric fields norm into the ASTM phantom and vicinity of the designed RF coil after the excitation of the birdcage coil at 63.8 MHz. Variation of electric field norms was observed when designed RF coil was a) parallel, b) 30^0 rotated, c) 45^0 rotated, d) 60^0 rotated, and e) perpendicular according to the birdcage coil. Red arrows show the direction of the electric field into volume of interest.

In Figure 12 the amount of electric field varies depending on the orientation of the RF coils. Electric field increases significantly with respect to the increase in rotation angle between the RF coil and the birdcage coil. The highest induced electric field is observed when the RF coil is placed perpendicular to the birdcage coil as it is expected in Maxwell's equations.

Similarly, with the excitation by the birdcage coil, electric field norms at the surface of the RF coil were examined in Figure 13. The most induced electric field was seen when the RF coil is oriented perpendicular to the birdcage coil.

Figure 13. Image shows induced electric field norms at the surface of the RF coil after the excitation by the birdcage coil. Electric field norms was observed when the designed RF coil was a) parallel, b) 30^0 rotated, c) 45^0 rotated, d) 60^0 rotated, and e) perpendicular according to the birdcage coil.

Electric Field Norm Analysis of Double Helical RF Coil in Different Orientation

Another orientation depended performance analysis of RF coil were performed into the birdcage coil by using a different geometric design. Electric fields norm of two helical RF coil into different orientations according to the birdcage coil were observed in Figure 14, in order to evaluate orientation dependency of RF markers with respect to the standard MRI coils.
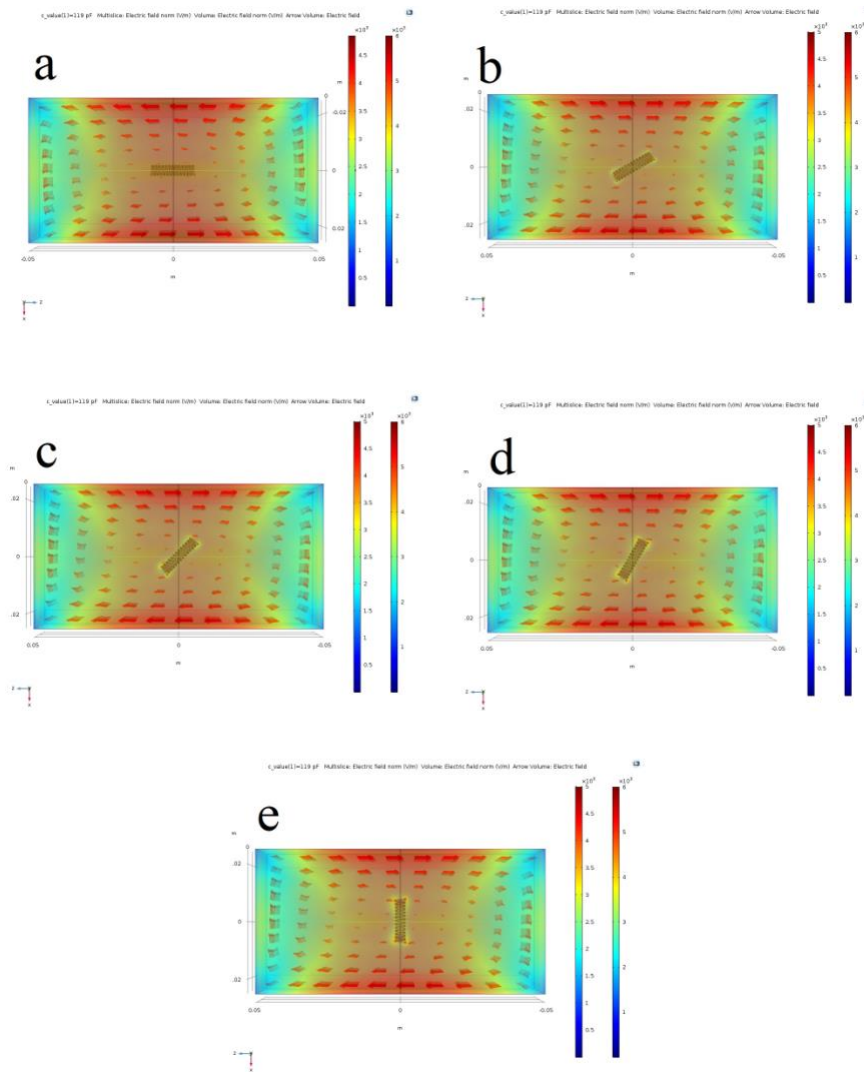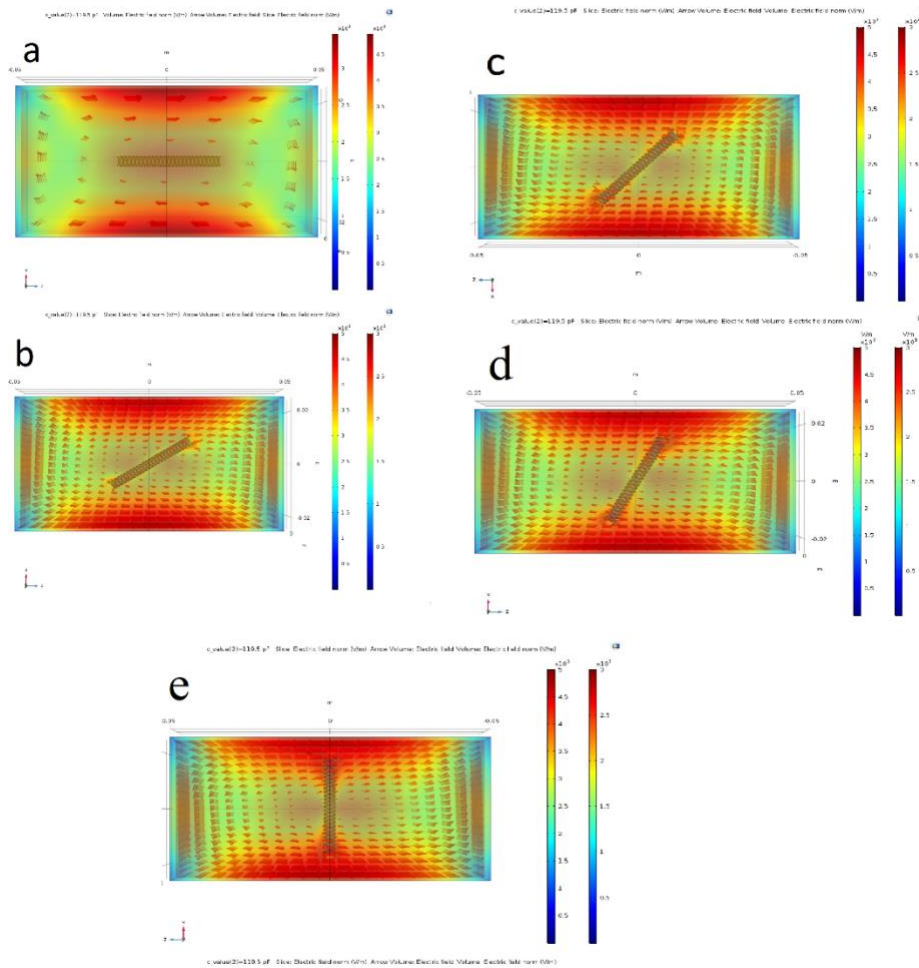
Figure 14. Image shows induced electric field norms into the ASTM phantom and vicinity of the designed double RF coil after the excittion of the birdcage coil at 63.8 MHz. Variation of electric field norms was observed when designed double RF coil was a) parallel, b) 30^0 rotated, c) 45^0 rotated, d) 60^0 rotated, and e) perpendicular according to the birdcage coil. Red arrows show the direction of the electric field into volume of interest.

Like single RF coil design, the amount of electric field varies depending on the orientation of the RF coils. Electric field increases significantly with respect to the increase in rotation angle between the double RF coil and the birdcage coil. The highest induced electric field is observed when the double RF coil is placed perpendicular to the birdcage coil as it is expected in Maxwell's equations.

Similarly, with the excitation by the birdcage coil, electric field norms at the surface of the double RF coil were examined in Figure 15. The most induced electric field was seen when the double RF coil is oriented perpendicular to the birdcage coil.
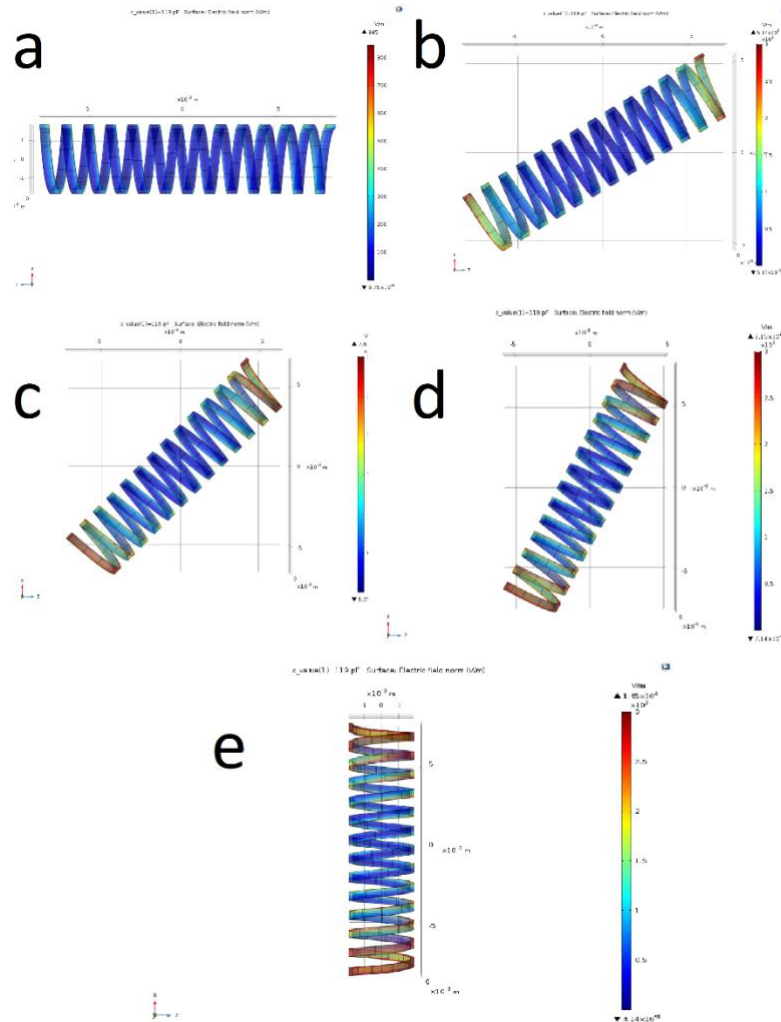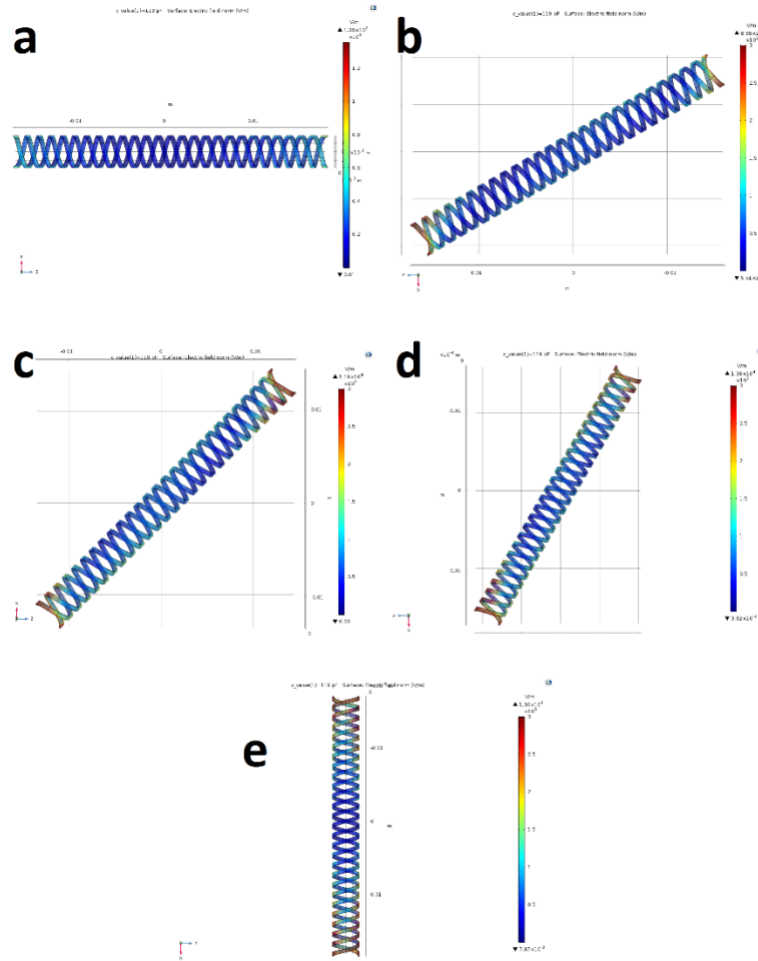
Figure 15. Image shows induced electric field norms at the surface of the double RF coil after the excitation by the birdcage coil. Electric fields norm was observed when the designed double RF coil was a) parallel, b) 30^0 rotated, c) 45^0 rotated, d) 60^0 rotated, and e) perpendicular according to the birdcage coil.

In conclusion, the results of simulations are consistent with former experimental works and results in the literature [1]. Although there are some difficulties at examining the interactions between micro size instruments and huge size environments such as micro coils and MRI platform, it is clear that the FEM simulations will be a reliable test and evaluation method in order to examine magnetic and electrical characteristics of designed RF coils and so RF markers.

4. CONCLUSION

In this study, 3D FEM modeling of manufactured RF marker prototype into a birdcage coil was figured out by using COMSOL Multiphysics software program. After ensuring the validation of performed MRI platform with compliance with ASTM phantom results, affectivity of the birdcage coil and MRI environment for 1.5 Tesla was examined with capacitance tuning. After obtaining optimum capacitance value, homogeneity of magnetic field was analyzed when the RF marker prototype was placed into center of the birdcage coil. Moreover, performances of 2 different RF coil designs were evaluated while coil designs were positioned into different orientation angles with respect to the birdcage coil.

Capability of the modeling the interactions between a RF marker and a birdcage coil into a MRI environment experienced in this study, will lead many new simulation designs including comparison of

different forms of RF markers, coil orientations and their characteristics. Accordingly, it is possible to construct custom made novel coil designs that can be used as a RF marker and as a standard MRI coil.

By providing these simulation models will be very beneficial for saving time to foresee the optimum coil parameters and RF marker performances without fabrication and real MRI experiments.

5. REFERENCES

1. Baysoy, E., Yildirim, D., Ozsoy, C., Mutlu, S., Kocaturk, O. (2016). Thin fillm based semi-active resonant marker design for low profile interventional cardiovascular MRI devices. Magnetic Resonance Materials in Physics, Biology and Medicine, 30(1), 93-101. Doi:10.1007/s10334-016-0586-8).

2. Lederman, R.J. (2006). NIH Public Access, 112(19), 3009-3017.

3. Barkhausen, J., Kahn, T., Krombach, G.A., Kuhl, C.K., Lotz, J., Maintz, D., Ricke, J., Schönberg, S.O., Vogl, T.J. and Wacker, F.K. (2017). White Paper: Interventional MRI: Current Status and Potential for Development Considering Economic Perspectives, Part 1: General Application. RoFo: Fortschritte auf dem Gebiete der Rontgenstrahlen und der Nuklearmedizin, 189(7), 611-623. Doi:10.1055/s-0043-110011.

4. Gurler, N. & Ider, Y.Z. (2015). Numerical methods and software tools for simulation, design, and resonant mode analysis of radio frequency birdcage coils used in MRI. Concepts Magn. Reson., 45, 13-32. Doi:10.1002/cmr.b.21279.

5. Tadesse, Y. (2015). The electromagnetic simulation of birdcage coils for MRI based on Finite element method. Master of degree thesis, Youngstown State University, Ohio, The United States of America.

6. Sonmez, M., Saikus, C.E., Bell, J.A., Franson, D.N., Halabi, M., Faranesh, A.Z., Ozturk, C., Lederman, R.J., Kocaturk, O. (2012). MRI active guidewire with an embedded temperature probe and providing a distinct tip signal to enhance clinical safety. Journal of Cardiovascular Magnetic Resonance, 14, 38. Doi:10.1186/1532-429X-14-38.

Determination of Exchangeable Cations and Residual Concentration of Herbicide Treated Soils and Analysis of The In-Vitro Biodegradation of The Herbicides

Research Article

Sebiomo Adewole[1]* iD , Banjo F.Mary

[1] Department of Biological Sciences, Tai Solarin University of Education Ijagun, Ijebu-Ode

Author E-mails
rev20032002@yahoo.com
*Correspondance to: Sebiomo Adewole, Department of Biological Sciences, Tai Solarin University of Education Ijagun, Ijebu-Ode
Tel: +2348077675121
DOI: 10.38061/idunas.759008

Abstract

This study determined the effect of Atrazine, Xtravest, Gramoxone and Glyphosate on exchangeable cations and also analysed the in-vitro biodegradation of this herbicides as well as assayed for their residual concentration in soils. Exchangeable cations were analysed in atomic absorption spectrophotometer. Utilisation of herbicides was determined while herbicide degradation and residual concentration of herbicide were analysed using Gas Chromatography. K+, Ca2+, Mg2+, and Na+ declined while Fe2+ and Zn+ accumulated significantly. Bacteria and fungi significantly utilised herbicides as carbon source resulting in herbicide degradation. The lowest herbicide concentration of 118.55 ppm was obtained from atrazine inoculated with bacteria, while the highest herbicide concentration of 449.23 ppm was obtained from xtravest inoculated with fungi. Bacteria and fungi such as: B. subtilis, P. aeruginosa, P. florescences, P. putida, Actinomyces viscous, A. niger, A. tamarii, F. oxysporum, and P. chrysogenum were isolated in all the herbicide treated soils. Continuous herbicide treatment should be avoided because of their ability to persist in soils hence limiting essential nutrients available to plants. Indigenous microorganisms can be employed to remediate soils polluted by herbicides.
Keywords: Cation exchange, Bacteria, Fungi, Herbicide, Biodegradation

1. INTRODUCTION

The population is constantly being exposed to increased use of crop protection products. The continual protection of plants and manufacture of synthetic chemicals, such as herbicides, widely contributed to the regularity of the production. However, today the systematic use of herbicides is questioned, with the increasing awareness of the risks, which they can generate for all the components of the environment, even for man health (Tahar et al., 2017). Toxicological consequences due to the exhibition

in these thousand chemical components by means of the food, water and ground are alarming. The sustainable agriculture involves optimizing agricultural resources and at the same time maintaining the quality of environment and sustaining natural resources. In achieving this optimization, the soil microbial community composition is of great importance, because they play a crucial role in carbon flow, nutrient cycling and litter decomposition, which in turn affect soil fertility and plant growth (Chauhan et al., 2006; Tripathi et al., 2006), and hence occupy a unique position in biological cycles in terrestrial habitat. The soil microbial biomass is considered as active nutrient pool to plants and plays an important role in nutrient cycling and decomposition in ecosystem (De-Lorenzo et al., 2001).

Herbicides are applied to control weeds in the crop field have direct (or) indirect consequences on non-targeted organisms including soil microflora. After application of herbicides, microorganisms are able to degrade and utilize them as energy source for their metabolic activities and also for physiological processes. While processing these activities there may be a chance of change in soil physicochemical characteristics. Diversified effect of both toxic and as well as beneficial effect of herbicides on soil microorganisms and soil characteristics were studied in different ways in the recent past (Trimurtulu et al., 2015).

The continuous use of environmentally persistent herbicides and other synthetic agricultural chemicals posed great risks to soil and water contamination. A viable alternative pesticide that is equally effective and less harmful to the environment is in demand (Souza et al., 2012). The persistence of a pesticide in the soil is defined as the period or extension of time in which it remains active.

There is serious concern about the increased use of herbicides, which may cause (i) environmental hazards such as water table and water body contamination, (ii) biological disruption in crop field populations, and (iii) reduced efficiency as a result of increased population of soil microorganisms more efficient in herbicide degradation. The herbicide that are used frequently eventually reach the soil from the crop plants and accumulates in top 0-15 cm layer of soil, where the activities of microbes are found to be maximum. Herbicides in the soil affect the non-target and beneficial microorganisms and their activities which are essential for maintaining soil fertility (Sethi et al., 2015).

Atrazine is a selective pre- and post- emergence herbicide providing knockdown and residual action. It has low rate of volatilization from soil and is moderately persistent (half-life of ~60 days). It is more persistent in neutral and alkaline soils than in soils with low pH. It is moderately mobile and able to be leached through soils into groundwater (Kruger et al., 1996). Metolachlor is a selective herbicide used in the control of grassy weeds in the cultivation of corn, soybeans, peanuts, cotton and other crops. Metolachlor is often used in combination with other broadleaved herbicides (e.g. atrazine, metobromuron and propazine) to extend the spectrum of activity (Ayansina and Oso, 2006). Glyphosate is a broad-spectrum systemic herbicide. It is nonvolatile, it is strongly adsorbed by soil particles and is essentially immobile in soil (AATSE, 2002). Paraquat is a broad-spectrum herbicide that destroys plant tissue by contact action. It is highly soluble in water and because of its ionic properties is strongly adsorbed by soil particles and is essentially immobile in soil. The strong binding of paraquat to clay minerals is the factor most likely associated with its long half-life in soils (Clive, 2006).

Fertilizers, pesticides, herbicides, and some other materials applied to soil often contribute to water and air pollution. Therefore, soil is a key component of environment chemical cycles. Dissolved mineral matter in soil is largely present as ions. Prominent among the cations are H^+, Ca^{2+}, Mg^{2+}, K^+, Na^+ and usually very low levels of Fe^{2+}, Mn^{2+} and Al^{3+}. Multivalent cations and anions form ion pairs with each other in soil, solutions (Maynard, 2000). Hence this study determined the effect of selected herbicides (Atrazine, Xtravest, Gramoxone and Glyphosate) on exchangeable cations and also analysed the in-vitro biodegradation of this herbicides as well as assayed for their residual concentration in soils after treatment.

2. MATERIALS AND METHODS

Soil Sampling

Soil samples were collected from depths of 0–15 cm. Samples were then mixed and homogenized. After removing recognizable plant debris, samples were air-dried and sieved through a 2-mm mesh sieve.

Study Site

The present study was carried out in the agricultural field located at Oke Odo Street Ago-Iwoye, Nigeria. The soils had no prior pesticide treatment. The site (open field) was divided into fifteen plots (5 m2 each) of land. The experiment was made up of five treatments which include control (no-treatment) and four herbicide treatments (atrazine, xtravest, glyphosate and gramoxone).

Herbicides

The herbicides used in this work were provided from a local agricultural dealership store in Ibadan, Nigeria. They were; Xtravest {atrazine[1-Chloro-3-ethylamino-5-isopropylamino-2,4,6-triazine, $C_8H_14CIN_5$] + metolachlor [2 -chloro -N- (2-ethyl-6-methylphenyl) -N- (1-methoxypropan-2-yl) acetamide], $C_{15}H_{22}CINO_2$, {27+15%} Suspo (SE)} (a product of Zhejiang Province Changxing First Chemical Co., Ltd., Xiaopu, Changxing, Zhejiang, China), Glyphosate [2,4-Dichlorophenoxyacetic acid, $C_3H_8NO_5P$] (Roundup, a product of Monsanto Europe S.A./N.V. Haven 627, Scheldelaan 460 2040 Antwerpen Belgium), Gramoxone [1,1-Dimethyl-4,4-bipyridinium dichloride, $C_{12}H_{14}C_{I2}N_2$] (Syngenta Crop Protection AG, Basle, Switzerland) and Atrazine [1-Chloro-3-ethylamino-5-isopropylamino-2,4,6-triazine, $C_8H_{14}CIN_5$] (Forward (Beihai) Hepu Pesticide Co. Ltd., 1, Quingshuijiang Liangzhou Hepu, Beihai, Guangxi, China, 536100).

Soil Treatments

The treatments were carried out in triplicates, using the complete randomized block design for a period of 8 weeks; at company recommended rates of 4 l/h (at 350 ml in 15 l sprayer). The herbicides were applied successively to the soils every week to the 8th week. Soil samples were then collected every 2 weeks to the 8th week of treatment. Fifteen soil samples were collected in separate polyethene bags every 2 weeks to the 8th week of treatment. A total of sixty soil samples were collected transported immediately to the laboratory for analysis.

Mineral Analysis

To 2.0 g of soil sample, 30ml of IN NH4OAC (ammonium acetate solution) was added and the flasks were shaken on a mechanical shaker for 2 h. Ca2+, Mg2+, K+, Na+ in soil samples were determined using the methods of Blakemore et al. (1987) and USDA, SCS (1972, 1982). Total wet digestion of soil samples in Nitric/Perchloric acid mixtures at ratio 2:1 was used to extract the Fe2+ and Zn+ from soil samples. Concentrations of Ca2+, K+, Na+, Mg2+, Fe2+ and Zn+ were determined in Atomic Absorption Spectrophotometer fitted with a hollow cathode lamp and a fuel rich flame (air acetylene), using the methods of Blakemore et al. (1987) and USDA, SCS (1972, 1982).

Atomic Absorption Spectrophotometry

The atomic absorption spectrophotometer consisted of a premix burner (water cooled, fishtail type) with a 10×0.05 cm2 slot. In addition, a monochromator with a diffraction grating of 1800 grooves/mm, wavelength range of 190 - 900 nm, focal length of 450 nm and giving an average dispersion of 1.2 nm/mm was positioned. An air– acetylene flame was used with an oxidant pressure of 1.60 kg/cm2. As a source of radiation, neon-filled hollow cathode lamps were used. Firstly, a blank solution was run by the instrument to retrieve the background signals. Then standard solutions of each element were measured to optimize the instrument response, and finally sample solutions of soil samples were analyzed in order to determine the concentration of each mineral element. Lead, nickel, cadmium and chromium composition was determined by electro-thermal atomic absorption spectroscopy. The analysis of Ca^{2+}, K^+, Na^+, Mg^{2+}, Fe^{2+} and Zn^+ was done by flame atomic absorption spectroscopy.

Determination of The Concentration of Residual Herbicides in Soils After Treatment Using Gas Chromatography

The modified method as described by Ayanthi et al. (2008) was used in sample preparation and extraction. The soil samples were homogenised. Extraction was carried out using 10g of the sample by adding acetone to sample bound water so that agglomeration of samples during extraction could be minimised, toluene was then added in equal volume of acetone and the samples were agitated using mechanical shaker. The samples were then filtered using vacuum filtration. Acetone was driven off leaving toluene in the mixture. Organic phase was drained using anhydrous sodium sulphate to remove the associated water during extraction. Methanol was added to dissolve the remaining analytes in the solid phase extracted. The filterate of the methanol and toluene phase was added together and then allowed to concentrate to about 2.0ml. The extract was loaded to pre-conditioned C-18 Mega Bond Elut cartridge. The analytes were eluted from the cartridge with ethyl acetate. The extract was collected and then concentrated with nitrogen stream to about 2.0 ml before gas chromatography analysis was used for the analysis. One micro-litre was injected into the Hewlett Packard Gas Chromatography (HP 6890 Powered with HP ChemStation Rev. A 09.01 [1206] Software).

Isolation of Herbicide Utilizing Bacteria and Fungi

Five grams of each soil sample was suspended in 250-ml Erlenmeyer flasks containing a mixture of 50 ml of mineral salts medium and 1 ml of each herbicide in separate flasks. This concentration was used because it is equivalent to the field application rate. The flasks were incubated on a rotary shaker (Gallenkamp, England) at 120 rpm for 7 days at 30°C. Isolation was then carried out using the spread plate method on the solid mineral salts medium with each herbicide added to separate plates. The plates were incubated at 30°C for 5 days for bacteria and 30°C for 7days for fungi. Morphologically distinct colonies of indigenous microbial isolates of bacteria and fungi isolated on nutrient agar for bacteria and potato dextrose agar for fungi respectively were used in the herbicide utilization experiments. Identity of the bacterial isolates was affirmed after characterization by standard bacteriological methods (Holt et al., 1994; Cheesbrough, 1984) while the fungal isolates were identified using morphological and cultural characteristics.

Determination of the Abilities of Bacteria and Fungi to Utilize Selected Herbicides

The ability of microbial isolates (bacterial consortium and fungal consortium) to utilise herbicide substrates as carbon source (atrazine, xtravest, glyphosate and gramoxone) in pure cultures were determined in minimal salt medium (g/l) (Moneke et al., 2010). The components were dissolved in 1000ml distilled

water, homogenized on hot plate magnetic stirrer to form uniform solution for 30 min. The pH of the basal medium was adjusted to pH 7.2. The basal medium of 150 ml was dispensed into 250 ml Erlenmeyer flasks and herbicide substrates were introduced into each flask respectively at 100 ppm after sterilisation which was done separately in an autoclave at 121°C for 15 min and cooled to ambient temperature. One ml aliquot of diluted overnight broth cultures of each test organisms ($\times 10^4$ cells/ml) were seeded into each flask respectively and the flasks were incubated in a gyratory shaker incubator at 150 rpm for a period of thirty days at 30°C (Bacterial isolates used in this study were those that had the highest turbidity, while the fungal isolates used in this study were those that had the highest counts on each of the herbicides). Utilisation of herbicides by microbial isolates were evaluated by monitoring bacterial and fungal growth using viable count on nutrient and potato dextrose agars, fungal dry-weights, optical density of bacteria and pH.

Determination of *in-vitro* Biodegradation of Herbicides by Bacteria and Fungi

The ability of herbicide degrading bacteria and fungi to degrade pure herbicide substrates was tested in minimal salt medium in 100 ml flasks using the method of Moneke et al. (2010). The flasks were then autoclaved and inoculated with 1.0 ml portion of each isolate (except one which serves as control). The flasks were subsequently incubated in an orbital shaker incubator at 150 rev/min at 30°C for 7days. Gas chromatography analysis was then used to determine the remaining herbicide after 7 days of incubation, in the orbital shaker incubator, using the method of Ayanthi et al. (2008) already described above.

Statistical Analysis

The data were statistically analysed, with SPSS 20 software, using a one-way analysis of variance (ANOVA). Means were compared at 5% level of significance using Duncan's multiple range test.

3. RESULTS

Pseudomonas spp and *Bacillus* spp were found to be of common occurrence in herbicide treated soils. *B. subtilis, P. aeruginosa, P. florescences, P. putida* and *Actinomyces viscous* were isolated in all the herbicide treated soils. Meanwhile fungi such as *Aspergillus, Fusarium* and *Penicillum* species were of common occurrence in all the herbicide treated soils. *A. niger, A. tamarii, F. oxysporum,* and *P. chrysogenum* were isolated in all the herbicide treated soils.

Microbiological and Physicochemical Properties of Soil at the Experimental Site

Presented in Table 1 are the microbiological and physicochemical properties of the soil at the experimental site before treatment with herbicides. Table 2 shows the effect of herbicide treatment on exchangeable Ca^{2+}, Mg^{2+}, K^+, Na^+, Fe^{2+} and Zn^+ in soil samples.

Table 1: Microbiological and physicochemical properties of soil at the experimental site

Soil properties	Values
Soil type	Ferric luvisols
Bacterial count (CFU/g$\times 10^5$)	9.70
Fungal count (CFU/g$\times 10^5$)	1.10
Actinomycetes count (CFU/g$\times 10^5$)	0.80
Total nitrogen (%)	0.12
Available phosphorus (ppm)	10.0
Organic carbon (%)	1.42
Sodium (Na) (cmolkg^{-1})	0.42
Potassium (K) (cmolkg^{-1})	0.44

Calcium (cmolkg^{-1})	4.62
Magnesium (Mg) (cmolkg^{-1})	1.41
Iron (Fe) (cmolkg^{-1})	1820
Zinc (Zn)(cmolkg^{-1})	19
Soil electrical conductivity (μS/cm)	250
pH	6.80
Soil moisture (%)	18.32
Sand (%)	67.6
Silt (%)	20
Clay (%)	12.4

Exchangeable Cations (cmolkg-1) of Soil Samples Obtained at the 2nd, 4th, 6th, and 8th Weeks of Herbicide Treatment

Exchangeable Na$^+$ declined considerably in atrazine, gramoxone and xtravest treated soils from the 2nd to the 8th week. Glyphosate treated soils had the highest exchangeable Na$^+$ content of 0.67 cmolkg^{-1}at the 6th week, while soils treated with gramoxone recorded the lowest exchangeable Na$^+$ value of 0.19 cmolkg^{-1} at the 8th week. In glyphosate treated soils exchangeable K$^+$ accumulated from the 2nd (0.78 cmolkg^{-1}) to the 6th (1.31 cmolkg^{-1}) weeks of treatment. Glyphosate treated soils had the highest exchangeable K$^+$ value of 1.31 cmolkg^{-1} at the 6th week while gramoxone treated soil samples recorded the lowest exchangeable K$^+$ value of 0.1 cmolkg^{-1} at the 8th week of treatment (Table 2). Soils treated with atrazine recorded the highest exchangeable Ca^{2+} value of 8.44 cmolkg^{-1} at the 6th week of treatment while soils treated with glyphosate and gramoxone had the lowest calcium content value of 3.27 cmolkg^{-1} at the 4th week of treatment (Table 2). Statistical analysis showed that treatment with the herbicide types resulted in significant changes at the 2nd ($p \leq 0.001$), 4th ($p \leq 0.004$), 6th ($p \leq 0.000$) and 8th ($p \leq 0.000$) weeks, in values of exchangeable Mg^{2+}. Glyphosate treated soils had the lowest exchangeable Fe^{2+} value of 2643 cmolkg^{-1} while gramoxone treated soils had the highest exchangeable Fe^{2+} value of 5862 cmolkg^{-1} at the 2nd week. Soils treated with glyphosate had the highest exchangeable Zn$^+$ value of 81.77cmolkg^{-1} at the 8th week of treatment. Glyphosate and xtravest treated soils had the lowest value of 29 cmolkg^{-1} at the 2nd week of treatment (Table 2).

Table 2: Exchangeable cations (cmolkg^{-1}) of soil samples obtained at the 2nd, 4th, 6th, and 8th weeks of herbicide treatment

		2ND WK	4TH WK	6TH WK	8TH WK
Na	CON	0.480±0.017^{bc}	0.550±0.075^{b}	0.440±0.015^{b}	0.280±0.017^{b}
	GLY	0.550±0.003^{c}	0.560±0.015^{b}	0.670±0.031^{c}	0.430±0.019^{c}
	ATR	0.420±0.009^{a}	0.260±0.009^{a}	0.260±0.018^{a}	0.220±0.006^{a}
	GRA	0.480±0.007^{b}	0.360±0.006^{a}	0.300±0.015^{a}	0.190±0.015^{a}
	XTR	0.490±0.015^{b}	0.330±0.015^{a}	0.280±0.009^{a}	0.210±0.003^{a}
K	CON	0.480±0.023^{b}	0.460±0.006^{c}	0.600±0.029^{b}	0.420±0.009^{b}
	GLY	0.780±0.012^{c}	0.880±0.009^{d}	1.310±0.047^{c}	0.800±0.032^{c}
	ATR	0.280±0.000^{a}	0.190±0.015a	0.270±0.006^{a}	0.120±0.020^{a}
	GRA	0.510±0.012^{b}	0.230±0.021^{b}	0.200±0.015^{a}	0.100±0.007^{a}
	XTR	0.500±0.015^{b}	0.430±0.000^{c}	0.250±0.021^{a}	0.140±0.012^{a}
Ca	CON	4.730±0.121^{a}	4.140±0.020^{c}	7.680±0.277^{c}	6.730±0.064^{b}
	GLY	4.960±0.037^{a}	3.270±0.038^{a}	5.650±0.165^{a}	6.070±0.035^{a}
	ATR	4.710±0.055^{a}	3.320±0.064^{a}	8.440±0.009^{d}	6.620±0.118^{b}

	GRA	5.130 ± 0.121^a	3.270 ± 0.038^a	6.790 ± 0.105^b	6.080 ± 0.064^a
	XTR	4.100 ± 0.078^a	4.010 ± 0.009^b	6.860 ± 0.032^b	6.310 ± 0.055^a
Mg	CON	1.480 ± 0.003^c	0.970 ± 0.072^b	1.990 ± 0.006^c	1.800 ± 0.020^c
	GLY	1.430 ± 0.010^{bc}	0.940 ± 0.012^b	2.720 ± 0.092^d	1.930 ± 0.037^d
	ATR	1.400 ± 0.012^b	0.780 ± 0.061^a	1.520 ± 0.006^b	1.360 ± 0.050^a
	GRA	1.490 ± 0.026^c	0.770 ± 0.012^a	1.140 ± 0.064^a	1.380 ± 0.040^a
	XTR	1.330 ± 0.029^a	1.040 ± 0.000^b	1.430 ± 0.069^b	1.500 ± 0.028^b
Fe	CON	1956 ± 182^a	3976 ± 183^a	5031 ± 223^c	4990 ± 491^a
	GLY	2643 ± 44^a	4049 ± 104^a	4283 ± 85^{ab}	4926 ± 6^a
	ATR	4087 ± 441^b	4463 ± 60^b	3888 ± 165^a	4605 ± 77^a
	GRA	5862 ± 512^c	4579 ± 68^b	4698 ± 34^{bc}	5348 ± 204^a
	XTR	5216 ± 379^c	4666 ± 65^b	5002 ± 55^c	4933 ± 150^a
Zn	CON	28.670 ± 0.880^a	40.670 ± 2.030^a	69.670 ± 0.880^d	90.000 ± 2.020^e
	GLY	29.000 ± 0.580^a	41.670 ± 1.450^a	63.000 ± 0.580^c	81.770 ± 1.590^d
	ATR	31.000 ± 0.580^a	62.670 ± 2.030^b	57.000 ± 2.000^b	61.270 ± 1.300^b
	GRA	44.670 ± 1.450^b	62.770 ± 0.720^b	46.930 ± 1.440^a	44.270 ± 0.720^a
	XTR	29.000 ± 1.730^a	67.770 ± 1.010^c	65.000 ± 0.000^c	73.000 ± 1.150^c

CON=Control, GLY= Glyphosate, ATR= Atrazine, GRA= Gramoxone, XTR= Xtravest, WK=Week. Columns with values that have the same letter show that there are no significant differences($p\geq0.05$) between the values; columns with values that have different letters show that there is a significant difference ($p\leq0.05$) between the values.

Changes in Viable Counts ([CFU/g] $\times10^5$) of Bacteria During Biodegradation

There were significant increases ($p\leq0.000$) in viable counts from the 2nd to the 12th day and at the 14th day ($p\leq0.001$) at the 2nd week. Glyphosate had the highest viable count value of 10.80×10^5 CFU/g at the 6th day of incubation, while xtravest recorded the lowest viable count value of 6.37×10^5 CFU/g at the 14th day (Table 3). Xtravest had lower viable count values between the 8th and 14th day compared to the control. Although all viable count values at the 2nd week dropped from the 6th to the 14th day. Glyphosate recorded the highest viable count of 12.76×10^5 CFU/g at the 10th day of incubation (Table 3). Control soil samples had lower viable count values than those of the herbicides.

Changes in Optical Density of Bacteria During Biodegradation

Optical density values increased significantly ($p\leq0.000$) from the 2nd to the 14th day at the 2nd week. Gramoxone had the lowest optical density value of 0.885 and 0.955 at the 2nd and 14th days of incubation respectively at the 8th week herbicide types had significant effect ($p\leq0.000$) on optical density values from the 2nd to the 14th day. Optical density values for control and glyphosate reduced from the 2nd to the 14th day. Xtravest had the highest optical density value of 0.974 at the 14th day of incubation. Atrazine had the lowest optical density value of 0.913 at the 2nd day of incubation, while at the 14th day of incubation glyphosate had the lowest optical density value of 0.929 (Table 4).

Table 3: Changes in viable counts ($[CFU/g] \times 10^5$) of bacteria during biodegradation

		2ND	4TH	6TH	8TH	10TH	12TH	14TH
2ND WK	CON	8.17±0.033a	8.57±0.033a	8.75±0.003a	7.37±0.088a	6.63±0.133a	6.84±0.003b	6.76±0.019ab
	GLY	10.33±0.067e	10.65±0.029e	10.80±0.000e	9.60±0.000d	8.20±0.118c	7.85±0.087d	7.38±0.053c
	ATR	9.83±0.033d	10.03±0.033d	10.41±0.007d	8.20±0.000b	7.34±0.125b	7.20±0.153bc	7.13±0.167bc
	XTR	8.65±0.047b	8.72±0.017b	8.94±0.020b	7.28±0.600a	6.53±0.203a	6.43±0.203a	6.37±0.233a
	GRA	9.33±0.067c	9.81±0.007c	9.90±0.000c	8.50±0.000c	7.66±0.030b	7.54±0.037cd	7.43±0.033c
4TH WK	CON	8.33±0.133a	8.73±0.133a	9.00±0.115a	6.83±0.015a	6.83±0.015a	6.73±0.015b	6.67±0.037c
	GLY	9.97±0.033c	10.30±0.058d	10.52±0.044d	9.38±0.028d	7.88±0.061c	7.45±0.024c	7.17±0.033d
	ATR	9.81±0.007c	10.03±0.033c	10.41±0.007d	9.22±0.012d	8.55±0.029d	8.37±0.033d	8.03±0.033e
	XTR	8.41±0.007a	8.87±0.067a	9.22±0.017b	8.13±0.033c	7.23±0.088b	6.89±0.047b	6.37±0.035b
	GRA	9.10±0.058b	9.38±0.017b	9.67±0.017c	7.57±0.145b	7.10±0.153b	6.43±0.120a	6.10±0.058a
6TH WK	CON	7.33±0.033a	7.43±0.033a	7.57±0.033a	7.63±0.033a	7.70±0.058a	7.57±0.033a	7.37±0.033a
	GLY	11.33±0.176d	11.41±0.174d	11.50±0.173d	11.60±0.173d	11.67±0.145d	11.57±0.145d	11.3±0.058d
	ATR	10.13± 0.133c	10.23±0.088c	10.33±0.088c	10.40±0.100c	11.43±0.033d	11.33±0.067d	11.03±0.033d
	XTR	8.87±0.037b	8.87±0.033b	9.20±0.058b	9.30±0.000b	9.43±0.033b	9.17±0.033b	8.80±0.200b
	GRA	10.10±0.153c	10.20±0.153c	10.37±0.088c	10.43±0.067c	10.53±0.067c	10.10±0.058c	9.30±0.058c
8TH WK	CON	7.50±0.000a	7.57±0.033a	7.67±0.033a	7.83±0.033a	7.83±0.033a	7.67±0.033a	7.37±0.033a
	GLY	12.23±0.145e	12.37±0.145e	12.47±0.133e	12.67±0.033e	12.77±0.033e	12.53±0.033e	12.17±0.033d
	ATR	10.57±0.088c	10.60±0.058c	10.70±0.000c	10.87±0.033c	11.00±0.058c	10.67±0.176c	9.67±0.176c
	XTR	9.33±0.067b	9.57±0.088b	9.67±0.088b	9.80±0.058b	9.83±0.033b	9.60±0.000b	9.07±0.033b
	GRA	10.83±0.033d	10.90±0.000d	11.00±0.000d	11.47±0.033d	11.60±0.058d	11.00±0.000d	9.90±0.058c

CON=Control, GLY= Glyphosate, ATR= Atrazine, GRA= Gramoxone, XTR= Xtravest, WK=Week. Columns with values that have the same letter show that there are no significant differences($p \geq 0.05$) between the values; columns with values that have different letters show that there is a significant difference ($p \leq 0.05$) between the values.

Table 4: Changes in optical density of bacteria during biodegradation

		2ND	4TH	6TH	8TH	10TH	12TH	14TH
2ND WK	CON	0.882±0.001a	0.886±0.001a	0.891±0.001a	0.893±0.001a	0.894±0.001a	0.896±0.001a	0.898±0.001a
	GLY	0.941±0.001b	0.945±0.001c	0.956±0.001c	0.961±0.001c	0.971±0.001d	0.976±0.002c	0.984±0.003c
	ATR	0.894±0.001a	0.903±0.003b	0.924±0.000b	0.941±0.001b	0.961±0.001c	0.970±0.002c	0.985±0.003c
	XTR	0.954±0.002c	0.965±0.001d	0.975±0.001d	0.983±0.001d	1.043±0.001e	1.045±0.001d	1.046±0.001d
	GRA	0.885±0.008a	0.887±0.001a	0.892±0.001a	0.895±0.001a	0.917±0.003b	0.938±0.004b	0.955±0.003b
4TH WK	CON	0.881±0.001a	0.888±0.000a	0.893±0.001a	0.895±0.001a	0.895±0.001a	0.898±0.001a	0.910±0.006a
	GLY	0.945±0.001c	0.947±0.001c	0.961±0.002c	0.965±0.001c	0.975±0.001d	0.977±0.001d	0.981±0.001d
	ATR	0.897±0.001b	0.909±0.003b	0.928±0.001b	0.945±0.001b	0.963±0.001c	0.967±0.002c	0.969±0.002c
	XTR	0.956±0.002d	0.956±0.002d	0.977±0.001d	0.986±0.000d	1.047±0.001e	1.138±0.001e	1.143±0.002e
	GRA	0.887±0.007ab	0.887±0.007a	0.894±0.001a	0.896±0.001a	0.925±0.004b	0.931±0.004b	0.939±0.003b
6TH WK	CON	0.885±0.001a	0.887±0.001a	0.890±0.001a	0.892±0.001a	0.898±0.001a	0.993±0.001c	1.086±0.031a
	GLY	0.946±0.002d	0.949±0.003d	0.952±0.003d	0.954±0.003c	0.960±0.003c	0.965±0.002ab	1.357±0.027b
	ATR	0.907±0.004b	0.915±0.001b	0.920±0.001b	0.930±0.001b	0.942±0.001b	0.971±0.004b	1.426±0.003c
	XTR	0.964±0.002e	0.967±0.001e	0.968±0.001e	0.972±0.001d	0.976±0.001d	0.988±0.001c	1.465±0.002c
	GRA	0.934±0.007c	0.937±0.007c	0.939±0.006c	0.936±0.003b	0.943±0.003b	0.956±0.004a	1.330±0.006b
8TH WK	CON	0.980±0.000e	0.980±0.000e	0.977±0.002e	0.970±0.000d	0.970±0.000d	0.961±0.001d	0.961±0.001d
	GLY	0.951±0.001c	0.950±0.000c	0.950±0.000c	0.941±0.001b	0.938±0.001b	0.931±0.001a	0.929±0.001a
	ATR	0.913±0.004a	0.917±0.002a	0.925±0.001a	0.927±0.001a	0.931±0.001a	0.935±0.001b	0.938±0.000b
	XTR	0.968±0.001d	0.963±0.001d	0.964±0.000d	0.966±0.000c	0.969±0.001d	0.971±0.000e	0.974±0.001e
	GRA	0.941±0.001b	0.940±0.000b	0.942±0.000b	0.943±0.001b	0.945±0.001c	0.945±0.000c	0.949±0.001c

CON=Control, GLY= Glyphosate, ATR= Atrazine, GRA= Gramoxone, XTR= Xtravest, WK=Week. Columns with values that have the same letter show that there are no significant differences($p \geq 0.05$) between the values; columns with values that have different letters show that there is a significant difference ($p \leq 0.05$) between the values.

Changes in Fungal Counts ([CFU/g] $\times 10^4$) During Biodegradation

Treatment with the herbicide types at the 2nd week showed significant changes ($p \leq 0.009$; $p \leq 0.005$; $p \leq 0.004$; $p \leq 0.000$; $p \leq 0.001$) in fungal counts at the 5th, 10th, 15th, 20th and 25th days respectively (Table 5). Fungal counts increased from the 5th day to the 20th day and dropped on the 25th day. xtravest had the lowest fungal count of 3.30×10^4 CFU/g at the 5th day. At the 8th week, significant changes ($p \leq 0.001$; $p \leq 0.002$; $p \leq 0.001$; $p \leq 0.005$; $p \leq 0.002$) in fungal counts occurred at 5th, 10th, 15th, 20th and 25th days of incubation respectively. Fungal counts increased from the 5th to the 15th days and then decreased from the 20th to the 25th day. Xtravest had the highest fungal count value of 1.17×10^5 CFU/g at the 15th day, while at the 5th day gramoxone had the lowest fungal count value of 4.00×10^4 CFU/g. At the 25th day gramoxone recorded the lowest fungal count value of 3.30×10^4 CFU/g.

Changes in Fungal dry-weights During Biodegradation

In Table 6, at the 2nd, 4th and 8th weeks, fungal dry weight values increased from the 5th to the 20th days and then dropped at the 25th day. At the 2nd week, fungal dry weight showed significant changes ($P \leq 0.000$) in values from the 5th to the 25th day (Table 6). At the 20th day xtravest recorded the highest fungal dry weight value of 0.020 g. At the 25th day gramoxone recorded the lowest fungal dry weight of 0.012 g. There were significant changes ($p \leq 0.000$) in fungal dry weight values from the 5th to the 25th days at the 8th week. Atrazine had the highest fungal dry weight value of 0.022 g at the 20th day while gramoxone and glyphosate had the lowest value of 0.012 g at the 5th day. At the 25th day gramoxone had the lowest value of 0.012 g (Table 6).

Table 5: Changes in fungal counts ([CFU/g] $\times 10^4$) during biodegradation

		5TH	10TH	15TH	20TH	25TH
2ND WK	CON	4.30 ± 0.033^a	5.70 ± 0.033^{ab}	8.00 ± 0.058^a	9.30 ± 0.067^{ab}	8.70 ± 0.033^a
	GLY	5.70 ± 0.033^b	7.70 ± 0.033^c	10.70 ± 0.088^b	13.70 ± 0.033^c	11.00 ± 0.058^b
	ATR	4.30 ± 0.033^a	6.30 ± 0.033^{ab}	8.30 ± 0.033^a	10.30 ± 0.033^b	8.70 ± 0.033^a
	XTR	3.30 ± 0.033^a	5.30 ± 0.033^a	6.70 ± 0.033^a	8.70 ± 0.033^a	7.70 ± 0.033^a
	GRA	4.30 ± 0.033^a	6.70 ± 0.033^{bc}	8.00 ± 0.000^a	12.70 ± 0.033^c	10.30 ± 0.033^b
4TH WK	CON	3.30 ± 0.033^a	5.70 ± 0.033^{ab}	6.70 ± 0.033^a	4.70 ± 0.033^{bc}	3.00 ± 0.000^{ab}
	GLY	4.70 ± 0.033^b	6.00 ± 0.000^{bc}	6.30 ± 0.033^a	4.00 ± 0.000^{ab}	2.30 ± 0.033^a
	ATR	4.30 ± 0.033^b	5.70 ± 0.03^{ab}	7.00 ± 0.058^{ab}	3.30 ± 0.033^a	2.70 ± 0.033^a
	XTR	5.70 ± 0.033^c	7.00 ± 0.058^c	8.00 ± 0.000^b	5.70 ± 0.033^{cd}	4.30 ± 0.033^c
	GRA	3.00 ± 0.000^a	4.70 ± 0.033^a	6.70 ± 0.033^a	5.00 ± 0.000^d	3.70 ± 0.033^{bc}
6TH WK	CON	4.00 ± 0.000^{ab}	4.70 ± 0.033^a	4.70 ± 0.033^b	4.30 ± 0.033^b	2.70 ± 0.033^a
	GLY	5.00 ± 0.000^{bc}	5.30 ± 0.033^{ab}	5.70 ± 0.067^{ab}	4.00 ± 0.000^{ab}	2.30 ± 0.033^a
	ATR	5.30 ± 0.067^c	5.70 ± 0.120^{ab}	6.00 ± 0.115^a	3.30 ± 0.033^a	1.70 ± 0.033^a
	XTR	6.70 ± 0.033^d	7.00 ± 0.058^b	6.70 ± 0.067^c	4.70 ± 0.033^b	2.70 ± 0.033^a
	GRA	3.00 ± 0.000^a	4.00 ± 0.000^a	4.30 ± 0.033^{ab}	4.00 ± 0.000^{ab}	2.00 ± 0.000^a
8TH WK	CON	5.70 ± 0.033^b	6.70 ± 0.033^{ab}	7.00 ± 0.058^a	4.30 ± 0.033^a	3.70 ± 0.033^a
	GLY	6.70 ± 0.033^b	7.70 ± 0.033^b	8.30 ± 0.067^a	6.30 ± 0.067^{ab}	4.70 ± 0.033^{ab}
	ATR	6.70 ± 0.088^b	7.70 ± 0.088^b	8.70 ± 0.088^a	7.30 ± 0.088^{bc}	5.70 ± 0.067^{bc}
	XTR	8.70 ± 0.033^c	10.30 ± 0.067^c	11.70 ± 0.033^b	8.70 ± 0.033^c	6.30 ± 0.033^c
	GRA	4.00 ± 0.000^a	5.70 ± 0.033^a	6.70 ± 0.033^a	5.70 ± 0.067^{ab}	3.30 ± 0.033^a

CON=Control, GLY= Glyphosate, ATR= Atrazine, GRA= Gramoxone, XTR= Xtravest, WK=Week.
Columns with values that have the same letter show that there are no significant differences($p \geq 0.05$) between the values; columns with values that have different letters show that there is a significant difference ($p \leq 0.05$) between the values.

Table 6: Changes in fungal dry-weights during biodegradation

		5TH	10TH	15TH	20TH	25TH
2ND WK	CON	0.010 ± 0.000^b	0.012 ± 0.000^b	0.014 ± 0.000^b	0.015 ± 0.000^b	0.015 ± 0.000^{bc}
	GLY	0.012 ± 0.000^c	0.015 ± 0.000^c	0.016 ± 0.001^c	0.018 ± 0.001^{cd}	0.016 ± 0.000^{cd}
	ATR	0.013 ± 0.000^{cd}	0.015 ± 0.001^c	0.016 ± 0.001^c	0.017 ± 0.001^c	0.015 ± 0.001^b
	XTR	0.014 ± 0.000^d	0.015 ± 0.000^c	0.017 ± 0.000^c	0.020 ± 0.000^d	0.017 ± 0.000^d
	GRA	0.008 ± 0.000^a	0.010 ± 0.000^a	0.012 ± 0.000^a	0.014 ± 0.000^a	0.012 ± 0.000^a
4TH WK	CON	0.011 ± 0.000^a	0.014 ± 0.000^a	0.016 ± 0.000^a	0.017 ± 0.000^a	0.013 ± 0.001^a
	GLY	0.014 ± 0.000^b	0.017 ± 0.001^b	0.019 ± 0.001^a	0.020 ± 0.000^{bc}	0.014 ± 0.001^a
	ATR	0.015 ± 0.000^c	0.017 ± 0.000^b	0.019 ± 0.001^a	0.023 ± 0.000^c	0.019 ± 0.000^b
	XTR	0.024 ± 0.000^d	0.026 ± 0.001^c	0.030 ± 0.001^b	0.032 ± 0.002^d	0.021 ± 0.000^c
	GRA	0.013 ± 0.000^b	0.015 ± 0.001^{ab}	0.019 ± 0.002^a	0.019 ± 0.001^{ab}	0.015 ± 0.001^a
6TH WK	CON	0.013 ± 0.000^b	0.014 ± 0.000^{ab}	0.015 ± 0.001^{ab}	0.014 ± 0.000^c	0.010 ± 0.000^c
	GLY	0.013 ± 0.000^{bc}	0.014 ± 0.000^{bc}	0.015 ± 0.000^{ab}	0.013 ± 0.000^b	0.010 ± 0.001^c
	ATR	0.014 ± 0.000^c	0.015 ± 0.000^c	0.016 ± 0.001^b	0.013 ± 0.001^b	0.009 ± 0.001^c
	XTR	0.018 ± 0.000^d	0.018 ± 0.000^d	0.020 ± 0.000^c	0.016 ± 0.000^d	0.006 ± 0.001^b
	GRA	0.011 ± 0.000^a	0.013 ± 0.000^a	0.014 ± 0.000^a	0.010 ± 0.000^a	0.004 ± 0.000^a
8TH WK	CON	0.012 ± 0.000^a	0.013 ± 0.000^a	0.014 ± 0.000^a	0.015 ± 0.000^a	0.012 ± 0.000^a
	GLY	0.015 ± 0.001^b	0.017 ± 0.000^b	0.019 ± 0.000^c	0.021 ± 0.001^b	0.016 ± 0.000^b
	ATR	0.016 ± 0.001^{bc}	0.019 ± 0.001^c	0.021 ± 0.000^d	0.022 ± 0.001^b	0.020 ± 0.001^c
	XTR	0.018 ± 0.001^c	0.019 ± 0.001^c	0.020 ± 0.001^d	0.021 ± 0.001^b	0.019 ± 0.001^c
	GRA	0.012 ± 0.000^a	0.014 ± 0.001^a	0.016 ± 0.000^b	0.014 ± 0.000^a	0.012 ± 0.000^a

CON=Control, GLY= Glyphosate, ATR= Atrazine, GRA= Gramoxone, XTR= Xtravest, WK=Week. Columns with values that have the same letter show that there are no significant differences($p\geq0.05$) between the values; columns with values that have different letters show that there is a significant difference ($p\leq0.05$) between the values.

Residual Concentration of Herbicides Obtained from Soil Samples

Fig.1 shows the residual the residual concentration of herbicides obtained from herbicide treated soils. Residual concentration of herbicides increased significantly ($p\leq0.024$) from the 2nd week to the 8th week of treatment. There was also significant difference ($p\leq0.001$) in residual concentration values of the herbicide types. The highest residual concentration value of 9.94×10^{-1} ppm was recovered from glyphosate treated soils at the 8th week of treatment, and peak detection time of 11.37 mins. Also, at the 2nd, 4th and 6th weeks of treatment it was noted that glyphosate treated soils had the highest residual concentration values of 4.13×10^{-1} ppm, 6.05×10^{-1} ppm, and 8.62×10^{-1} ppm respectively (at peak detection times of 12.41 mins, 12.30 mins and 17.53 mins respectively) compared to other herbicide treated soils. The lowest residual concentration of 2.53×10^{-1} ppm (atrazine) was obtained from atrazine treated soils at the 2nd week of treatment at peak detection time of 14.95 mins, while also at the 8th week of treatment atrazine treated soils had the lowest concentration of atrazine (6.67×10^{-1} ppm), at peak detection time of 15.26 mins compared to other herbicides at the 8th week of treatment.

Biodegradation of Herbicides by Bacteria and Fungi

In Figure 2, the concentrations of the control were higher than the concentrations of the bacteria and fungi inoculated herbicides. There was significant reduction ($p\leq0.001$) in the herbicide concentrations after degradation by bacteria and fungi. All herbicides inoculated with bacteria were found to contain lower concentrations of the corresponding herbicide compared to those that had been inoculated with fungi after 7 days of incubation on rotatory shaker incubator. The bacteria and fungi inoculated into each of the herbicides caused sharp reduction in herbicide concentrations compared to the control. The lowest herbicide concentration of 118.55 ppm was obtained from atrazine inoculated with bacteria, while the highest

herbicide concentration of 449.23ppm was obtained from xtravest inoculated with fungi at the 7th day of incubation.
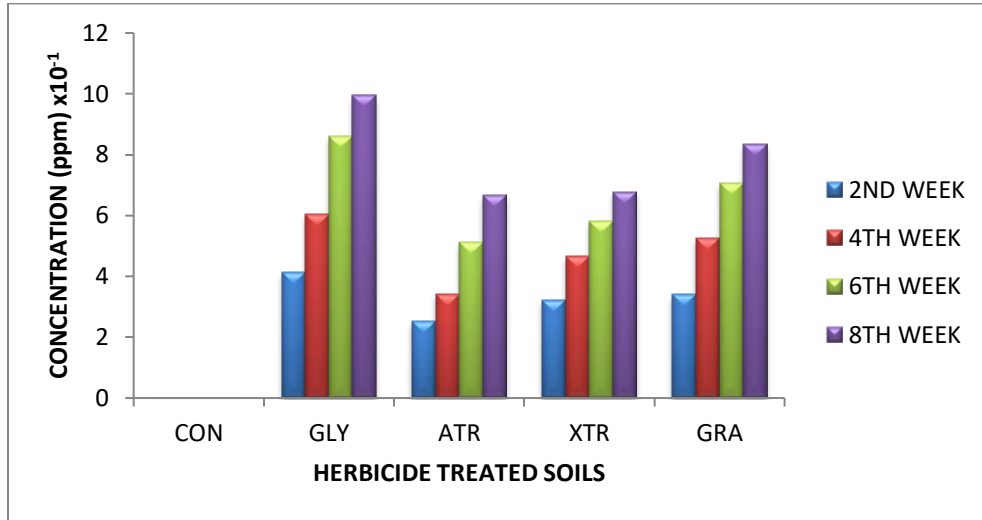

Figure 1: Residual concentration of herbicides obtained from soil samples.
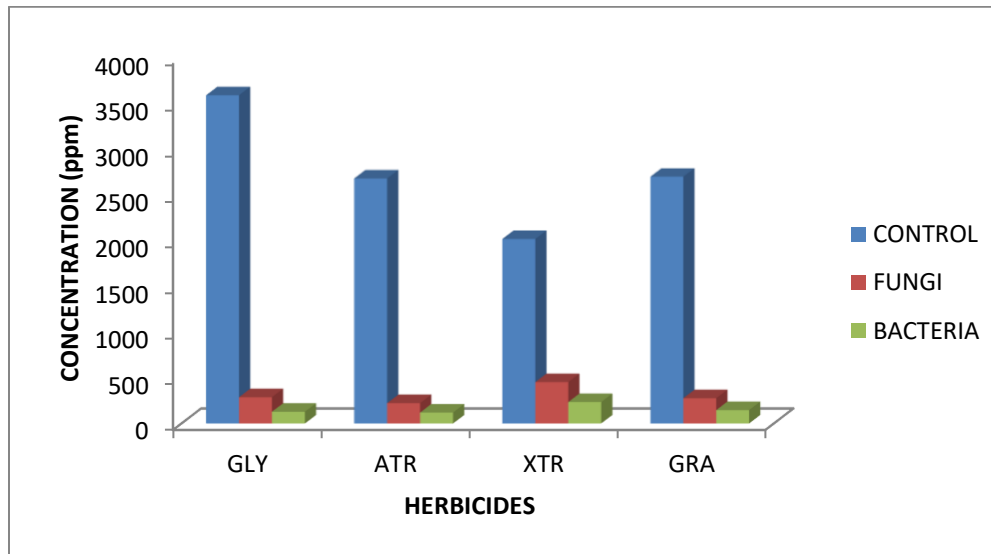

Figure 2: Biodegradation of herbicides by bacteria and fungi.

4. DISCUSSION

In this study Zn and Fe cations accumulated in soils after treatment with herbicides. Similar observation were also reported by Abah et al. (2012). The levels of Fe and Zn recorded in this study were found to be above critical limits of 10-20 mg/kg Fe and 60-400 mg/kg Zn which cause phytotoxicity in plants (FAO/WHO, 1976). This might be due to the chelation ability of these herbicides (allowing them to accumulate in this form in soils) where they form complexes with these metal co-factors essential for enzyme activities thus immobilizing them in soil reducing their availability to plants. Iron deficiency chlorosis is also becoming increasingly prevalent in cropping systems receiving frequent or prolonged applications of glyphosate (Ozturk et al., 2008). Cations in the soil solution are bonded to the surface of clay minerals by electrostatic interactions and can return in solution by the substitution of other cations or by dilution. The most representative exchange cations are K^+, Ca^{2+}, Mg^{2+}, and Na^+ (Blasioli et al., 2011).

The strong negative correlation of exchangeable Ca^{2+} with residual concentration of herbicides indicates that as the herbicides accumulated in the soils, as a result of successive treatment, there was concomitant reduction in exchangeable Ca^{2+} in the soils. The accumulation of K^+ in glyphosate treated soils occurred because K^+ is a constituent component of glyphosate chemical compound ($C_3H_7KNO_5P$). The reduction in concentration of some soil minerals (K^+, Ca^{2+}, Mg^{2+}, and Na^+) in this study might have occurred as a result of leaching of the minerals in solution and the degradation of the herbicides consequent upon the utilisation of these soil minerals by soil microbes and also their resultant uptake by plants. Benzon et al. (2015) reported that the data on available P, exchangeable Mg, Na, Ca, and K. CEC showed no significant difference among treatments. They also reported that relatively lower values were obtained compared to the control. Cucci et al. (2015) reported that the variations in available phosphorus and exchangeable potassium were negligible and not statistically different between the various treatments.

Herbicides used in this study persisted in soils upon successive treatments with the herbicides. GC analysis used in this study revealed that the herbicides accumulated in the soils throughout the period of treatment. This might be as a result of strong bonding interactions between the herbicides and soil organic matter resulting in their accumulation in soils. Glyphosate showed more persistence in soils as a result of its strong binding interaction with organic matter. Jilani and Khan (2004) reported that the residues of an applied pesticide may remain in the environment for variable periods of time.

The bacterial and fungal isolates used in the determination of the time utilisation of the herbicides showed appreciable growth in culture medium containing the herbicides as carbon source. The differences observed in the growth of the isolates in the media are indications of the differences between the organisms in tolerating the herbicides. This study showed that the bacterial and fungal isolates grew maximally on all the herbicides. The utilisation of herbicides in minimal salt medium have shown that none of the bacterial and fungal isolates exhibited lag phases, because the microorganisms used in this study are indigenous to the soil from which they were obtained and consequently have adapted to the herbicides used in treatment. Xtravest and glyphosate were better utilised by the indigenous bacteria and fungi in minimal salt medium compared to other herbicides tested in this study. According to Andy et al. (2017), microbial degradation of paraquat involves the action of some fungi and bacteria organisms. The genera of organisms that degrades paraquat include fungi: *Rhizopus*, *Penicillium*, *Aspergillus* and *Mucor* species and sole source of carbon and energy revealed that the isolates utilized paraquat at different rates. This indicates the varying ability of microorganisms to breakdown paraquat. In the work of Moneke et al. (2010), of the seven bacterial species they identified, two (*Acetobacter* sp. and *P. fluorescens*) were selected for further biodegradation studies based on their short lag phase and rapid utilisation of glyphosate. Many *Pseudomonas* species have been used extensively in the degradation and metabolism of glyphosate. Cheloufi et al. (2017) state that, glyphosate and 2.4-D have a negative effect on production of P_2O_5 and NO_3 - in two Soils Types of the Bou Namoussa irrigable perimeter (Algerian Extreme Northeast), while herbicide 2.4-D exerts a more depressive action than that of Glyphosate towards microflora in both related soils from the point of view of texture and structure, loamy ground and other sandy in the irrigable perimeter of Bou Namoussa. Inhibition by these two herbicides decreases the two microbial activities concerning mineralisation of assimilable phosphorus and organic nitrogen in nitrate. The sharp reduction in herbicide concentrations after 7 days of incubation caused by the indigenous bacterial and fungal consortium indicates high rate of degradation by the indigenous bacteria and fungi, hence pointing to the ability of the microorganisms to use herbicides as carbon source. The bacterial consortium degraded herbicides faster than the fungal consortium because of their rapid rate of proliferation in aquatic environments. Bacteria degraded atrazine faster than any of the other herbicides used in this study. Moreno *et al.* (2007) reported that after 16 days of incubation there was, at a maximum, 50% of the added atrazine remaining. Shaner and Henry (2007) reported that there was approximately a 3- to 5- fold difference between the rates of degradation in the rapid assay compared to field dissipation.

5. CONCLUSION

There were considerable reductions of exchangeable Na^+, K^+ and Mg^{2+} in soils after herbicide treatment. The indigenous bacteria and fungi were able to utilize the herbicides as carbon source and consequently degrading them *in-vitro*. Continuous herbicide treatment should be avoided because of their ability to accumulate and persist in soils resulting in soil pollution and limiting essential nutrients available to plants. Indigenous microorganisms can be employed to remediate soils polluted by herbicides. Future studies on acceleration of biodegradation rates by indigenous microbial consortium should be examined.

6. REFERENCES

1. Abah, J., Akan, J.C., Uwah, E.I., Ogugbuaja, V.O. (2007). Determination of some anions levels in some tubers grown in Benue State, Nigeria. Trend in Applied Science Research, 3(2), 196-202.

2. Abah, J.A., Abdulrahaman, F.I., Ndahi, N.P. (2012). Study of the effects of chemical fertilizers and herbicides on the levels of some heavy metals and anions in soils and corn (Zea mays) growth in selected parts of Benue state, Nigeria. Journal of Physical Sciences and Innovation, 4, 62-72.

3. Andy, I. E., Edu, G. S., Bassey, I. U., Markson, A. A., Umana, E. I., Udo, S. E. (2017). Biodegradation of Paraquat. Journal of Biopesticides and Environment, 1, 80-85.

4. Australian Academy of Technological Sciences and Engineering (2002). Pesticide use in Australia. A review undertaken by the Australian Academy of Technological Sciences and Engineering. Anl Publishing, www.atse.org.au

5. Ayansina, A.D.V., and Oso, B.A. (2006). Effect of two commonly used herbicide on soil microflora at two different concentrations. African Journal of Biotechnology, 5 (2): 129-132.

6. Ayanthi, N., Priyantha, N., and Rodrigo, U (2008). Analytical Methods for the Investigation of Reactivity of Propanil. Journal of National Science Foundation, 36(3), 199-203.

7. Benzon, H.R.L., Rubenecia, M.R.U., Ultra, V.U., Lee, S.C. (2015). Chemical and Biological Properties of Paddy Soil Treated with Herbicides and Pyroligneous Acid. Journal of Agricultural Science 7: 1-10.

8. Blakemore, L.C., Searle, P.L., Daly, B.K. (1987). Methods for chemical analysis of soils. N.Z. Soil Bureau Sci. Rep. 80. Soil Bureau, Lower Hutt.

9. Blasioli, S., Braschi, I., Gessa, C.E. (2011). The fate of herbicides in soil: In Herbicides and the environment pp. 175-194. www.intechopen.com/download/pdf/pdfs_id/1258 6.

10. Chauhan, A.K. Das, A., Kharkwal, H., Kharkwal, A.C., Varma, A. (2006). Impact of microorganisms on environment and health, in A.K. Chauhan and A. Varma ed., Microbes: Health and environment.

11. Cheesbrough, M. (1984). Medical Laboratory Manual for Tropical Countries. Microbiology. Linacre House, Jordan Hill, Oxford. Vol.11.

12. Cheloufi, R., Messaadia, H., Alayat, H. (2017). Biodegradation of Herbicides by Pseudomonas aeruginosa in two Soils Types of the Bou Namoussa irrigable perimeter (Algerian Extreme Northeast): Effects on mineral nutrition (P2O5 and NO3 -). Journal of Materials and Environmental Sciences, 8(7), 2513-2521.

13. Clive, P. (2006). Effects of pesticides used in sugarcane cropping systems on soil Organisms and biological functions associated with soil health. A report prepared for the Sugar Yield Decline Joint Venture

14. Cucci, G., Lacolla, G., Crecchio, C., Pascazio, S., Giorgio, D.D. (2015). Impact of long term soil management practices on the fertility and weed

flora of an almond orchard. Turkish Journal of Agriculture and Forestry, 39,1-9.

15. De-Lorenzo M. N., M., Domiguez A., Moldes D., Cameselle C., Sanroman, A. (2001). Enhanced ligninolytic enzyme production and degrading capability of Phanerochaete chrysosporium and Trametes versicolor. World Journal Microbiology and Biotechnology, 19, 665-669.

16. Ferrey, M.L., Koskinen, W.C., Blanchette, R.A., Burnes, T.A. (1994). Mineralisation of Alachlor by lignin-degrading fungi. Canadian Journal of Microbiology, 40 (9), 795-798.

17. Food and Agriculture Organisation/World Health Organisation (1976). List of maximum levels recommended for contaminants by joint FAO/WHO codex alimentary commission, 2nd series. CAC/FAI, Rome 3. Pp. 1-8.

18. Holt, J.G., Krieg, N.R., Sneath, P.H.A., Staley, J.T., Williams, S.T. (1994). Bergye's Manual of Determinative Bacteriology. 9th Ed. Williams and Wilkins, Baltimore, Maryland, USA.

19. Jilani, S., Khan, M.A. (2004). Isolation, characterisation and growth response of pesticide degrading bacteria. Journal of Biological Sciences, 4, 15-20

20. Kruger, E.L, Rice, P.J., Anhalt, J.C., Anderson, T.A., and Coats, J.R. (1996). Use ofundisturbed soil columns under controlled conditions to study the fate of [14C] diethylatrazine. Journal of Agriculture and Food Chemistry, 44, 1144-1149.

21. Maynard, E. (2000) Heavy metal contamination in soils of urban highways, Cincinati, Ohio. Journal of Water and Soil Pollution, 133, 293-314.

22. Moneke, A.N., Okpala, G.N., Anyanwu, C.U. (2010). Biodegradation of glyphosate herbicide in vitro using bacterial isolates from four rice fields. African Journal of Biotechnology, 9 (26), 4067-4074.

23. Moreno, J.L., Aliaga, A., Navarro, S., Hernandez, T., Garcia, C. (2007). Effect of atrazine

on microbial activity in semiarid soil. Applied Soil Ecology, 35, 120-127.

24. Ozturk, L., Yazici, A., Eker, S., Gokmen, O., Roemheld, V., Cakmak, I. (2008). Glyphosate inhibition of ferric reductase activity in iron deficient sunflower roots. New Phytology, 177, 899-906.

25. Sethi, S., Pophle, S., Varte, N., Salve, C., Waghela, S. (2015). Microbial population response exposed to Different pesticides. International Journal of Scientific Engineering and Applied Science, 1(5), 250-255.

26. Shaner, D., Henry, W.F. (2007). Field history and dissipation of atrazine and metolachlor in Colorado. Journal of Environmental Quality, 36, 128-134.

27. Souza, J. B. G., Re-Poppi, N., Raposo Jr., J. L. (2012). Characterization of pyroligneous acid used in Agriculture by Gas Chromatography-Mass Spectrometry. Journal of Brazil Chemical Society, 23(4), 610-617.

28. Tahar, W., BordJiba, O., Mezedjri, L. (2017). Impact of two Pesticides on soil Physicochemical Characteristics and the Biological Activity. Journal of Chemical and Pharmaceutical Sciences, 10(2), 803-808

29. Trimurtulu, N., Ashok, S., Latha, V., Subramanyeswara R.A. (2015). Influence of Pre-Emergence Herbicides on the Soil Microflora during the Crop growth of Blackgram, Vigna mungo.L. International. Journal Current Microbiology and Applied Sciences, 4(6), 539-546

30. Tripathi, S.K., Sumida, A., Ono, K., Shibata, H., Uemura, S., Kodama, Y., Hara, T. (2006). Leaf litter fall and decomposition of different above-and below ground parts of birch (Betula ermanii) tree and dwarf bamboo (Sasa kurilensis) shrub in a young secondary forest of Northern Japan, Biology and Fertility of Soils, 43, 237-246.

31. United States Department of Agriculture, Soil Conservation Service (1972, 1982). Soil Survey

Laboratory Methods Manual. Soil Survey Investigations Report no. 1. United States Department of Agriculture, Washington, D.C.

Biogas Potentials of Anaerobic Co-Digestion of Rumen Contents and Sewage Sludge

Research Article

Francis James OGBOZIGE[1*] iD , Tanimu Shamsudeen USMAN[2] iD , Umar Alfa ABUBAKAR[3] iD

[1]Department of Civil Engineering, Federal University Otuoke, Nigeria

[2]Depatment of Water Resources & Environmental Engineering, Ahmadu Bello University, Zaria, Nigeria

[3]Depatment of Water Resources & Environmental Engineering, Ahmadu Bello University, Zaria, Nigeria

Author E-mails
engr.ogbozige@gmail.com
    *Correspondance to: Francis James Ogbozige, Department of Civil Engineering, Federal University Otuoke, Nigeria

Abstract

Sewage sludge (SS) and rumen contents (RC) are produced daily in waste stabilization ponds and abattoirs respectively as organic wastes. However, these wastes could pose a threat to the environment if not properly managed hence, this research investigated the potentials of these wastes in generating biogas. This was achieved by digesting different SS/RC ratios anaerobically for 75days and recording the biogas produced under mesophilic condition. The SS and RC were obtained from Ahmadu Bello University (ABU) waste stabilization pond and cattle (*Bos indicus*) respectively, while the SS/RC ratios considered are 1:0, 0:1, 1:1, 1:2 and 2:1. Results showed that co-digestion at SS/RC ratios 1:1, 1:2 and 2:1 produced more biogas compared to mono-digestions of equivalent volumes of SS (1:0) and RC (0:1). This is because the daily biogas potentials for SS/RC ratios 1:0, 0:1, 1:1, 1:2 and 2:1 are 3.59, 5.61, 6.09, 6.67 and 5.79ml per gram of TS added respective. In other words, biogas potential for SS improved by 69.64, 85.79 and 61.28% when co-digested with RC at SS/RC ratios 1:1, 1:2 and 2:1 respectively, while that of RC improved by 8.56, 18.89 and 3.21% at SS/RC ratios 1:1, 1:2 and 2:1 respective. Hence, it was concluded that co-digestion of SS and RC at SS/RC ratio 1:2 produced more biogas followed by 1:1 and 2:1 accordingly.

1. INTRODUCTION

The discharge of untreated sewage into the environment could cause a lot of adverse effects on human health since sewage usually contains numerous life threatening pathogens including *Vibrio cholerae* and *Salmonella typhi*. It could also lead to eutrophication of streams and rivers with its associated effects. Hence, in 1979, the management of Ahmadu Bello University (ABU), Zaria-Nigeria decided to design and construct a Waste Stabilization Pond (WSP) that could treat the wastewater generated within the university community before discharging to the nearby Kubani stream. However, during the operation of a WSP, sludges are frequently formed as byproduct and needs to be removed periodically in order not to reduce the volume and treatment efficiency of the pond thus, increasing the operating cost of WSP. Zaria, been the host community of Ahmadu Bello University is known to have numerous abattoirs especially for the ruminants. Usually, the ingesta (rumen contents) in these abattoirs are disposed by merely dumping on the ground surface until they accumulate to form heaps, allowed to dry and then burnt openly. This is not environmentally friendly because rumen contents contain so much bacteria [1-3]. Hence, if disposed in this manner, the watery component could leached into the ground to contaminate groundwater. In addition, the open burning of these dried heaps of rumen contents pollutes the atmosphere.

Global warming is one of the main environmental problems disturbing the world however, researchers have shown that the use of renewable energy at homes, institutions and industries could reduce its effects considerably [4, 5]. Biogas has been identified for long as one the sources of renewable energy and it is generated when bacteria decompose organic materials in the absence of oxygen to produce mostly methane and carbon dioxide in a process known as anaerobic digestion [6-7]. The gas produced usually consist of 55 – 75% methane and 25 – 45% carbon dioxide with trace amount of other gases especially nitrogen [8]. However, the anaerobic digestion (AD) comprises four stages known as hydrolysis, acidogenesis, acetogenesis and methanogenesis as shown in Figure 1.
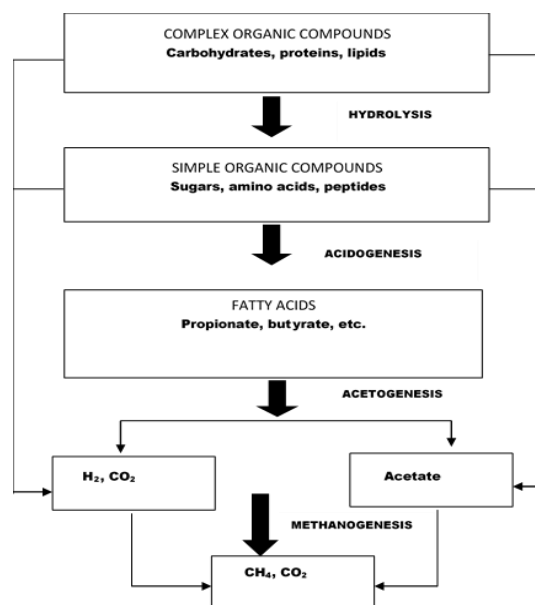

Figure 1. Stages for anaerobic digestion and formation of biogas

During the first stage, hydrolytic bacteria decompose complex organic matters into simple soluble organic molecules using water to split the chemical bonds between the substances. In the second stage, acidogenic or fermentative bacteria convert the small and simple molecules (monomers) resulted from the first stage

(hydrolysis) to a mixture of volatile fatty acids (VFAs) such as acetic, propionic and butyric acids and other minor products like alcohols, hydrogen and carbon dioxide (CO_2). The third stage (acetogenesis) involves the formation of acetate through the reduction of the carbon dioxide (CO_2) or organic acids formed during the second stage by a group of anaerobic bacteria known as acetogens. However, the fourth and final stage (methanogenesis) involves the overall anaerobic conversion of organic matter to methane and CO_2. This is achieved by the cleavage of two acetic acid molecules to generate methane and carbon dioxide, or by reduction of carbon dioxide with hydrogen by methane forming bacteria (methanogens).

The sludge in WSP and rumen contents in abattoirs are all biodegradables hence, could be used as feedstock for anaerobic digestion. However, the mono-digestion of abattoir wastes have been reported of creating technical challenges due to the inhibitory effects of ammonia and fatty acids on methanogens [9]. Besides, Mono-digestion of sewage sludge also have the limitation of low quantity of biogas production compared to the volume of feedstock added in a digester, as some of the organic matters in the sludge are already stabilized by the bacteria present [10]. In other words, the bacteria in sewage sludge are activated and would readily digest organic wastes more than those present in fresh rumen contents. Hence, co-digestion been the simultaneous anaerobic treatment of two or more biodegradables of different characteristics with the aim of enhancing biogas production, could be applied on these wastes (sewage sludge and rumen contents). Apart from improving the overall biogas production, the co-digestion of these wastes will reduce the cost of biogas production as both the sewage sludge and rumen contents can jointly be treated in a single installation or digester. Hence, it is important to investigate the biogas potentials of the said wastes when co-digested at different ratios in order to make necessary recommendations based on their performances.

2. MATERIALS AND METHOD

Sewage sludge from the anaerobic tank of Ahmadu Bello University WSP (11°8'17.05"N, 7°39'27.47"E) and fresh rumen contents of a cattle (*Bos indicus*) from Zango Shanu abattoir, Zaria (11°8'11.82"N, 7°39'59.88"E) were separately collected in a 5-liter container. The sludge and rumen contents were properly decanted in order to ensure that only the solid proportions are retained for the experiment. Sewage sludge to rumen contents (SS/RC) ratios of 1:0, 0:1, 1:1, 1:2 and 2:1 were prepared based on the total solids (TS) contents of the sludge and rumen contents, and were identified as A, B, C, D and E respectively. Since the both organic materials (sewage sludge and rumen contents) already contain anaerobic bacteria, additional bacteria were not introduced as inoculum into the various SS/RC ratios prepared. The SS/RC ratios 1:0 and 0:1 (i.e. A and B) were prepared for the sake of serving as controls in order to compare the results of the co-digestions with the mono-digestions of sewage sludge and rumen contents respectively. However, the exact quantities of sewage sludge and rumen contents used in preparing the various SS/RC ratios are given in Table 1.

Table 1. Proportions of feedstock components in digester

Assay ID	SS/RC ratio	Sewage sludge (ml)	Rumen contents (ml)	volume of feedstock (ml)
A	1:0	1000	0.0	1000
B	0:1	0.0	1000	1000
C	1:1	500	500	1000
D	1:2	333.3	666.6	1000
E	2:1	666.6	333.3	1000

The various SS/RC ratios showed in Table 1 were measured into 2000ml conical flasks (digesters) using a graduated cylinder and were thoroughly mixed. Thereafter, samples were immediately obtained and analysed for concentrations of total solids (TS) added in the digesters using standard method [11]. The pH values of the mixtures were adjusted by adding few drops of 10M NaOH solution to each mixture until the pH readings were between 6.5 and 7.8. Thereafter, the conical flasks were corked in order to maintain anaerobic (oxygen free) conditions and kept in a mesophilic environment (30°C to 37°C) during retention period.

The daily quantity of biogas generated in the digesters were measured using the downward water displacement method. This was achieved by filling 1200ml beaker up to 90% capacity (1080ml) thereafter, 1200ml graduated cylinder fully filled with water was inverted and submerged below the water surface in the beaker, and clamped vertically by means of retort stand. A delivery tube was connected from the digester to the inverted graduated cylinder as shown in Figure 2. Thus, the biogas formed in the digester moved to the inverted graduated cylinder through the delivery tube. This consequently displaced corresponding volume of water from the inverted graduated cylinder to the beaker. Hence, the observed drop in water level in the graduated cylinder was recorded as the amount of biogas produced at the ambient temperature and pressure.
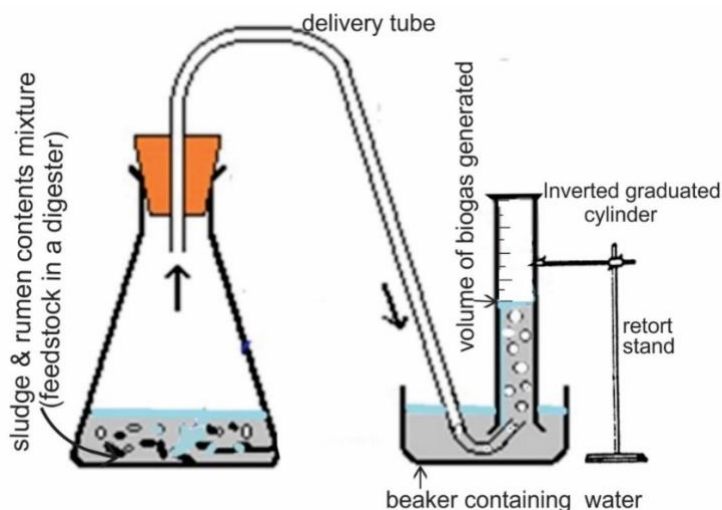

Figure 2. Determination of volume of biogas produced by water displacement method

The daily and cumulative biogas production for each experimental assay was recorded for a period of 75days. Hence, the average daily biogas production was determined by dividing the cumulative biogas produced at the 75th day by 75. The result obtained was divided by the quantity (grams) of TS added in the digester thus, obtaining the daily biogas potential or yield in ml per gram of TS added. However, the quantity (grams) of TS added in each digester was known by multiplying the volume of feedstock in the digester (1000ml) by the concentration of TS.

3. RESULTS AND DISCUSSION

The concentrations of TS added in the digesters with SS/RC ratios 1:0, 0:1, 1:1, 1:2 and 2:1 are 2.38, 1.94, 2.16, 2.09 and 2.23g/l respectively while the results of the cumulative biogas production for the various experimental conditions (assays) are presented in Figure 3. The figure revealed that the cumulative biogas produced in the mono-digestion of sewage sludge (SS/RC ratio 1:0) during the first 25days (260ml) was higher than the mono-digestion of rumen contents (SS/RC ratio 0:1) which was 230ml. This might be

attributed to the fact that bacteria in the sewage sludge were already active in degrading organic matters in the WSP prior to the experiment while those in the rumen contents were still acclimatizing during the said period. Nevertheless, the reverse occurred for the remaining 50 days as the final cumulative volumes of biogas produced for SS/RC ratios 1:0 and 0:1 are 640 and 817ml respectively. This is because the quantity of degradable organic matters present in fresh rumen contents is usually higher than that of sewage sludge since the former often contain undigested ingesta (mostly grasses). Thus, explaining the reason why more biogas were produced in the mono-digestion of the rumen contents during the remaining 50 days compared to the mono-digestion of sewage sludge, after the bacteria in the sewage sludge have acclimatized. It is also revealed in Figure 3 that more quantities of biogas were produced in all the cases involving co-digestion (SS/RC ratios 1:1, 1:2 and 2:1) compared to the mono-digestions (1:0 and 0:1) which is in agreement with past related literatures [12-14]. However, the cumulative biogas produced in co-digestion with SS/RC ratios 1:1, 1:2 and 2:1 are 987, 1045 and 968ml respectively.
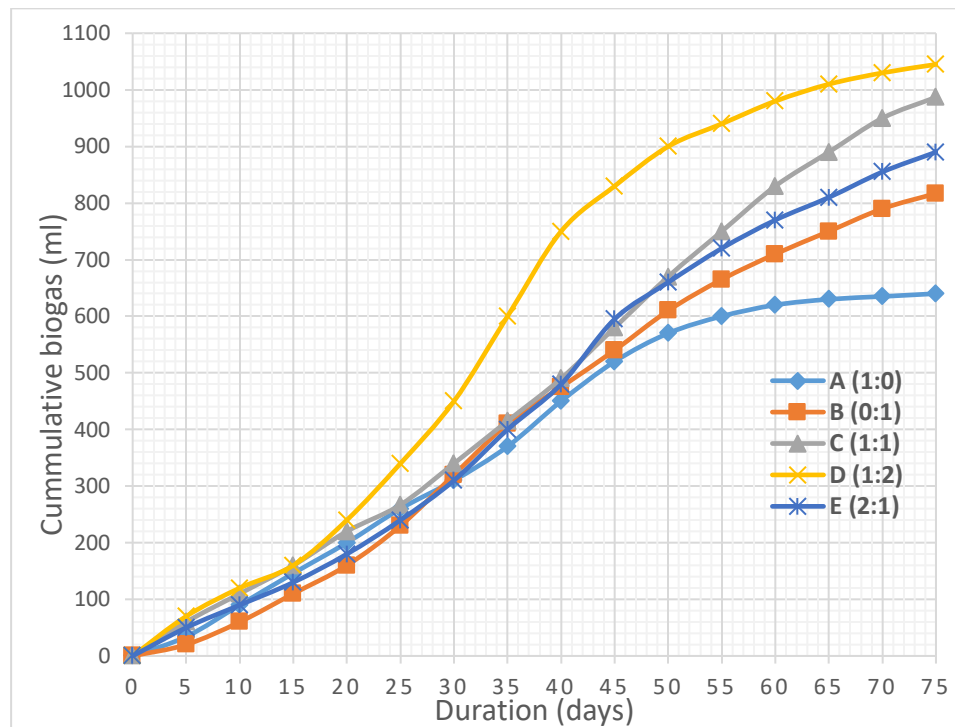

Figure 3. Cumulative biogas production

In other words, the biogas production in the co-digestions improved with an increase in rumen contents in the feedstock (SS/RC ratio). This might be due to the spike in activities of bacteria present in the rumen contents, caused by the already activated bacteria in the sewage sludge, which in turns degrade the numerous undigested organic matters usually present in rumen contents.

Based on the values obtained as concentrations of TS added in the digesters as well as the final cumulative volumes of biogas shown in Figure 3, the daily biogas potentials are calculated as shown in Table 2.

Table 2. Biogas potential of various experimental assays

Assay ID (a)	SS/RC ratio (b)	Conc. of TS added in g/l (c)	Volume of feedstock in ml (d)	Quantity of TS added in grams $= \frac{(c) \times (d)}{1000}$ (e)	Final cum. biogas in ml (f)	Average daily biogas in ml $= \frac{(f)}{75}$ (g)	Average daily biogas potential in ml per gram of TS added $= \frac{(g)}{(e)}$
A	1:0	2.38	1000	2.38	640	8.53	3.59
B	0:1	1.94	1000	1.94	817	10.89	5.61
C	1:1	2.16	1000	2.16	987	13.16	6.09
D	1:2	2.09	1000	2.09	1045	13.93	6.67
E	2:1	2.23	1000	2.23	968	12.91	5.79

Conc. = concentration, cum. = cumulative, SS = sewage sludge, RC = rumen contents, TS = total solids
(a), (b), (c), ………., (g) = column 1, 2, 3,………., 7 respectively.

It is clearly revealed in Table 2 that daily biogas potentials for mono-digestions of the sewage sludge (SS/RC 1:0) and rumen contents (SS/RC ratio 0:1) are 3.59 and 5.61ml per gram of TS added respectively. On the other hand, the values for co-digestions with SS/RC ratios 1:1, 1:2 and 2:1 are correspondingly 6.09, 6.67 and 5.79ml per gram of TS added. In other words, the highest daily biogas potential occurred when the SS/RC ratio is 1:2. Hence, biogas potential of the sewage sludge (SS) improved by 69.64, 85.79 and 61.28% when co-digested with rumen contents (RC) at SS/RC ratios 1:1, 1:2 and 2:1 respectively, while that of rumen contents (RC) improved by 8.56, 18.89 and 3.21% at SS/RC ratios 1:1, 1:2 and 2:1 respective.

4. CONCLUSIONS

Based on the analysed results acquired from this research, the following deductions are drawn:

i. Sewage sludge from ABU Waste Stabilization Pond and rumen contents from cattle (*Bos indicus*) have daily biogas potentials of 3.59 and 5.61ml per gram of TS added respectively when mono-digested anaerobically without inoculum under mesophilic condition. However, more biogas are produced at the initial stage (first 25days of retention) for mono-digestion of the sewage sludge compared to rumen contents.

ii. Anaerobic co-digestion of the sewage sludge (SS) and rumen contents (RC) at SS/RC ratios 1:1, 1:2 and 2:1 produced more biogas compared to mono-digestions of equivalent volumes of SS and RC. Nevertheless, average daily biogas potential for SS/RC ratio 1:2 (6.67ml per gram of TS added) is the highest, followed by SS/RC ratio 1:1 (6.09ml per gram of TS added) and SS/RC ratio 2:1 (5.79ml per gram of TS added).

iii. Biogas potential of the sewage sludge (SS) improved by 69.64, 85.79 and 61.28% when co-digested with rumen contents (RC) at SS/RC ratios 1:1, 1:2 and 2:1 respectively, while that of rumen contents improved by 8.56, 18.89 and 3.21% at SS/RC ratios 1:1, 1:2 and 2:1 respective.

5. ACKNOWLEDGEMENTS

6. REFERENCES

1. Matthews, C., Crispie, F., Lewis, E., Reid, M., O'Toole, P. W., & Cotter, P. D. (2019). The rumen microbiome: a crucial consideration when optimising milk and meat production and nitrogen utilisation efficiency. *Gut microbes*, *10*(2), 115-132.

2. Cammack, K. M., Austin, K. J., Lamberson, W. R., Conant, G. C., & Cunningham, H. C. (2018). RUMINNAT NUTRITION SYMPOSIUM: Tiny but mighty: the role of the rumen microbes in livestock production. *Journal of animal science*, *96*(2), 752-770.

3. Dayyani, N., Karkudi, K., & Zakerian, A. (2013). Special rumen microbiology. *International Journal of Advanced Biological and Biomedical Research*, *1*(11), 1397-1402.

4. Hasnisah, A., Azlina, A. A., & Che, C. M. I. (2019). The impact of renewable energy consumption on carbon dioxide emissions: Empirical evidence from developing countries in Asia. *International Journal of Energy Economics and Policy*, *9*(3), 135.

5. Gielen, D., Boshell, F., Saygin, D., Bazilian, M. D., Wagner, N., & Gorini, R. (2019). The role of renewable energy in the global energy transformation. *Energy Strategy Reviews*, *24*, 38-50.

6. Arthur, R., Baidoo, M. F., & Antwi, E. (2011). Biogas as a potential renewable energy source: A Ghanaian case study. *Renewable Energy*, *36*(5), 1510-1516.

7. Balat, M., & Balat, H. (2009). Biogas as a renewable energy source—a review. *Energy Sources, Part A*, *31*(14), 1280-1293.

8. Demirbas, A., Taylan, O., & Kaya, D. (2016). Biogas production from municipal sewage sludge (MSS). *Energy Sources Part A Recovery Utilization and Environmental Effects*, *38*(20), 3027–3033.

9. Borowski, S., & Kubacki, P. (2015). Co-digestion of pig slaughterhouse waste with sewage sludge. *Waste management*, *40*, 119-126.

10. Garg, S. K. (2012). *Sewage disposal and air pollution engineering*. Khanna Publsihers.

11. American Public Health Association, American Water Works Association, Water Pollution Control Federation, & Water Environment Federation. (1915). *Standard methods for the examination of water and wastewater* (Vol. 2). American Public Health Association..

12. Almomani, F., & Bhosale, R. (2020). Enhancing the production of biogas through anaerobic co-digestion of agricultural waste and chemical pre-treatments. *Chemosphere*, 126805.

13. Nkodi, M. T., Mulaji, K. C., Mabela, M. R., Kayembe, S. J., Biey, M. E., Ekoko, G., & Taba, K. M. (2020). Investigation of Factors Affecting Biogas Production from Cassava Peels by Fractional Factorial Design Experimental Methodology. *Journal of Applied Life Sciences International*, 49-56.

14. Achinas, S., & Euverink, G. J. W. (2019). Elevated biogas production from the anaerobic co-digestion of farmhouse waste: Insight into the process performance and kinetics. *Waste Management & Research*, *37*(12), 1240-1249.